INTESTINAL TRANSPORT PROBLEMS INVOLVING MICHAELIS-MENTEN KINETICS

by

DONALD A. JOHNSON

A thesis submitted in partial fulfillment of the requirements for the degree of

DOCTOR OF PHILOSOPHY
(Pharmacy)

at the

UNIVERSITY OF WISCONSIN-MADISON

1985

INTESTINAL TRANSPORT PROBLEMS INVOLVING MICHAELIS-MENTEN KINETICS

Donald A. Johnson

Under the supervision of Assistant Professor Ronald Burnette and Professor Gordon Amidon (University of Michigan)

Two pharmaceutical problems are identified involving interphase transport and Michaelis-Menten kinetics. One is the analysis of the intestinal perfusion experiment. The other is the dissolution of solid substrates into enzymic solutions. In both systems interphase transport rates are analysed through mass balance statements composed of convection, diffusion and chemical reaction.

A laminar flow model is used for the intestinal perfusion analysis. The general membrane transport scheme is simultaneous passive diffusion and carrier mediated transport. A boundary layer analysis allowed direct determination of the intrinsic uptake parameters. A film model was also developed where the film thickness, which is related to the aqueous resistance, is determined from the boundary layer solution. The derived aqueous resistance was compared to experimental data for progesterone, a highly permeable compound, and leucine, which is taken up by a saturable carrier system. Experimental results and theoretical estimates were in close agreement for both compounds. Also shown was that the apparent

Michaelis constant of a saturable scheme could be shifted beyond the concentration range of study or the solubility limit due to aqueous resistance. Compounds with simultaneous passive uptake can especially have the saturable mechanism masked if the aqueous resistance is kept large.

The dissolution behavior of N-benzoyltyrosine ethyl ester (BTEE) and N-acetylphenylalanine (APEE) from a rotating disc into solutions of alpha-chymotrypsin was also investigated. Dimensional analysis identifies the importance of the parameter R*, the ratio of the diffusion time to reaction time. It was found that enzymatic reaction had little effect on dissolution of the highly soluble APEE while having a large effect on the slightly soluble BTEE. The dissolution rate of BTEE as a function of pH was studied to determine the dependence of the catalytic rate constant on pH. Other experiments included the variation of bulk enzyme concentration and rotational speed of the disc. Results of all experiments were correctly predicted by the R* parameter.

To: _____

Mom, Dad, Christopher, and Ingrid

ACKNOWLEDGEMENTS

I wish to acknowledge my major professor, Dr. Gordon Amidon who, although present at this thesis defense, was unable to serve as an official committee member due to the length of time which has lapsed since his departure from the University of Wisconsin. I sincerely appreciate his patience and tolerance which afforded me a great degree of independence in my work. I always found his encouragement to be very motivating. As his student I was able to spend some time at each of the three best departments of pharmaceutics in the nation. These are the Universities of Wisconsin, Kansas, and Michigan.

I wish to thank all the students and faculty members of those three institutes who have contributed in any way to the development of my scientific thinking as well as my personal philosophy of science and education. I am especially grateful to Professor E.N. Lightfoot of the chemical engineering department at the University of Wisconsin. He together with Drs. Elliott and Amidon laid the theoretical groundwork for the intestinal perfusion modelling. Dr. Lightfoot was also very instrumental in the early development of the enzyme dissolution work.

There are too many graduate students that I've been associated with over the past several years to name them all. However, I would like to express my thanks to Andreas de Meere, a

graduate student of the University of Amsterdam who spent four months of his training at the University of Michigan. During that time he collected much of the L-leucine data. Also Ming Hu, a graduate student at the University of Michigan, collected the proline data presented here. I further acknowledge the use of the published progesterone data of Drs. Komiya, Park, Kamani, Ho, and W. Higuchi.

I would like to thank Sue Knitter of Word Designs who did the word processing of this thesis. Her help enormously simplified putting this work into final form.

Finally, and most importantly, I wish to express my deepest appreciation to my entire family for all their generous love and support. I am proud to belong to such a wonderful family.

TABLE OF CONTENTS

LIST OF FIGURES

Part I

LIST OF TABLES

INTRODUCTION

In order for most orally administered drugs to be effective, they must first be absorbed through the gastrointestinal membrane and into the systemic circulation. The majority of drugs are absorbed by a simple passive-diffusive mechanism. There are however, many examples of compounds which are transported across the intestinal membrane by a saturable process of either facilitative or active transport. Active transport is distinguished from facilitative transport in that it requires metabolic energy and also has the ability to concentrate against a chemical gradient.

Some examples of compounds which show a saturable mechanism for intestinal absorption include: sugars (1-2), amino acids (3-18), dipeptides (19-23), bile acids (24,25), riboflavin (26), ascorbic acid, thiamine, beta-carotene and alpha-tocopherol (27, 28), and the amino-acid like substance, carnatine (29-31). Pharmaceutical compounds demonstrating a saturable uptake mechanism include cimetidine (32) and a large number of the beta-lactam antibiotics (33-42). Although not all beta-lactam antibiotics are taken up by a carrier mediated process, the ones that are may be taken up by one of two carrier types or both. One carrier is characterized by facilitative diffusion and the other is the active transport process common to the uptake of intact dipeptides (35, 38). Some of these antibiotics, as well as some of the other compounds mentioned, have been shown to be taken up by simple passive diffusion and a saturable

carrier system simultaneously (24,25,29-32,34,35,41).

Prodrugs which are targeted for bioreconversion in the gastrointestinal tract may also demonstrate a saturable uptake scheme due to saturation of the enzymic systems involved in the digestion or absorption of nutrients. An example is a prodrug to which an amino acid is attached to the parent drug with an amide or ester linkage (43).

The prodrug approach may be used to increase drug solubility in order to increase bioavailability of orally administered drugs (43). On the other hand, it may be used to decrease drug solubility and thereby prolong intestinal absorption (44,45). Decreasing the drug solubility may also increase the shelf life of a solid suspension formulation (46). However, a low aqueous solubility may also mean a low dissolution rate and hence poor bioavailability. It will be shown though, that if the prodrug is a substrate for one of the luminal enzymes, the rapid chemical reaction after oral administration of a prodrug suspension may result in rapid dissolution rates. Therefore, it may be possible to achieve greater shelf life stability without compromising bioavailability.

The need for evaluating intestinal membrane permeabilities and dissolution rates of drugs applies whether they permeate by a passive mechanism or a saturable one and whether they are prodrugs or not. Poor bioavailability of a pharmaceutical compound may be due to several factors. Three common ones are: 1) first pass metabolism,

ii) poor permeation through the intestinal membrane and, iii) poor drug dissolution and/or poor drug solubility. In order to assess the reason for lack of good bioavailability, experimental systems should be designed to isolate and evaluate each of the above three factors. The present work is concerned with the latter two.

Membrane permeabilities are studied by a variety of in vitro and in vivo techniques. Unfortunately, the permeabilities determined experimentally are effective permeabilities and are strongly dependent on the hydrodynamic conditions of the experimental system. Therefore, for a given compound, the effective permeability will vary from technique to technique. How to extract the aqueous resistance out of the effective permeability to give the intrinsic membrane permeability is not always clear.

For the dissolution of solid substances under assumed sink conditions, the chemical concentration potential is fixed and is equal to the solubility of the compound. Therefore, the dissolution rate depends primarily on the geometric form of the solid and the aqueous resistance determined by the convective mixing of the bulk dissolution media. Again, the hydrodynamics is not always known.

Aside from convective considerations, mass transport analysis may be further complicated by the presence of a chemical reaction. Two different strategies for gastrointestinal bioreconversion of prodrugs are luminal and membrane surface reconversion. A chemical bulk reaction (luminal reconversion) will generally appear as a term

in the mass transport differential equations while surface reactions are generally incorporated into the boundary conditions of the transport equations. In either case, the problem becomes even more complex when considering the non-linear functional form of a saturable process demonstrating Michaelis-Menten type kinetics.

In this thesis, two problems associated with oral absorption of drugs in the small intestine are analyzed. The first problem analyzes the experimental technique of the in situ perfusion of the rat intestine. The aqueous resistance for the system is derived, thus allowing calculation of the intrinsic membrane parameters by experimental determination of the effective permeability and knowledge of that aqueous resistance. Here the membrane permeability is viewed as a surface reaction. The second problem involves the luminal reconversion of prodrugs targeted for one of the protease enzymes of the gastrointestinal tract (e.g. alpha-chymotrypsin). This problem is analyzed using the in vitro method of the rotating disc. This system is chosen because of its well characterized hydrodynamics. This allows one to concentrate on the effect chemical reaction has on dissolution rate. Here, the solid substrate dissolves into a bulk solution containing the enzyme.

A general flux equation for both problems can be written as:

$$J = P_{aq} \Delta C$$

which has the electrical analogy $I=(1/R)V$. The concentration

potential, ΔC, in the dissolution problem equals the drug solubility and the aqueous resistance, (1/Paq), is dependent on the hydrodynamics. If a bulk chemical reaction is included, the concentration gradient remains the same. However, there can be a significant decrease in the aqueous resistance. The reason for this is that the dissolved drug at the solid surface must diffuse through the diffusional boundary layer to reach the bulk media. The boundary layer thickness is determined by the convective mixing. If the reaction time is much faster than the time required for diffusion through the boundary layer, the diffusional pathlength is shortened due to reaction. The result is that the mass sink (bulk media) is brought closer to the solid surface.

In the intestinal perfusion problem, ΔC equals the bulk fluid concentration minus the membrane surface concentration. The aqueous resistance is determined solely by the distance a drug is able to diffuse radially in the intestine within the mean residence time of the drug in the intestine based on the flow rate and intestinal length of perfused segment. The membrane surface reaction (uptake) will affect only the concentration potential, ΔC, and not the aqueous resistance. Even when the membrane is impermeable to a drug ($J=0$), the aqueous resistance still exists. It is the chemical potential, in this case, which goes to zero.

Therefore, it is seen that if the chemical reaction occurs in the bulk, the aqueous resistance is affected but not the

concentration potential. On the other hand, if the reaction occurs at a surface, it is the concentration potential and not the aqueous resistance which is affected.

ANALYSIS OF THE INTESTINAL PERFUSION EXPERIMENTS

BACKGROUND

Physiology of the Small Intestine

The organizational structure that makes up the wall of the gastrointestinal tract is shown in figure one. As fluid flows through the small intestine, it encounters many folds called the valvulae conniventes which are most prominent in the duodenum and jejunum and less in the ileum (47). These folds are covered with many villi. In the human, there are 20-40 villi per square millimeter of mucosa. Each intestinal villus is a fingerlike projection 0.5-1.0 millimeters in length in humans (4) and approximately 0.4 millimeters in rats (48) (see figure two). The relative and absolute lengths and depths of the villi and crypts change along the intestine (49-52). The villi are covered by a single layer of columnar epithelium and contain a network of capillaries and lymphatic vessels. The free edges of the epithelial cells are further divided into microvilli.

The epitheleal cells contain large quantities of digestive enzymes. These enzymes include: i) dipeptidases (21, 23, 53), ii) amino-oligopeptidases (53-55), and iii) enzymes for splitting disacch- arides into monosaccharides - sucrase, maltase, isomaltase, and lactase (55-57), and iv) lipases (57). Most of these enzymes are located mainly in the brush border of the epithelial cells and therefore presumably cause hydrolysis of nutrients on the outer surface of the microvilli prior to absorption (57).

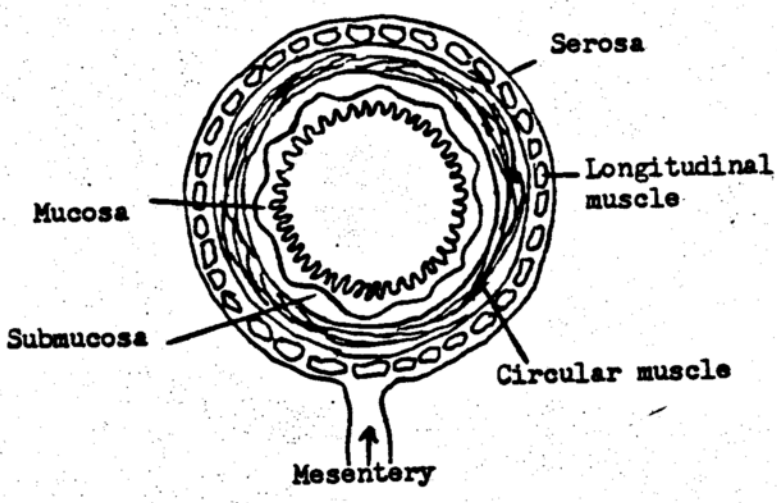

Figure 1

Schematic representation of the layers of the small intestine.

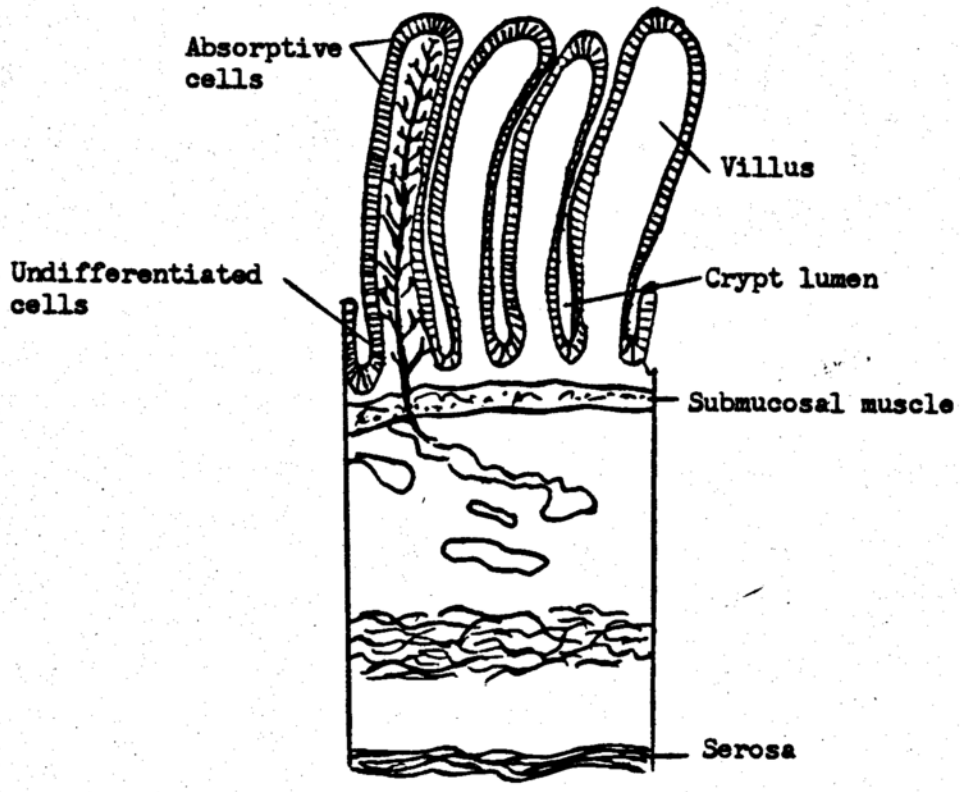

Figure 2

Diagram of small intestine section showing villi and crypt region.

In the crypt region, the epithelial cell population includes the undifferentiated cells. These cells mature while migrating to the villus tips where they are shed in two to five days (58, 59). This process continuously renews the epithelial lining of the villus. During migration to the villi tips, functional as well as morphological maturation of the undifferentiated cells is believed to occur (60, 61). For example, the absorption cells involved in amino acid absorption are located high up on the villus tip (4, 13, 62).

It seems plausible that most solutes are absorbed in the uppermost positions of the villi and that the lateral surface of the lower two-thirds has little role in absorption (1, 63). It has been suggested that the function of the villi folds is not so much to increase absorptive surface area as it is to provide time for the differentiation and maturation of the absorptive enzyme systems in the epithelial cells as they migrate upward from the crypts (63). For highly permeable solutes such as long chain fatty acids, it has been shown that the absorptive surface area is approximately (1/100) - (1/200) the actual anatomical surface area provided by the folds of the villi and microvilli. It is concluded then, that for highly permeable solutes at least, the absorptive surface area is close to the minimum cylindrical surface area at the tips of the villi (1, 63, 64).

It has also been shown that with in vitro techniques, the villi become swollen causing occlusion of the intervilli space thus

restricting absorption to the villus tip region (65). Other investigations have shown that there is little, if any, effective stirring in the intervilli space (1, 63). These studies further support the appropriateness of estimating the absorptive surface area to be that of the minimal cylindrical surface area.

The membrane permeability may be a composite of many physical processes (64). All the inhomogeneities of the membrane tend to be averaged out in the permeability term. For instance, if a drug is absorbed at the villi tips but also diffuses into the crypt lumen with subsequent absorption into the lower villus region, then this diffusional process in the crypt lumen becomes incorporated into the membrane permeability. Although the fluid of the crypt lumen is aqueous in nature, the resistance to diffusion in this region is not part of the aqueous resistance of the experimental system, say an intestinal perfusion, since the external bulk flow conditions have no effect on this resistance. Hence, it is incorporated into the membrane resistance.

There is a term quite frequently used, and perhaps misused, called the "unstirred water layer". This is the aqueous region, adjacent to the membrane surface, through which the drug molecule must diffuse to go from the bulk fluid to the membrane surface. The resistance to aqueous diffusion in this region is highly dependent on the bulk flow. It is this aqueous resistance that shall be derived in the analysis.

Physically, the unstirred water layer should not be considered a region of fluid stasis (albeit fluid flow is slower near a stationary surface). Rather, it should be considered the region over which the concentration potential exists. Further discussion on the unstirred layer is in a subsequent section.

Experimental Methods For Determining Intestinal Membrane Permeabilities

There are a variety of techniques for determining membrane permeabilities. The membrane parameters determined however, usually depend on the technique chosen. The reason for this may be due to a variety of factors including the hydrodynamic conditions of the experiment as well as the physical distribution of sites on the membrane available for absorption. To help in understanding the discrepancies seen among the various techniques, a brief description of the more common methods for studying intestinal membrane permeabilities are given.

Everted Sacs

The everted sac technique was first introduced in 1954 by Wilson and Wiseman (66). Segments of small intestine about ten centimeters in length are removed from the rat, rinsed with normal saline and everted over a glass rod. The drug solutions are prepared in modified Ringer's solution. One milliliter of drug solution is placed in the interior of the sac and is incubated for one hour in

100 milliliters of Ringer's solution gassed with 5% carbon dioxide in oxygen. The incubating media may or may not also contain drug. Putting equal drug concentrations on the serosal and mucosal sides may be used to distinguish between active and facilitative transport. The same may be accomplished by use of metabolic inhibitors such as 2, 4-dinitrophenol (32, 42). If equal concentrations on both sides are used, the concentration should be kept low so as to maximize the final ratio between serosal and mucosal fluid concentrations (36, 67).

In addition to analyzing the final drug concentrations of the fluids, the tissue may also be analyzed for drug taken up. This usually requires the addition of a non-permeable probe molecule to correct for the drug in the fluid adherent to the membrane surface (1, 68).

The shaking rate during incubation has been shown to markedly affect the uptake rate (1, 68). In addition to this, the nonsteady-state nature of this technique makes it difficult to obtain the intrinisic uptake parameters from the measured effective ones.

Rings of Everted Intestine

This method involves taking slices of everted intestine 0.2-0.5 centimeters long (42, 69). The slices are placed in a Ringer's solution containing drug. The flask is gassed with 5% carbon dioxide in oxygen for a period of one hour after which time the slices are rinsed and blotted dry. A tissue homogenate is then prepared using a

Teflon homogenizer.

The same comments for the everted sacs about shaking rate during incubation apply here. In addition, this technique requires use of radio-labelled compounds or tissue extraction. Use of radio-labelled compounds is a severe disadvantage if a commercially labelled compound is unavailable, as well as a cost disadvantage for ones which are. Tissue extraction on the other hand, requires determination of an extraction efficiency curve. Aside from these points, the actual experimental procedure is an easy one and can give good statistical results (8, 70, 71).

Another disadvantage, not mentioned but common to the everted sac, is that by everting the intestine, the villi are turned inward and can close some of the subepithelial space. This may restrict access to the incubating media (13). Finally, in the everted ring method, the flux is measured across both the baso-lateral membrane as well as the brush-border membrane. A change in the convective mixing of the incubating media will probably have a greater effect on transport across the baso-lateral side since this side is more exposed to the incubating media.

Intestinal Loops

The method of the in-situ ligated loop has the advantage that the blood supply to the small intestine can be left intact (72). Intestinal lengths of approximately 5-10 centimeters are used. The lumen is washed with isotonic phosphate buffer. Six milliliters of

air are introduced to expel the residual buffer and then the air is gently removed (33). One milliliter of drug solution is injected into the loop where it remains for one hour, after which time the animal is killed. The loop is then removed, the contents emptied and analyzed.

As mentioned, this method has the advantage of leaving the blood supply to the small intestine intact. The disadvantage arises from the absence of stirring within the lumen which may result in a large aqueous resistance. The analysis can further be complicated by the lack of steady state conditions.

In Situ Perfusion

In this technique the blood supply to the small intestine is also left intact. The surgery described by Elliott is summarized as follows (73). The intestine is exposed by a midline longitudinal incision. The segment of intestine to be perfused is identified and an incision is made. A tefion cannula is inserted and tied in place with surgical thread. Approximately 5 to 15 centimeters distal to the first cannula, a second cannula is introduced. The tubing of the proximal cannula leading to the rat is passed through a water bath and is connected to a syringe containing drug solution. The syringe is placed in a constant flow infusion pump (Harvard Apparatus Model 931, S. Natick, MA) from which the perfusional flow rate can be regulated. The intestinal segments are perfused until the effluent is clear (usually 20 minutes) and then an additional 60-90 minutes

(see figure 3). Further details of this experimental method can be found in references 43 and 74.

The drug concentration in the effluent is assayed and compared to the known influent concentration. Steady state effluent concentrations are usually seen within 30 minutes and maintained fora full 90 minutes (75).

Several advantages arise with this technique. As mentioned the blood supply is left intact. Secondly, one needs only to assay the effluent concentration. This can be done by such standard means as HPLC, for example. Finally, the hydrodynamic flow can be controlled and one can now begin to estimate the contribution of the aqueous resistance to the overall resistance to membrane uptake (74, 76).

The everted sac technique and the everted ring technique are in vitro ones while the ligated loop and the perfusion systems are in vivo. Although there are seemingly advantages and disadvantages to each method, the in vitro techniques may not provide insight into actual function in vivo, particularly because the transport processes may depend upon adequate blood flow. For example, Smithson and Gray, compared intestinal uptake of the tetrapeptide Gly-Leu-Gly-Gly in gut sacs and in perfused segments (54). The rates of disappearance of the tetrapeptide were the same in both preparations. However, the hydrolytic products accumulated in the mucosal fluid of the in vitro system. This implies that the tetrapeptide is handled differently in

vivo or that the hydrolytic products are transported more efficiently in vivo.

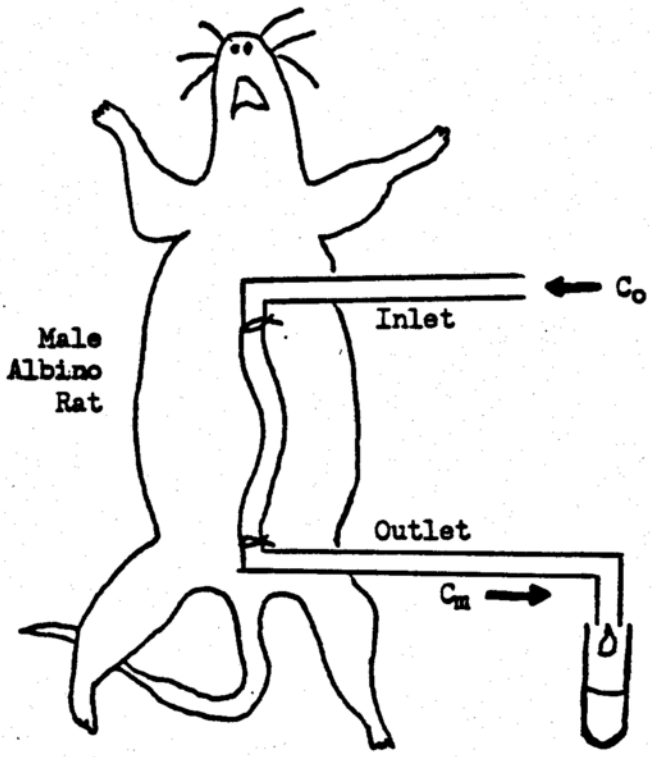

Figure 3

Schematic diagram of the in vivo perfusion of the rat intestine.

The "Unstirred" Layer

It has been recognized for some time that the measurements of membrane permeabilities may be strongly influenced by the presence of "unstirred" or aqueous diffusion layers adjacent to the membrane surface (77). It is with some trepidation that the term "unstirred" layer is used. Physically speaking, there cannot be a macroscopic zone of stasis separated from a moving bulk phase by a sharp boundary. The diffusion boundary layer merely reflects the drug concentration gradient in the direction perpendicular to the membrane surface. More often then not, the fluid in this region adjacent to the membrane surface is in motion. In particular, the fluid flow in the intestinal perfusion experiments is in the axial direction, including the region of radial concentration gradient. Increasing the flow rate will, in fact, convectively bring more mass into this region thereby decreasing the concentration gradient.

Confusion can arise when it is not certain what one is referring to as the unstirred layer. If the luminal crypts of the intervilli space is meant by the unstirred layer, then this region probably is really stagnent or unstirred. However, as mentioned earlier, it is better not to incorporate this region into the aqueous resistance term since the external flow conditions will have little, if any, effect on the diffusional resistance of this region.

The boundary layer thickness is most commonly defined through a flux equation:

$$\frac{\Delta C}{\delta} = \frac{dC}{dy}\Big|_{y=0}$$

A common misconception is that the boundary layer thickness, δ, describes an actual stagnent film, when in fact, it is more of an operational quantity. Further discussion of this point can be found in a review by Pedley (78).

"Unstirred layer" is perhaps a poor choice of words. Yet its appearance is quite frequent in the biological literature. In this work the unstirred layer will be taken to mean the region of concentration gradient adjacent to and in the direction perpendicular to the membrane surface with full cognition of fluid motion in this region. More often this will be referred to as the diffusional boundary layer.

The diffusional resistance in the aqueous diffusional boundary layer has been shown to have profound effects on the kinetics of both active and passive transport processes of the gastrointestinal tract (79-82). Under certain circumstances, diffusion through this layer may actually be the rate limiting step to absorption (65, 74, 80, 83). This is particularly true for very lipophilic compounds.

The unstirred layer has been shown experimentally to markedly affect the apparent Michaelis constant for carrier mediated uptake and to have little effect on the maximal uptake (1, 79, 84-89). The apparent Michaelis constants are determined to be too high when an

unstirred layer is present. Failure to show a saturable uptake may merely indicate a very high unstirred layer resistance. Theoretical considerations have been given to correct the bias in the Michaelis term due to the aqueous diffusional resistance (1, 64, 79, 81, 83, 84, 86, 90-93). However, these corrections require knowledge of the unstirred layer thickness and, unfortunately, there are few good theoretical considerations for this aspect of the problem. Also, only one of the references cited considers the effect of the unstirred layer on the parameters of an uptake scheme comprised of saturable and passive mechanisms in parallel (91).

The effect of the unstirred layer on the Michaelis constant is demonstrated by the work of Wilson and Dietschy (1). The effect of the stirring rate on the uptake of glucose, L-serine, and taurocholate into everted rings was studied. The results for glucose, which are typical, are shown in figure 4. The Michaelis constant determined by a double recipricol plot was markedly affected by the degree of stirring. The stirring rate had little effect on the maximal uptake, Jmax, when determined from these same plots. The maximal uptake was also determined experimentally at concentrations high enough such that the maximal uptake was independent of concentration. It was discovered that these values were consistently lower than those determined from double recipricol plots. This is not surprising since it has been shown that it is theoretically

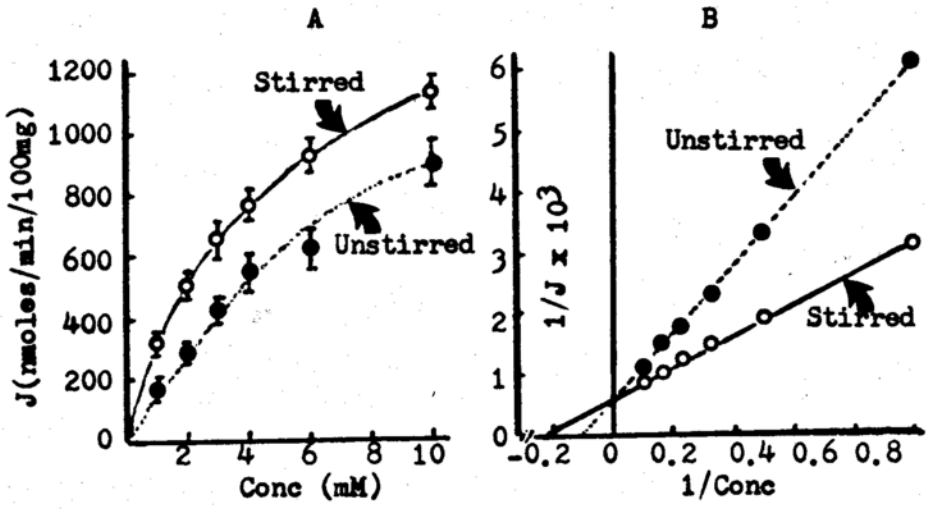

Figure 4
Active transport rates of glucose into intestinal rings as a function of concentration in the bulk buffer phase. Panel A shows the uptake rate, J, under stirred and unstirred conditions. The same data are plotted as reciprocals in Panel B. (Redrawn from reference 1)

incorrect to use a double recipricol plot for these types of studies because of the presence of the unstirred layer (1, 81, 83).

In order to understand the failure of the double recipricol plot, the equation describing the flux across the membrane surface is examined.

$$J = \frac{D}{\delta} (Co - Cw)$$

The concentration at the membrane surface is symbolized as Cw. Usually, this concentration is unknown and is approximated to be the bulk concentration, Co, which is the concentration of the sample medium. If one knows what the boundary layer thickness is, the concentration at the membrane surface can be derived by setting the above flux equation equal to the flux through the aqueous boundary layer (83).

$$C_w = \frac{(Co - Km - J_{max} \cdot \delta/D) + \sqrt{(Co - Km - J_{max} \cdot \delta/D)^2 + 4CoKm}}{2}$$

It is therefore easy to see how simple substitution of the bulk concentration for the membrane concentration can lead to serious errors in determination of the Michaelis-Menten parameters. Also, it is not surprising that the parameter values are dependent on the degree of stirring, since the membrane concentration depends on the

boundary layer thickness, a function of stirring rate.

Although the effect of the unstirred layer is known, the problem lies in the lack of knowledge concerning the thickness of this layer. Some investigators have circumvented this problem with in vitro systems by increasing the stirring until a plateau Km value is obtained (84) or by stepwise increasing the stirring rate, determining Km and Jmax, and extrapolating to infinite stirring (87). For the in vivo perfusion method, this is not possible since increasing the flow rate too much makes it impossible to distinguish between the concentration of the perfusate going into and coming out of the perfused segment. Intuitively, it seems correct to set the flow rate as high as possible to decrease the aqueous resistance as much as possible, yet the flow rate should be slow enough to allow sufficient mass absorption allowing distinction between effluent and influent concentrations. This may guarantee that the aqueous resistance does not become rate limiting. However, it is still necessary to know the aqueous resistance such that it can be factored out of the overall resistance to membrane uptake.

The effect of increasing the perfusion flow rate then, is to increase absorption by decreasing the overall resistance to uptake. This has been demonstrated experimentally in rat (74, 94-100) as well as with luminal perfusions in man using a double tube (101-104).

Although derivation of the aqueous resistance is a complex problem, it is possible to obtain estimates experimentally. This is

done by assuming that the total resistance to membrane uptake of highly permeable lipophilic compounds is due solely to the aqueous resistance (1, 67, 74). Ho, Higuchi and co-workers used this method in the perfused rat intestine and found an empirical relationship between the flow rate and aqueous resistance (74). A method by Smithson et al. (105) calculates the unstirred layer thickness by comparing the kinetic constants of isolated brush border enzymes in vitro to the kinetic constants of the rat jejunum enzymes in an in vivo perfusion.

The theoretical analysis of Elliott et al. (76) derives the intrinsic first order membrane permeability constant directly for the perfusion system by assuming the intestine is a cylindrical tube with laminar flow (106). Here, the aqueous resistance is not needed to calculate the intrinsic permeability constant.

The convective-diffusive equation described by Elliott et al. was solved using a separation of variables technique (107). Since this procedure requires linear boundary conditions, the solution has limited applicability to the Michaelis-Menten uptake scheme. The present work shall extend the boundary layer analysis for laminar flow in a circular duct, described by Levich (108). The boundary conditions in this approach can be arbitrary.

STATEMENT OF THE PROBLEM

The diffusional resistance in the fluid adjacent to the membrane surface greatly affects the membrane uptake of a drug. The effect of this aqueous resistance is to bias the intrinsic membrane parameters, especially the Michaelis constant of a saturable carrier. The degree of bias depends on the size of the aqueous resistance, which is a function of the experimental conditions. The nature of the intestinal perfusion experiments requires that there be a significant difference in the effluent and influent concentrations. This much loss of mass means that a significant aqueous resistance must be allowed to exist. The problem is that there is a lack of theory for determination of the aqueous resistance in this system so that the intrinsic parameters may be obtained.

The problem statement is perhaps best put into the form of these three questions:

1) What is the aqueous resistance for the intestinal perfusion experiment and what parameters does it depend on?

2) Once the aqueous resistance is found and one is able to calculate the intrinsic membrane permeability, how does one relate this to the intrinsic membrane parameters, Jmax, Km and Pm, where Jmax is the maximal flux, Km the Michaelis constant for a saturable carrier system and Pm is a passive permeability constant?

3) Having the answer to 1 and 2, how can this be expressed in a

form practical for the experimentalist?

The objectives of the analysis will be to answer these three questions.

MODEL

The mass transport model for intestinal perfusion with dilute solutions is shown schematically in Fig. 5. The rate of mass entering the intestine is given by the flow rate, Q, times the inlet concentration, Co. The rate of mass flowing out of the distal end of the intestine is given by the flow rate times the exit concentration, Cm. A mass balance statement is: the difference between the rate of mass flowing in and out through the cross-sectional areas is equal to the rate of mass absorbed through the membrane surface. The steady-state macroscopic mass balance is:

$$Q\,(C_o - C_m) = 2\,\pi\,R \int_0^L J\,(x)\,dx \qquad (1)$$

The radius of the intestine is R and the perfused intestinal length is L. THe flux of the drug across the membrane, J(x), is integrated over the membrane surface.

The most general expression for the membrane flux to be considered is that consisting of a saturable carrier system and a passive diffusion component in parallel.

$$J(x) = \frac{J_{max}\,C_w(x)}{K_m + C_w(x)} + P_m\,C_w(x) \qquad (2)$$

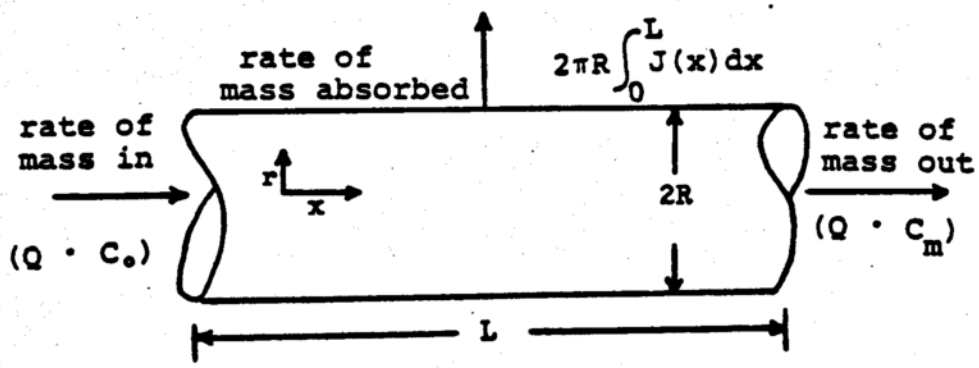

Figure 5
The Macroscopic Model for Intestinal Perfusion. The difference between the rate of mass flowing into and out of the intestine is equal to the rate of mass absorbed. The perfusional flow rate is Q and the inlet and outlet concentrations are Co and Cm respectively. The mass flux J(x) is integrated over the membrane surface.

The kinetic parameters for the saturable system, Jmax and Km, are the maximal flux and the intrinsic Michaelis constant, respectively. The membrane permeability constant for passive diffusion is represented by Pm. The membrane flux, J(x), has units of mass/area/time and is a function of axial distance, x. The concentration at the membrane surface, Cw(x), is also a functional of axial distance down the intestine. Permeability has units of velocity and is defined as a flux divided by a concentration.

The limiting cases to the above general flux equation are when the membrane surface concentration is either much higher or much lower than the Michaelis constant (zero order and first order regions of the saturable mechanism) and/or the passive permeability constant is zero. The flux across the membrane surface depends upon the concentration at the surface. Experimentally, however, only the inlet and outlet perfusate concentrations are measurable. Typically, the membrane surface concentration is approximated by the inlet concentration, Co. Doing this ignores the presence of a aqueous resistance and therefore leads to a biased determination of the kinetic parameters, as discussed in the background section. When this is done, the macroscopic mass balance of equation one can be written as:

$$Q\,(C_o - C_m) = 2\,\pi\,R\,L\,P_{eff}\,C_o \qquad (3)$$

or rewritten as:

$$P_{eff} = \frac{Q\,(1 - C_m/C_o)}{2\,\pi\,R\,L} \qquad (4)$$

The effective permeability, Peff, is determined by the experimental flow rate Q, the measured ratio of outlet to inlet concentration, Cm/Co, and the intestinal length and radius, L and R. The effective permeability is therefore the quantity one obtains experimentally. It is related to the intrinsic membrane permeability by the following expression:

$$\frac{1}{P_{eff}} = \frac{1}{P_{aq}} + \frac{1}{P_w} \qquad (5)$$

which states that the total resistance to membrane uptake is equal to the sum of the aqueous resistance and the membrane resistance. The intrinsic membrane permeability, Pw, is a function of the perfused concentration, due to the presence of a saturable mechanism. Therefore, the objectives of the analysis are twofold: 1) to determine the aqueous resistance term such that the intrinsic permeability can be derived from the experimentally determined effective permeability and 2) to relate the concentration dependent intrinsic permeability to the intrinsic membrane parameters Jmax, Km, and Pm.

In order to achieve the objectives set forth, it becomes necessary to determine the functional form of the membrane surface concentration so that the flux scheme of equation 2 can be substituted into equation 1 and the integration performed. Since it is not physically possible to measure the surface concentration at each position along the intestinal membrane surface, the function must be derived. This is accomplished by doing a microscopic mass balance on a differential volume element within the lumen. This microscopic mass balance, also known as the equation of continuity (109), takes the following form under steady-state conditions (73,76):

(6)

$$V_x \frac{\partial c}{\partial x} = D \frac{1}{r} \frac{\partial}{\partial r} r \frac{\partial c}{\partial r}$$

where Vx is the fluid velocity in the axial direction and D is the aqueous diffusion coefficient of the drug. The term on the left describes the movement of mass into and out of the volume element due to the convective flow. The term on the right describes the diffusion of mass into and out of the element. The diffusion is driven by the concentration gradient, which is a result of the flux across the membrane surface and is in the direction perpendicular to the convective flow. The form of the above equation assumes no significant fluid flow in the radial direction. Consideration of two dimensional flow is given by others (110-112).

Residence time distribution studies have shown that, to a good approximation, the hydrodynamics of the perfused rat intestine is laminar in nature (106). The velocity profile for laminar flow in a circular duct is a parabolic function (109).

$$V_x = 2 \frac{Q}{\pi R^2} \left(1 - \left(\frac{r}{R}\right)^2\right) \quad (7)$$

The fluid has maximum velocity at the luminal center (r=0) and goes to zero at the membrane surface (r=R).

The boundary conditions for equation 6 are:

$$\text{B.C.} \quad 1 \quad \text{at } x = 0 \qquad C = C_o \tag{8}$$

$$\text{B. C.} \quad 2 \qquad -D \left.\frac{dc}{dr}\right|_{r=o} = 0 \tag{9}$$

$$\text{B.C.} \quad 3 \qquad -D \left.\frac{dc}{dr}\right|_{r=R} = J(x) \tag{10}$$

The membrane flux, J(x), is given by equation 2 or one of its limiting cases. At the entrance of the perfused segment (x = 0), the concentration is equal to the inlet concentration, Co. The second boundary condition merely states that the center of the intestine is neither a source nor sink for mass. This boundary condition arises out of the axial symmetry of the problem.

The solution to equations (6-10) using the first-order flux at the membrane, i.e., J (x) = Pm Cw(x), was found using separation of variables technique (76).

$$C_m/C_o = \sum_{j=1}^{\infty} u_j \exp(- B_j^2 Gz) \qquad (11)$$

$$Gz = \pi DL/2Q \qquad (12)$$

In this expression, each uj and Bj is a function of the permeability constant Pm. The values of uj's and Bj's are tabulated in the cited reference for some specific values of the permeability constant.

As mentioned previously, the separation of variables technique requires linear boundary conditions. This solution therefore, has limited applicability to the flux scheme of equation 2. The boundary layer analysis overcomes this deficiency. However, the boundary layer analysis uses an approximation for the parabolic fluid velocity of equation 7 and therefore the solution derived is also approximate. The importance of the exact solution of equation 11 is that the accuracy of the boundary layer solution can be checked against the exact solution at least for the first order case. It should be

pointed out that for the limiting zero order case with no passive permeability, integration of equation 1 can be done with no further analysis. Using the notation of equation 4, it is found that in this case, the effective permeability is equal to the membrane permeability.

$$P_{eff} = \frac{J_{max}}{C_o} \tag{13}$$

Therefore, as the carrier system becomes saturated, the membrane resistance becomes rate limiting and the aqueous resistance is negligible.

Before discussing the boundary layer analysis, it is beneficial to briefly describe the Graetz number, Gz, due to its importance and frequent recurrence. For flow in a tube, the mean residence time of a fluid element in the tube is the volume divided by the flow rate.

$$t_{Res} = \frac{\pi R^2 L}{2 Q} \tag{14}$$

The mean time it takes a solute to diffuse a given distance radially is twice the distance squared divided by the diffusion coefficient. In a tube, the greatest distance over which diffusion can occur is the radius. Therefore, the radial diffusion time is:

$$t_D = \frac{2R^2}{D} \tag{15}$$

The ratio of the mean residence time to the radial diffusion time is the Graetz number.

$$Gz = \frac{t_R}{t_D} \tag{16}$$

The Graetz number is a dimensionless quantity.

Consider a tube with infinite wall permeability. If the Graetz number is very high, then most of the solute that enters the tube is absorbed. The ratio of the exit to inlet concentrations will be low. If the Graetz number is very low, the ratio will be high. Typically Graetz numbers for the perfusion of the rat intestine (which has a finite permeability in most cases) are in the range of 0.01 to 0.10 (43, 74).

BOUNDARY LAYER SOLUTION

The boundary layer approach was used previously by Levich (108) to solve the convective diffusion problem for laminar flow in a tube under assumed sink conditions at the tube wall. For the intestinal perfusion system this would represent the limiting case of infinite membrane permeability. All the resistance to absorption is aqueous in nature and no resistance is offered by the membrane. Most drugs, however, have finite membrane permeabilities and, in fact, this is the quantity of interest in a perfusion experiment.

The boundary layer approach is depicted schematically in Fig. 6. Due to the parabolic nature of the fluid velocity profile (see eq. 7), the fastest moving fluid is at the luminal center. The flow is much slower in regions close to the membrane surface where mass transfer occurs. When flow conditions result in low Graetz numbers, Gz, the faster moving fluid in the central core of the lumen exits the intestine with negligible change in concentration. Only the slower moving fluid within the boundary layer becomes depleted of drug. Since all the fluid entering the intestine is of uniform concentration the boundary layer thickness, $\delta(x)$, is zero at the entrance. The boundary layer grows in size as the fluid proceeds down the intestine and an increasing amount of drug is absorbed by the membrane. The aqueous diffusional resistance increases with the boundary layer thickness since the boundary layer is the distance over which the drug must diffuse to get from the bulk to the membrane

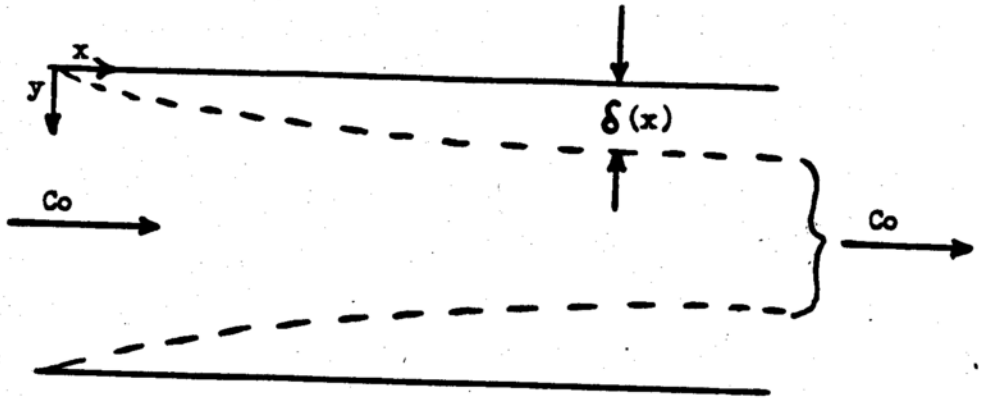

Figure 6
Schematic of the Boundary Layer Approximation. For laminar flow in a circular duct the fluid velocity profile is parabolic with a maximum velocity at the tube center. If the flow rate results in low Graetz numbers, there exists a central core of fluid which enters and exits the tube with no change in concentration. Only the slower moving fluid in the boundary layer becomes depleted in mass. The boundary layer thickness is zero at the tube entrance and increases in size in the axial direction.

surface.

Under the flow conditions described above, the mass transport of interest is in the region close to the membrane surface, the boundary layer. It is therefore convenient to define a new variable y as the distance from the membrane surface:

$$y = R - r \tag{17}$$

Substitution of y into the equation of continuity (see equations 6 and 7), gives the following approximate equation for small y:

$$4 \frac{Q}{\pi R^2} y/R \frac{\partial c}{\partial x} = D \frac{\partial^2 c}{\partial y^2} \tag{18}$$

The approximation is in the parabolic velocity profile of equation 7, which in terms of the new variable y becomes:

$$V_x = \frac{2Q}{\pi R^2} \left(\frac{2y}{R} + \frac{y^2}{R^2} \right) \tag{19}$$

which for small y values reduces to:

$$V_x = \frac{4Q}{\pi R^2} \frac{y}{R} \tag{20}$$

This approximation is valid if the flow rate is fast enough to keep the boundary layer thickness small (i.e. low Gz number).

The boundary conditions of equations 8-12 become:

$$\text{B.C. 1} \quad \text{at } x = 0 \qquad C = C_o \tag{21}$$

$$\text{B.C. 2} \quad \text{as } y \to \infty \qquad C \to C_o \tag{22}$$

$$\text{B.C. 3} \quad D \left.\frac{\partial c}{\partial y}\right|_{y=o} = J(x) \tag{23}$$

The significance of the above manipulations is that the equation of continuity can now be solved by the method of combination of variables. As opposed to the separation of variables technique, combination of variables does not have the strict limitation on the boundary conditions.

Combining the x and y variables, the new variable n is defined;

$$n = \left(\frac{4}{9}\,\frac{Q}{\pi R^3 D}\right)^{1/3} \frac{y}{x^{1/3}} \tag{24}$$

This variable is chosen since by viewing equation 18, it is seen that the variables appear as the ratio y^3/x (ignoring the partial signs). The coefficient in equation 24 is chosen such that the partial differential equation of equation 18 will be in self-adjoint form when written as the total differential equation.

$$\frac{d}{dn}\left[\exp(n^3)\,\frac{dc}{dn}\right] = 0 \tag{25}$$

The success of the combination of variables technique also depends on the ability to combine two of the boundary conditions since only two boundary conditions are needed to solve equation 25 uniquely. Fortunately this is the case with equations 21 and 22 which form the following single boundary condition:

$$\text{B.C. 1} \quad \text{as} \quad n \to \infty \qquad C \to C_o \tag{26}$$

Using the chain rule, equation 23 becomes:

$$\text{B.C. 2} \quad \left.\frac{dc}{dn}\right|_{n=0} = 1.65\ Gz^{1/3} \left(\frac{x}{L}\right)^{1/3} \frac{R}{D}\ J(x) \qquad (27)$$

The solution to equations 25-27 is:

$$C = C_o - 1.65\ Gz^{1/3} \left[\frac{x}{L}\right]^{1/3} \frac{R}{D}\ J(x) \left[0.893 - \int_o^n \exp(-\beta^3)\, d\beta\right] \qquad (28)$$

The values of the integral

$$\int_o^n \exp(-\beta^3)\, d\beta$$

are tabulated for various values of n (113). The limit of this integral as n goes to infinity is 0.893.

It is the concentration at the membrane surface (i.e., n=0) that is of interest. Setting n equal to zero, equation (26) becomes:

$$C_w(x) = C_o - 1.47\ Gz^{1/3} \left(\frac{x}{L}\right)^{1/3} \frac{R}{D}\ J(x) \qquad (29)$$

This expression is the general solution for the membrane surface concentration since J (x) has yet to be specified. For the first order boundary condition case (i.e. J(x) = Pm Cw(x)) the membrane surface concentration is:

$$C_w(x)/C_o = 1/\left[1 + K\left[\frac{x}{L}\right]^{1/3}\right] \tag{30}$$

$$K = 1.47\, Gz^{1/3}\, \frac{R}{D}\, P_m \tag{31}$$

The macroscopic mass balance for the first-order case is:

$$Q(C_o - C_m) = 2\pi R \int_o^L P_m C_w(x)\, dx \tag{32}$$

Putting equation (30) into the integral and performing the integration, the following boundary layer solution results:

$$Gz^{-2/3}\,(1 - C_m/C_o) = 4.08 - \frac{8.16}{K} + \frac{8.16}{K^2}\,\mathrm{Ln}\,(1 + K) \tag{33}$$

By experimentally setting the Graetz number (flow rate and

intestinal length) and measuring Cm/Co, one can calculate the first order permeability constant, Pm, using equation 31. This solution applies equally as well when the saturable mechanism is in the first order region, with or without a passive permeability component.

For the saturable uptake scheme with no passive permeability

$$J(x) = \frac{J_{max}\, C_w(x)}{K_m + C_w(x)} \tag{34}$$

the membrane surface concentration is solved by substitution of equation 34 into equation 29):

$$C_w(x) = \frac{Co - Km - (x/L)^{1/3}\, Ko + \sqrt{\left[(x/L)^{1/3}\, Ko + Km - Co\right]^2 + 4Km}}{2}$$

$$Ko = 1.47\, \frac{R}{D}\, Gz^{1/3}\, Jmax \tag{36}$$

Therefore the solution for the Michaelis-Menten kinetic scheme is obtained by substituting equation 35 into equation 34 and performing the integration of equation 1. This solution is:

$$Gz^{-2/3}(1-Cm/Co) = 2.04(1+Km) + 1.36(Ko/Co) - 1.36(int) \qquad (37)$$

$$int = \frac{S^3 - T^3 + 1.5(1-Km)(U\cdot S - V\cdot T + 4\cdot Km\cdot L)}{(Ko/Co)^2}$$

$$L = Ln((U+S)/(V+T))$$

$$S = \sqrt{U^2 + 4\cdot Km} \qquad T = \sqrt{V^2 + 4\cdot Km}$$

$$U = Km + Ko/Co - 1$$

$$V = Km - 1$$

In a similar manner the solution for the Michaelis-Menten scheme in parallel with a passive diffusion mechanism can be obtained:

$$J(x) = \frac{J_{max}\, C_w(x)}{K_m + C_w(x)} + P_m\, C_w(x)$$

The membrane surface concentration is found to be:

$$C_w(x) = \frac{B + \sqrt{B^2 + 4\cdot Km/(1+Pm\cdot(x/L)^{1/3})}}{2}$$

$$B = \frac{Co - Km - (Ko/Co)(x/L)^{1/3} - Pm\,(x/L)^{1/3}}{1 + Pm\,(x/L)^{1/3}}$$

The integration of this flux scheme (equation 38), however, requires numerical integration and is not given here.

As can be seen, the boundary layer approach allows one to use any arbitrary flux scheme. The solutions, however, are complex and not easy to use in practice when trying to determine the intrinsic membrane parameters Jmax, Km and Pm.

It will be shown how the general boundary layer solution can lead to a definition of the aqueous resistance. Once this is done, one can extract the aqueous resistance from the total resistance. The remaining membrane resistance will then be put into a simple form relating to the intrinsic parameters. This will be done in the modified boundary layer analysis which will follow the section on the definition of the aqueous resistance.

THE AQUEOUS RESISTANCE

As seen from the boundary layer solutions, it is not necessary to know the thickness of the boundary layer and hence the aqueous resistance in order to calculate the intrinsic membrane parameters from experimental data. However, the advantages to describing the aqueous resistance will become evident in the modified boundary layer analysis. The criterion here is that the aqueous resistance should be defined in such a way that it is totally independent of the membrane parameters.

There are a couple of ways to define the boundary layer thickness. One is to define it as the distance from the membrane surface where concentration becomes, say, 95% or 98% of the bulk concentration. This definition, however, is somewhat arbitrary and furthermore is dependent upon the membrane flux, J(x), (see equation 28). Another way to define the aqueous resistance is through a flux condition. At steady-state, the flux through the membrane equals the net diffusional flux through the boundary layer.

$$J(x) = P_{aq}(x)\,[C_o - C_w(x)] \tag{38}$$

$$P_{aq}(x) = \frac{D}{\delta(x)} \tag{39}$$

The aqueous permeability, Paq (x) is the reciprocal of the aqueous resistance. Putting the general expression for the membrane surface concentration, (equation 29), into equation 38 results in the following expression:

$$P^{*}_{aq}{}^{-1} = 1.47\ Gz^{1/3} \left[\frac{x}{L}\right]^{1/3} \tag{40}$$

$$P^{*}_{aq} = \frac{R}{D}\ P_{aq} \tag{41}$$

The coefficient R/D has the units of resistance. Therefore P^{*}_{aq} is a dimensionless permeability. Its reciprocal, $P^{*}_{aq}{}^{-1}$, is the dimensionless aqueous resistance, which is the ratio of the boundary layer thickness over the radius of rat intestine. The expression for the membrane flux, J(x), cancels and does not appear in the expression for the aqueous resistance. Equation 40 is therefore valid for any arbitrary kinetic uptake scheme and can be called a true aqueous resistance. As seen from the expression, the aqueous resistance is zero at the entrance of the

intestine for the perfused system and increases to its maximum value at $x = L$ (see figure 6).

The expression derived for the aqueous resistance here is equivalent to the one derived by Levich (108) for the case of infinite membrane permeability. De Simone (114) also recognized its use in the perfusion experiments for diffusion controlled uptake (infinite membrane permeability).

MODIFIED BOUNDARY LAYER SOLUTION

The boundary layer solution was shown to be applicable to any arbitrary uptake scheme. Unfortunately, the solutions in some cases are not easy to use. In this section a film model is developed. The solutions in the film model can be compared to those of the boundary layer analysis and in the case of the first order flux directly to the solution of Elliott (73) (equation 11). Therefore, the film thickness is not arbitrarily assigned. It will also be shown that due to the semi-empirical nature of this approach, the film model solution will be even more accurate than the boundary layer model, at least when the first order solutions of the film and boundary layer model are compared to the exact solution of equation (11).

Because the solution of the film model is based on the concepts of the boundary layer analysis and uses a form of the aqueous resistance derived from it, the solution of the film model is called the modified boundary layer solution. The first order case will be done first and then the more general Michaelis-Menten scheme and finally, the most general scheme of Michaelis-Menten uptake in parallel with passive diffusion.

First Order--The macroscopic mass balance for the first order case is written as:

$$Q\,(C_o - C_m) = 2\pi R \int_0^L P_m\, C_w\,(x)\, dx \qquad (42)$$

At steady-state the net flux through the boundary layer is equal to the flux through the membrane surface.

$$P_{aq}(x)\,(C_o - C_w(x)) = P_m\,C_w(x) \tag{43}$$

Solving for the concentration at the membrane surface, the following is obtained:

$$C_w(x) = \frac{P_{aq}(x)}{P_{aq}(x) + P_m}\,C_o \tag{44}$$

where Paq (x) is derived from the boundary layer solution (see equations 40 and 41). With this expression for the membrane surface concentration, the macroscopic balance is rewritten as:

$$Q\,(C_o - C_m) = 2\pi R\,C_o \int_0^L \left[\frac{1}{\frac{1}{P_{aq}(x)} + \frac{1}{P_m}}\right] dx \tag{45}$$

The aqueous resistance is zero at the entrance of the intestine and

reaches its maximum value at $x = L$.

$$0 \leq (P_{aq}(x))^{-1} \leq 1.47 \frac{R}{D} Gz^{1/3} \tag{46}$$

Since the upper and lower limits of the aqueous resistance are known, the upper and lower bounds on the integral of equation 45 are also known.

Rather than letting the aqueous resistance vary as a function of x, it will be considered as having a constant value throughout the intestine. Furthermore, it will be considered proportional to the Graetz number to the one-third power.

$$(P_{aq})^{-1} = A \frac{R}{D} Gz^{1/3} \tag{47}$$

The proportionality constant A remains to be determined. It is a dimensionless parameter. The above expression for the aqueous resistance replaces the variable expression in equation 45. The result after some algebraic rearrangement, is the modified boundary layer solution.

$$\frac{(1 - C_m/C_o)}{4\ Gz - A\ Gz^{1/3}\ (1 - C_m/C_o)} = P_m^* \qquad (48)$$

$$P_m^* = \frac{R}{D} P_m \qquad (49)$$

As with the aqueous permeability, multiplication of the membrane permeability by R/D scales it and makes it a dimensionless parameter. The values of A are determined empirically by comparing the modified boundary layer solution to the exact solution (see equation 11). An important finding is that A is a function of only the Graetz number, Gz, a known quantity. The empirical correlation between A and the Graetz number is shown in Fig. 7. Although it is possible to find a single equation to describe the functional dependence of A on Gz, it is perhaps easiest to consider three linear portions of the graph. The variable A as a function of Gz is therefore:

$$\begin{aligned} &0.004 \leq Gz < 0.01 \quad && A = 10.0\ Gz + 1.01 \\ &0.01 \leq Gz < 0.03 \quad && A = 4.5\ Gz + 1.065 \\ &0.03 \leq Gz \quad && A = 2.5\ Gz + 1.125 \end{aligned} \qquad (50)$$

By taking the aqueous resistance as some constant value in the axial direction, the membrane concentration, Cw, also becomes independent of x (see eq. 44 with Paq constant). Equation 42 can then be written as:

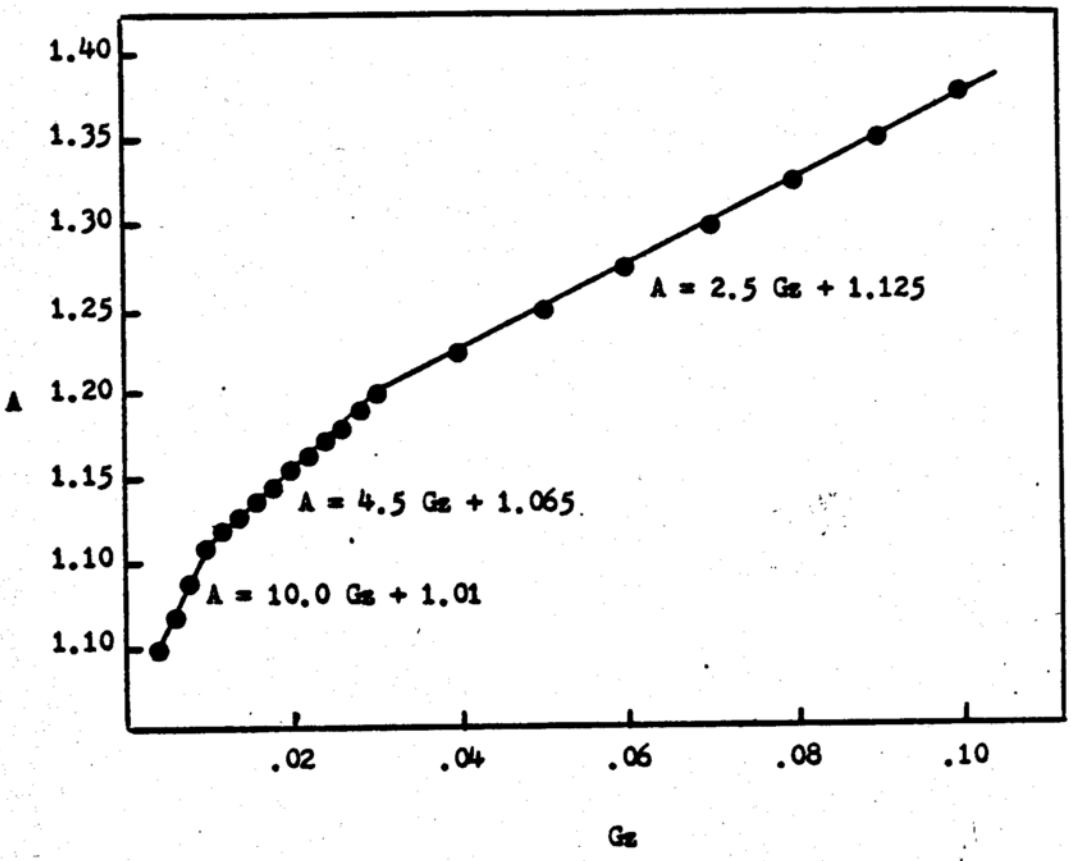

Figure 7
The coefficient A for the aqueous resistance of the film model. The coefficient is found by comparing the solutions of the film model and the convective-diffusive model. It was determined that A is a function of only the Graetz number.

$$Q(Co - Cm) = 2\pi RL \frac{P_m P_{aq}}{P_m + P_{aq}} Co \qquad (51)$$

After rearrangement equation 51 takes the form:

$$P_m^* = \frac{P_{eff}^*}{1 - \frac{P_{eff}^*}{P_{aq}^*}} \qquad (52)$$

where

$$P_{eff}^* = \frac{R}{D} P_{eff} = \frac{(1 - Cm/Co)}{4Gz} \qquad (53)$$

The expression in equation 52 is equivalent to equation 48. Therefore the aqueous resistance has been successfully factored out of the effective permeability to give the intrinsic membrane permeability. The solution of equation 52 will be compared to the exact solution in a subsequent section.

Michaelis-Menten--As stated, when the aqueous resistance is considered constant, the membrane surface concentration also becomes constant. Therefore the macroscopic mass balance can be written as:

$$Q (Co - Cm) = 2\pi R \cdot L \cdot J \qquad (54)$$

where J is the membrane flux. For the Michaelis Menten scheme J is:

$$J = \frac{J_{max}\, C_w}{Km + C_w} \tag{55}$$

In accordance with equations 3 and 4, equation 54 can be rewritten as

$$P_{eff} = \frac{J}{Co} \tag{56}$$

The membrane permeability is defined through the following equation:

$$J = P_w\, C_w \tag{57}$$

which for the Michaelis-Menten scheme is:

$$P_w = \frac{J_{max}}{Km + C_w} \tag{58}$$

The subscript w on the membrane permeability is used to denote the concentration dependence of the permeability. In fact it will be seen that how this permeability changes with concentration determines Jmax and Km.

At steady state the flux through the aqueous boundary layer is equal to the flux through the membrane

$$P_{aq}\,(\,Co - Cw\,) = P_w\, C_w \tag{59}$$

Solving for Cw:

$$C_w = \frac{P_{aq}}{P_{aq} + P_w} Co \tag{60}$$

Substituting this into equation 57, one can rewrite equation 56 as

$$P_w = \frac{P_{eff}}{1 - \frac{P_{eff}}{P_{aq}}} \tag{61}$$

However, Pw still has the membrane surface concentration in it, an unknown quantity (see equation 58). It can be derived though, through the quadratic equation obtained from the following relationship at steady state:

$$P_{aq}(Co - C_w) = \frac{J_{max} C_w}{Km + C_w} \tag{62}$$

$$\frac{C_w}{Co} = \frac{1 - Km/Co - J_{max}/(CoP_{aq}) + \sqrt{(1 - Km/Co - J_{max}/(CoP_{aq}))^2 + 4Km/Co}}{2} \tag{63}$$

It is possible therefore to experimentally measure the membrane permeability as a function of perfusate concentration, Co, and relate this to the intrinsic parameters, Jmax and Km using equations 61, 58 and 63. The effective permeability is what one actually measures. Also it is found, and shown in a subsequent section, that the aqueous permeability, Paq, is the same as that defined in equations 47 and

50.

Admittedly, the solution is more simple than the boundary layer solution but still not convenient to use. The form of the solution is simplified by looking at the limiting cases in the first and zero order region and then matching the solutions.

For the first order limiting case, the solution is that found in equation 52 where now the first order permeability constant is Jmax/Km.

$$\frac{J^*_{max}}{Km} = \frac{P^*_{eff}}{1 - \frac{P^*_{eff}}{P^*_{aq}}} \qquad (64)$$

Again, multiplication by R/D is indicated by the superscript '*'. The term on the left is therefore a dimensionless first order permeability constant.

In the zero order case, the flux across the membrane is equal to the maximal flux. Therefore equation 56 can be written as:

$$P^*_{eff} = \frac{J^*_{max}}{Co} \qquad (65)$$

This can be rewritten as

$$\frac{P^*_{eff}}{1 - \frac{P^*_{eff}}{P^*_{aq}}} = \frac{J^*_{max}}{Co\left(1 - \frac{P^*_{eff}}{P^*_{aq}}\right)} \qquad (66)$$

Putting equations 67 and 66 together gives the final result:

$$P_w^* = \frac{J_{max}^*}{Km + Co\left(1 - \frac{P_{eff}^*}{P_{aq}^*}\right)} \tag{67}$$

where

$$P_w^* = \frac{P_{eff}^*}{1 - \frac{P_{eff}^*}{P_{aq}^*}} \tag{68}$$

Although it cannot be derived mathematically it can be shown by numerical example that equation 67 is equilavent to equations 58 and 63. Not even one point could be found in the Gz, Km, Co, Jmax space where the expressions were not identical.

Michaelis-Menten Flux Passive Diffusion--In this case the flux across the membrane is written as

$$J = P_w C_w \tag{69}$$

$$P_w = \frac{J_{max}}{Km + C_w} + P_m C_w \tag{70}$$

Similar to the previous example, Pw is found to be related to the aqueous and effective membrane permeability by equation 61. Again, Pw is concentration dependent.

The membrane surface concentration is derived from the following relationship:

$$P_{aq}(Co - C_w) = \frac{J_{max}\, C_w}{Km + C_w} + P_m\, C_w \qquad (71)$$

$$C_w = \frac{D + \sqrt{D^2 + E}}{2} \qquad (72)$$

$$D = \frac{P_{aq}}{P_{aq} + P_m} Co\left(1 - \frac{Km}{Co} - \frac{J_{max}}{Co\, P_{aq}} - \frac{P_m}{P_{aq}} \frac{K_m}{Co} \right)$$

$$E = \frac{P_{aq}}{P_{aq} + P_m} Km$$

As in the previous example, the solution (equations 70 and 72) can be simplified by matching limiting case solutions. For the limiting first order case, a solution is obtained in the same manner as equation 52 where the first order permeability constant is the sum of the first order constant from the saturable system and first order passive constant.

$$\frac{J^*_{max}}{Km} + P^*_m = \frac{P^*_{eff}}{1 - \frac{P^*_{eff}}{P^*_{aq}}} \qquad (73)$$

The limiting case for zero order plus passive permeability is

represented by the following flux scheme:

$$J = J_{max} + P_m C_w \tag{74}$$

This limiting case itself has the two limiting cases; I) J = Jmax and II) J = Pm Cw matching those limiting cases gives the following solution for a zero order flux in parallel with a first order flux scheme:

$$\frac{P^*_{eff}}{\left(1 - \frac{P^*_{eff}}{P^*_{aq}}\right)} = \frac{J^*_{max}}{Co\left(1 - \frac{P^*_{eff}}{P^*_{aq}}\right)} + P^*_m \tag{75}$$

The final result when equations 75 and 73 are matched up is the most general expression for an uptake scheme which is composed of saturable and passive flux components in parallel.

$$P^*_w = \frac{J^*_{max}}{Km + Co\left(1 - \frac{P^*_{eff}}{P^*_{aq}}\right)} + P^*_m \tag{76}$$

When this solution was checked against the solution given by equations 70 and 72, it was found that again, the solutions were identical over the entire Gz, Km, Co, Jmax, and Pm space.

COMPARISON OF SOLUTIONS

The solution of equation 11 solved by the separation of variables technique is considered to be the exact solution for the laminar flow in a tube problem. The solution however, only applies to the linear first order case. The modified boundary layer solution is the solution to be used in practice for determination of the membrane permeability as a function of inlet concentration in order to obtain the intrinsic membrane parameters Jmax, Km and Pm. Only for the first order case can the modifled boundary layer solution be compared to the exact solution.

The modified boundary layer problem is really a film model. The question is: Does the same film thickness for the first order case apply to the more general case (i.e. do the same A values of equation 50 apply?). The answer seems to be yes. This answer is based on the fact that as the carrier system becomes saturated, the aqueous resistance becomes insignificant due to membrane controlled uptake. The correction for aqueous resistance is needed most in the first order region and somewhat less in the intermediate transition region where concentrations are on the order of Km. Also, in the first order case, it was found that the aqueous resistance (A in particular) was independent of the membrane permeability constant. This alone suggests that the A values determined for the first order case apply to a saturable mechanism since the zero order permeability

constant divided by any arbitrary concentration is really just another first order permeability constant. The fact is that the aqueous resistance is determined solely by the mean residence time and the mean diffusion time (i.e. the Graetz number, Gz). The reaction at the surface only sets up the concentration potential. Just as with the electrical resistor, which exists whether a current flows through it or not, so does the aqueous resistance exist.

In tables IA-IC a comparison of the three first order solutions is tabulated for given Gz and Cm/Co, the experimental quantities needed to calculate the membrane permeability. The permeability for the exact solution is given in the dimensionless form P_m^*. The other permeabilities given are for the boundary layer solution, Pmbl, and the modified boundary layer solution, Pmod.

The dimensionless permeability for all practical purposes is in the range of 0.1 to 10. Below 0.1 the membrane is considered impermeable since it becomes an analytical problem to distinguish between Cm and Co. If the membrane permeability gets much above 10, the aqueous resistance starts to dominate. For instance, the aqueous resistance at Gz = .1 is .64 and at Gz = .01 is .24, which is 6.4 and 2.4 times the membrane resistance when the membrane permeability is 10. If one should encounter high permeabilities, it is seen from the tables that the modified boundary layer solution works better at lower Gz numbers. Frankly, dimensionless permeabilities as high as 10 are seldom encountered (43, 74, 75).

Table I - Comparison of the Permeabilities Calculated from the Exact Solution, Pm, the Boundary Layer Solution, Pmbl, and the Modified Boundary Layer Solution, Pmod. Pm is given in the dimensionless form.

IA.
Gz = 0.01

Cm/Co	P*m	Pm/Pmbl	Pm/Pmod
0.995	0.1 0	0.840	0.842
0.990	0.25	0.984	0.984
0.982	0.50	0.965	0.964
0.974	0.75	0.959	0.957
0.968	1.00	1.00	1.00
0.945	2.00	1.00	0.986
0.918	4.00	1.03	0.991
0.900	0.60	1.05	0.974
0.888	8.00	1.06	0.946
0.881	10.0	1.12	0.965
0.857	25.0	1.50	1.03

Table I cont.

IB Gz = 0.04

Cm/Co	P*m	Pm/Pmbl	Pm/Pmod
0.984	0.10	0.958	0.954
0.963	0.25	1.00	0.990
0.933	0.50	1.00	0.978
0.907	0.75	1.01	0.975
0.886	1.00	1.03	0.981
0.823	2.00	1.07	0.970
0.760	4.00	1.23	1.00
0.724	6.00	1.33	0.978
0.704	8.00	1.47	0.984
0.691	10.0	1.63	1.01
0.656	25.0	2.84	1.20

IC Gz = 0.10

0.962	0.10	0.990	0.978
0.913	0.25	1.02	0.986
0.845	0.50	1.04	0.972
0.792	0.75	1.07	0.967
0.750	1.00	1.10	0.964
0.641	2.00	1.24	0.955
0.551	4.00	1.61	1.02
0.502	6.00	1.90	1.00
0.478	8.00	2.24	1.04
0.463	10.0	2.60	1.08
0.424	25.0	5.32	1.46

As seen from the tables, the modified boundary layer solution far outperforms the boundary layer solution. The boundary layer solution does fine however, as long as the ratio Cm/Co is high, say above 0.85. A plot of the ratio Pm/Pmbl versus the Graetz number times Pmbl was found to give good empirical correlations for determining the accuracy of the boundary layer solution (see figure 8). For example, if the boundary layer solution is to be within 5% of the exact solution, $0.95 < Pm/Pmbl < 1.05$, then the Graetz number times Pmbl must be in the range $.004 < GzPmbl < .06$. This correlation can be expressed in a different manner. In figure 9 it is shown that the ratio Cm/Co and the Graetz number can predict the accuracy of the boundary layer solution. It is seen that the boundary layer solution is within 5% of the exact solution if Cm/Co is greater than .9 at low Gz and greater than about .85 at higher Gz values.

To see whether the A values determined from the first order film model apply to the saturable case, the modified boundary layer solution for the Michaelis-Menten scheme (equations 67, 68) is compared to the corresponding boundary layer solution (equation 37). Examples of the comparison are given in tables IIA - IIC. It is seen that discrepancies arise when the ratio Cm/Co is low. This is probably due to the boundary layer solution and not the modified boundary layer solution, based on the correlations seen in figure 9. Therefore it is concluded that the A values used to determine the

aqueous resistance in equations 47 and 50 for the first order case are the same for the case of a saturable carrier. This is true at least in the region where the boundary layer solution holds and probably more likely in the region where the first order modified boundary layer solution holds.

The above results are extrapolated to the case of Michaelis-Menten plus passive diffusion. For very low perfusate concentrations (Co<<Km) the permeability of the membrane is a first order sum of the passive permeability and the first order Michaelis term, Pw = Jmax/Km + Pm. Therefore the aqueous resistance term certainly applies here. Furthermore as Co becomes much greater than Km, the membrane permeability limits to the first order passive term (see equation 76). The aqueous resistance term applies here as well. The aqueous resistance term was also shown to hold as the saturable mechanism went through the transition region to the zero order region. Therefore it is concluded that the aqueous resistance determined by the Gz number and the A values in equations 47 and 50 apply over the entire region for a mechanism of saturable uptake and passive diffusion in parallel.

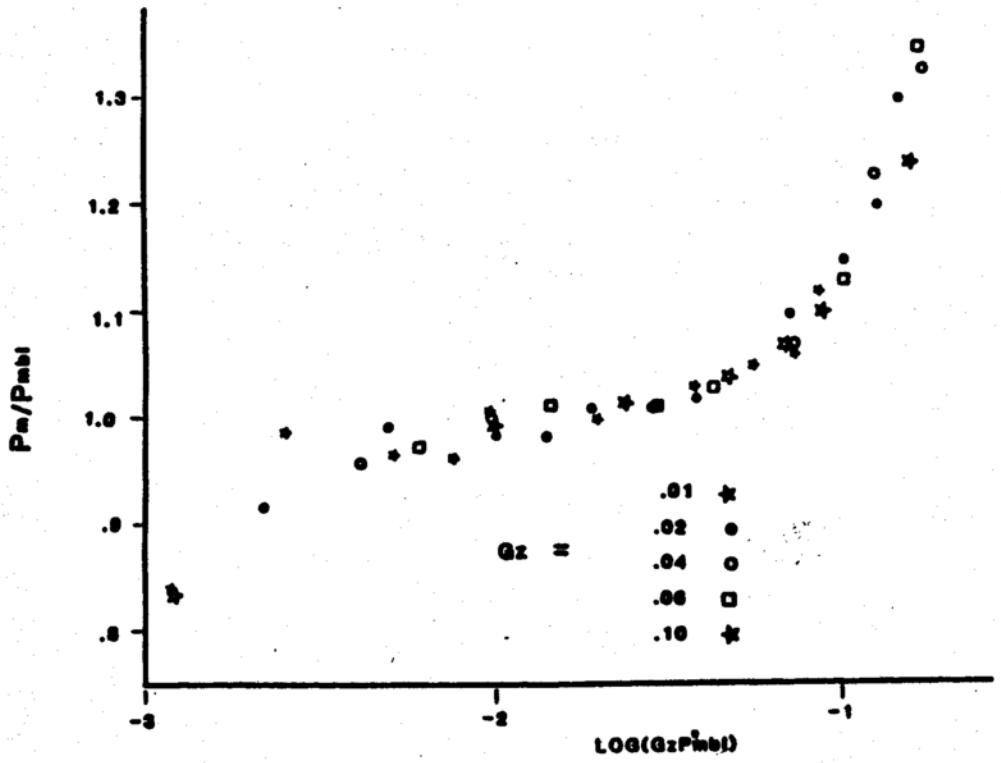

Figure 8
The first order permeability constant of the boundary layer solution, Pmbl, is compared to the permeability constant of the exact solution in equation 11, Pm. The emperical correlation between the ratio Pm/Pmbl and the Graetz number times the permeability constant of the boundary layer solution is shown in the figure.

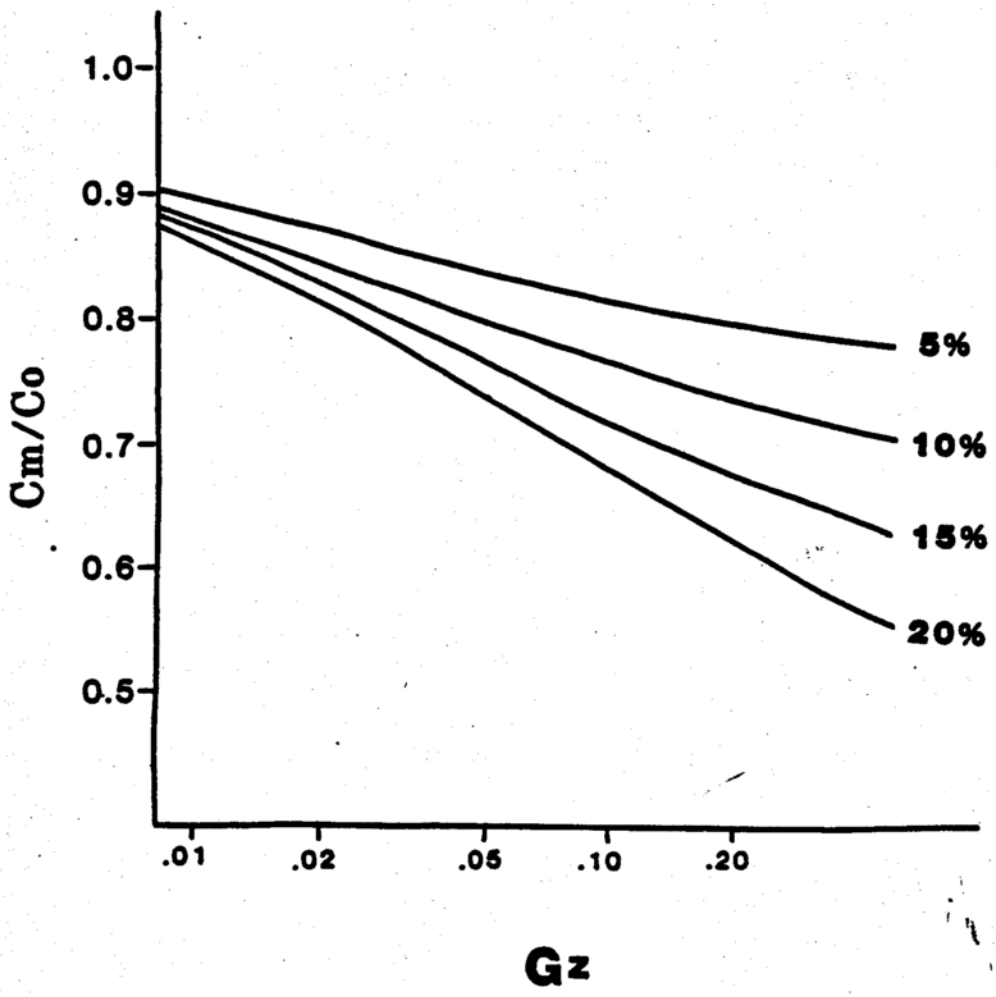

Figure 9
The first order permeability constant is determine by the Graetz number, Gz, and the ratio of the outlet to inlet concentrations. The permeability constant was calculated from the exact solution of equation 11 and the boundary layer solution. The accuracy of the boundary layer solution is represented in the graph. For instance, for Gz numbers and Cm/Co values in the region above the line marked 5%, the boundary layer solution is within 5% of the exact solution.

Table II - Comparison of the Boundary layer and Modified Boundary Layer Solutions. For a J^*max/Km and Gz, the ratio Km/Co is varied.

IIA.
$J^*max/Km = 7$
$Gz = .01$

Km/Co	P^*mbl	P^*mod	P^*mod/P^*mbl	Cm/Co
.1	.626	.626	1	.975
.2	1.1	1.1	1	.956
.3	1.44	1.44	1	.942
.4	1.68	1.68	1	.933
.5	1.85	1.85	1	.926
.6	1.98	1.97	.996	.921
.7	2.07	2.06	.994	.917
.8	2.15	2.13	.992	.914
.9	2.21	2.18	.99	.912
1	2.26	2.23	.988	.91
2	2.48	2.43	.978	.901
3	2.56	2.49	.974	.898
4	2.60	2.52	.972	.896
5	2.62	2.54	.97	.895
6	2.64	2.56	.969	.895
7	2.65	2.56	.969	.894
8	2.66	2.57	.968	.894
9	2.66	2.58	.968	.893
10	2.67	2.58	.967	.893

Table II cont.

IIB
J*max/Km = 4
Gz = .05

Km/Co	P*mbl	P*mod	P*mod/P*mbl	Cm/Co
.1	.358	.357	.997	.929
.2	.63	.625	.992	.875
.3	.825	.811	.983	.838
.4	.964	.939	.974	.812
.5	1.06	1.03	.965	.795
.6	1.14	1.09	.958	.782
.7	1.19	1.14	.951	.773
.8	1.24	1.17	.946	.766
.9	1.27	1.20	.941	.761
1	1.30	1.22	.937	.756
2	1.43	1.32	.918	.737
3	1.48	1.35	.91	.731
4	1.50	1.36	.907	.727
5	1.52	1.37	.904	.726
6	1.53	1.38	.903	.724
7	1.53	1.38	.902	.724
8	1.54	1.38	.901	.723
9	1.54	1.39	.90	.722
10	1.54	1.39	.90	.722

Table II cont.

IIC
J*max/Km = 1
Gz = 0.1

Km/Co	P*mbl	P*mod	P*mod/P*mbl	Cm/Co
.1	.09	.09	1	.964
.2	.164	.163	.994	.935
.3	.224	.222	.991	.911
.4	.273	.27	.989	.892
.5	.313	.308	.984	.877
.6	.347	.34	.98	.864
.7	.375	.366	.976	.854
.8	.399	.388	.972	.845
.9	.419	.406	.969	.837
1	.437	.422	.966	.831
2	.534	.506	.948	.798
3	.574	.539	.939	.785
4	.596	.556	.933	.778
5	.609	.566	.929	.773
6	.618	.573	.927	.771
7	.625	.579	.926	.769
8	.63	.582	.924	.767
9	.634	.586	.924	.766
10	.637	.588	.923	.765

RESULTS OF ANALYSIS

In the analysis an aqueous resistance was found which is independent of the membrane parameters. The dimensionless aqueous resistance is found to be a function of only the Gz number, which is interpreted as the convective mean residence time divided by the mean radial diffusion time.

$$(P^*_{aq})^{-1} = A \cdot Gz^{1/3} \tag{77}$$

$$\begin{aligned} 0.004 \leq Gz \leq 0.01 \quad & A = 10.0\ Gz + 1.01 \\ 0.01 \leq Gz \leq 0.03 \quad & A = 4.5\ Gz + 1.065 \\ 0.03 \leq Gz \quad & A = 2.5\ Gz + 1.125 \end{aligned} \tag{78}$$

$$Gz = \frac{\pi DL}{2Q} \tag{79}$$

Once the aqueous resistance was obtained, it was possible to factor the aqueous resistance out of the experimentally determined effective permeability to give the intrinsic membrane permeability.

$$P^*_w = \frac{P^*_{eff}}{1 - \frac{P^*_{eff}}{P^*_{aq}}} \tag{80}$$

$$P^*_{eff} = \frac{1 - Cm/Co}{4\ Gz} \qquad (81)$$

Furthermore, it was shown how the intrinsic permeability can be related to the intrinsic membrane parameters. For the most general case of saturable uptake plus passive diffusion in parallel, the membrane permeability is given as:

$$P^*_w = \frac{J^*_{max}}{Km + Co\left(1 - \frac{P^*_{eff}}{P^*_{aq}}\right)} + P^*_m \qquad (82)$$

where the superscript '*' indicates multiplication by R/D, the intestinal radius divided by the aqueous diffusion coefficient. The maximal uptake rate for the saturable mechanism is Jmax, the Michaelis constant is Km, and Pm is the passive first order permeability constant. The above solution applies whether there is only passive diffusion or only the saturable mechanism in operation (i.e. either Jmax or Pm equals zero).

The solution can be used as follows: The flow rate, Q, and the

length of intestine, L, are chosen to give Gz numbers on the order of 0.01 to 0.1. As a guide, the chosen Gz should give values of the ratio of outlet to inlet concentrations, Cm/Co, of around 0.85-0.90. This usually means intestinal lengths of about 10 centimeters and flow rates on the order of a half a milliliter per minute. Once Gz is chosen, one can calculate the aqueous resistance from equation 77. The perfusion experiment is performed and the effective permeability is calculated from measurement of the ratio Cm/Co and Gz as in equation 81. This leads to the calculation of the intrinsic membrane permeability (equation 80). The next step is to find the intrinsic membrane permeability as a function of the inlet concentration Co. A non-linear regression of P_w^* on Co(1 - Peff/Paq) will yield the intrinsic membrane parameters (see equation 82).

A typical graph of P_w^* versus Co (1 - Peff/Paq) is shown in figure 10. If there is no passive permeability, the membrane permeability will fall down to the x-axis at high concentrations. Also, if there is no saturable mechanism, the membrane permeability is independent of Co and will be represented by a straight line parallel to the x-axis.

A point to be made here is that since the flow rate is a variable, investigators may be inclined to keep this constant throughout the entire concentration range. However, since the membrane permeability changes with concentrations, so does the ratio of aqueous to membrane resistances. If the flow rate is not adjusted

accordingly, one can get into aqueous controlled uptake at the higher membrane permeabilities.

If no passive permeability is present, the intrinsic membrane permeability reduces to:

$$P_w^* = \frac{J_{max}^*}{Km + Co\left(1 - \frac{P_{eff}^*}{P_{aq}^*}\right)} \qquad (83)$$

This has the form of a rectangular hyperbola when P_w is considered a function of Co (1 - Peff/Paq). As discussed in the background section, the double reciprocal plot is in error if the inlet concentration is not corrected for the unknown "unstirred layer". This problem has now been overcome. A double reciprocal plot of equation 83 will give a slope of 1/Jmax and an intercept of Km/Jmax when the reciprocal of the membrane permeability is plotted against the reciprocal of Co(1 - Peff/Paq).

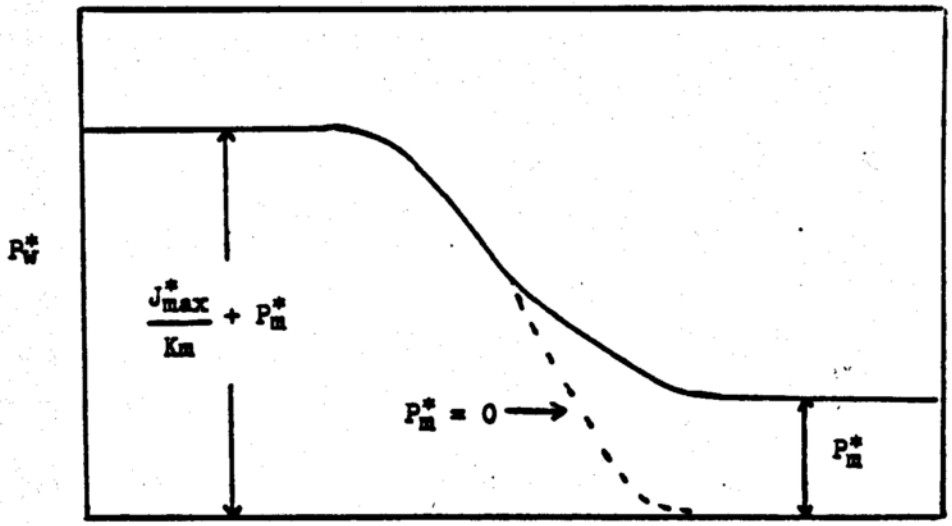

Figure 10
The dimensionless membrane permeability is plotted against Co(1-P*eff/P*aq). The membrane permeability is constant at low concentrations. The membrane permeability in this region is the sum of two first order constants. As the concentration increases, the carrier system begins to become saturated and the permeability starts to decrease. At high inlet concentrations, the carrier system is fully saturated and its contribution to membrane uptake is negligible compared to the first order passive uptake. In this region the permeability is again constant. If there is no passive uptake, the membrane permeability goes to zero at high concentrations.

EXPERIMENTAL

Materials. The amino acid L-leucine (Sigma Chemical Co., St. Louis, MO.) its radiochemical ^{3}H-labeled analog (New England Nuclear, Boston, MA), polyethylene glycol 3350 (Sigma Chemical CO.) with its ^{14}C-isotope (New England Nuclear Corp.) and all the buffer components (analytical grade) were used as received.

Freshly distilled water was deionized over a mix-bed ion-exchanger (Milli-Q reagent water system, Millipore Corp., El Paso, TX).

The perfusion solution consisted of a Sorensen phosphate buffer of pH = 7, 0.01% (w/v) polyethylene glycol 3350 with a tracer amount of its ^{14}C-isotope, and leucine in concentrations ranging from 0.01 to 100 mM with a tracer amount of its ^{3}H-isotope. A certain amount of NaCl is added to adjust the final solution to 300 mOsm Kg^{-1} H_2O. The osmolarity was measured with an automatic osmometer (Precision Systems Inc., Sudbury, MA).

Method. All experiments were performed on male Charles River rats, 300-350 g, who were maintained in fully accredited animal care facilities. The rats were fasted 12-18 hr before each experiment. Anesthesia was induced by injection of urethane (1.5 mg Kg^{-1} i.m.).

The rats were kept on a slide warmer (GCA Corp., Chicago, IL) and under a heating lamp to maintain their body temperature at

37°C. The abdominal cavity was opened by a mid-line incision of 3-4 cm. The jejunum was located and cannulated at 2-4 cm below the ligament of Treitz and 6-12 cm aboral to the first incision. The cannulae were secured with surgical silk suture (4-0 Chromic Gut, Ethicon Inc., Somerville, NJ).

All tubing and cannulae were made of polytetrafluoroethylene (Teflon^{R}). Care was taken to maintain the inlet and outlet cannulae at the same height to avoid gravitational flow.

After cannulation the intestinal segment was placed within the abdominal cavity, carefully avoiding crimping or kinking of the segment. The abdominal incision then was covered with plastic wrap (Saran wrap).

The jejunal segments were perfused with amino acid solution using an infusion pump (Harvard apparatus, Model 931, S. Natick, MA) for about 20 min until the effluent was clear. The intestine then was perfused for an additional 60 to 90 min and samples were collected every 15 min. Steady-state was usually achieved in 30 min. In the experiments the rate of perfusion varied from 0.074 ml/min to 0.764 ml/min. The tubing between the syringe and the inlet cannulae was placed in a water bath of 37°C (Tek-Pro, American Dade, Miami, FL).

The pH of the outlet solutions were measured and varied by less than 0.02 units from the pH of the inlet solution.

After the perfusion, blood samples were taken from the vena

porta to assure [^{14}C]-polyethylene glycol was not absorbed, whereas the radioactive amino acid was absorbed. None of the plasma samples had counts of ^{14}C above background. The tritium labeled amino acid counts were significantly higher than background and on the order of 2.5% of the perfusate counts.

The length of the intestine was measured by wetting it with a 0.9% w/v solution of NaCl and carefully laying it flat without stretching.

The kinetic parameters were calculated from the data using a nonlinear least squares analysis program for microcomputers (115). The calculations were performed on a Hewlett-Packatd 87 XM microcomputer.

Assay Method

The samples were analyzed by liquid scintillation counting. Samples of 0.5 ml were counted in 10 ml of scintillation fluid (Ready-solv Hp/b, Beckman Instruments Inc., Fullerton, CA). The samples were counted on a scintillation counter (Beckman LS9000) with automatic quench correction. All samples had Horrock numbers, a measuring of quenching, varying from 37 to 42. The tritium labeled amino acid and the [^{14}C]-polyethylene glycol 3350 were counted simultaneously using a double channel technique. The ratio of the isotopes between the two channels were measured using standards, which had the same Horrock numbers as the samples, so that the counts of the samples did not need to be calculated back to disintegrations

per minute.

From the known ratios of the isotopes between the two channels and the measured background, the total amount of tritium labeled amino acid and [^{14}C]-polyethylene glycol 3350 in the samples could be calculated (116). By assuming that polyethylene glycol 3350 would not be absorbed in the small intestine, the percentage of water absorbed in the jejunum during the perfusion experiment was calculated from:

$$\frac{A_i - A_f}{A_f} \times 100 = \% \text{ water absorbed}$$

where Ai and Af were the initial and the final counts per minute of ^{14}C, respectively. The volume change was never found to exceed more than 0.4%/length of intestine except for the variable flow experiments where volume change was as high as 0.8%/length in some instances of low flow rate. The outlet concentration was corrected for the volume change by means of the ratio Ai/Af.

EXPERIMENTAL RESULTS

The permeability of the amino acid leucine was studied in the concentration range of 0.01-100 mM, a range covering 4 orders of magnitude. The results are given in table III. In a second set of experiments, the inlet concentration was held constant at 0.1 mM while the flow rate and intestinal length was varied. This was done to see how the effective permeability was affected by the aqueous resistance. These results are given in table IV.

Finally, the experimental results for the perfusion of progesterone reported by Ho, Higuchi and co-workers (74) are presented in table V. In these experiments the investigators measured the effective membrane permeabilities at various flow rates and intestinal lengths. The aqueous resistances and intrinsic membrane permeabilities seen in table V were calculated from the data using equations 77 and 80. They reported an aqueous diffusion coefficient for progesterone of 8×10^{-6} cm^2/sec.

It is seen in table V that some of the membrane permeabilities for progesterone are negative. The intention of their study was to investigate the aqueous resistance. They chose progesterone as their model compound because of its high membrane permeability. Therefore, it was believed that the total resistance to uptake would be due to the aqueous resistance. The negative values can be understood by examining the following relationship which states that the total resistance is the sum of the aqueous and membrane resistance.

$$\frac{1}{P_{eff}} = \frac{1}{P_{aq}} + \frac{1}{P_w} \qquad (84)$$

If the aqueous resistance dominates, the difference between the total resistance and the aqueous resistance can be very small. In fact, in this case it is possible that the calculated aqueous resistance may actually be larger than the measured total membrane resistance due to experimental error.

Another very important point is in the actual perfusion technique used to generate the progesterone data. The intestinal lengths used by the investigators tended to be very long (up to 33 centimeters in most cases). These long lengths were shaped in multi-S patterns with up to five bends. This will probably cause a little more mixing than if the intestinal length was kept straight. Therefore the aqueous resistance calculated from equation 77, which assumes a straight tube may be a little higher than actual (hence the negative intrinsic permeabilities). Even so, the deviations are small and the aqueous reistance calculated is very close to the measured total resistance under these aqueous controlled conditions.

Table III - Permeability of L-leucine as a function of concentration

Conc. (mM)	P^*_{eff}	Co(1-Peff/Paq) (mM)	P^*_w
.01	2.57 (.084)¶	.0043 (.0002)¶	6.35 (.40)¶
0.1	2.67 (.036)	.040 (.001)	6.94 (.22)
1	2.60 (.082)	.343 (.018)	8.37 (.53)
4	1.87 (.043)	2.18 (.10)	3.54 (.23)
10	1.80 (.067)	5.36 (.21)	3.56 (.23)
30	0.87 (.072)	22.49 (.568)	1.22 (.13)
100	0.21 (.050)	94.47 (1.43)	0.26 (.054)

¶ Standard error of the mean (n = 4)

Table IV - Permeability of L-leucine as a Function of Perfusional Flow Rate. The Gz number is a function of the various flow rates and intestinal lengths used (D=0.94 x 105 cm2/sec). The theoretical aqueous resistance, $P^*_{aq}{}^{-1}$, is calculated from the Gz number. The effective total resistance, $P^*_{eff}{}^{-1}$, is measured experimentally.

Gz	$P^*_{aq}{}^{-1}$	$P^*_{eff}{}^{-1}$
.0066	.202	.370
.0074	.211	.354
.0086	.227	.373
.0100	.240	.404
.0168	.292	.381
.0263	.352	.425
.0311	.378	.424
.0335	.390	.482
.0421	.426	.664
.0460	.442	.488
.0470	.446	.791
.0512	.463	.647
.0909	.606	.808
.0957	.622	.639
.133	.710	.756
.148	.789	.877

Table V - Permeability of Progesterone as a function of Perfusional Flow Rate. (Data taken from reference 74). The aqueous resistance, $P^*_{aq}{}^{-1}$, is calculated from the theory using experiment flow rates and intestinal lengths. The total resistance, $P^*_{eff}{}^{-1}$, was measured experimentally.

$P^*_{aq}{}^{-1}$	$P^*_{eff}{}^{-1}$
.194	.130
.254	.203
.281	.279
.311	.269
.375	.327
.375	.324
.375	.406
.464	.403
.464	.393
.503	.576
.644	.669

Discussion

The progesterone data of Ho, Higuchi and co-workers are shown in figure 11. Progesterone is a very lipophilic compound with a log n-octanol/water partition coeficient of 3.99 (74). The resistance to intestinal uptake is believed to be entirely due to the aqueous resistance. Therefore, a plot of the total resistance versus the aqueous resistance should result in a line of slope one passing through the origin. In figure 11, the aqueous resistance is that predicted by equations 77-79 of the theory. The total resistance on the y-axis is the experimentally determined total resistance. The predicted and experimental values are in close agreement, although it appears that the predicted aqueous resistance may be a little on the high side. As stated earlier, this is probably because of the experimental technique of these workers. They took long lengths of intestine and arranged them in a multi S-shaped pattern with up to 5 bends. It is probable that this arrangement leads to greater mixing during perfusion and therefore the actual aqueous resistance may be slightly lower than that predicted by equations 77-79, which assumes laminar flow in a straight tube. However, in almost all cases, the predicted aqueous reistance is still within 15% of that found experimentally.

From the progesterone data, the investigators found an empirical relationship between the aqueous resistance and the flow rate. They

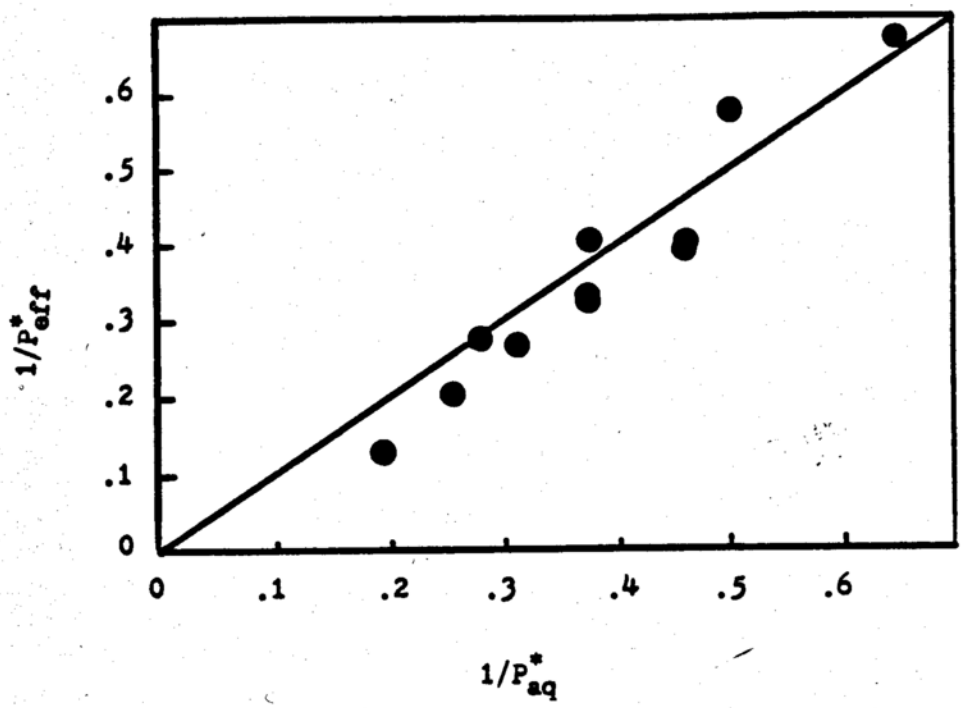

Figure 11
The permeability of progesterone was determined as a function of flow rate. Since progesterone is a highly permeable compound, the total resistance to uptake is assumed to be the aqueous resistance. This is represented by the solid line of slope one passing through the origin. The total resistance on the y-axis was experimentally measured and the aqueous resistance on the x-axis was calculated from the theory. (Data taken from reference 74)

found the resistance to be proportional to flow rate to the negative 0.44 power. Using equations 77-79, the aqueous resistance was calculated for $0.01 \leq Gz \leq 0.10$. This is the range of the Gz number used in the progesterone experiments. The negative logarithm of the aqueous resistance predicted from the equations is plotted against the negative logarithm of Gz. The plot is shown in figure 12. Linear regression of the points gives a slope equal to 0.426 ± 0.001 S.E. and an intercept of -0.51 ± 0.002 S.E. The correlation coefficient of the points is 0.9987. The slope found from the log-log plot of the theoretical calculations is almost equivalent to the value 0.44 found experimentally. Therefore, an alternate expression to equations 77-79 for the aqueous resistance is given below.

$$(P^*_{aq})^{-1} = 1.67\ Gz^{0.426} \qquad 0.01 \leq Gz \leq 0.1 \qquad (85)$$

The absorption of the amino acid leucine was studied at a constant concentration of 0.1 millimolar and at various flow rates. This compound is taken up by a saturable carrier mediated system. In contrast to progesterone, this compound has a membrane resistance large enough to contribute to the total resistance. A plot of the total resistance versus the aqueous resistance should yield a straight line with a slope of one and an intercept equal to the

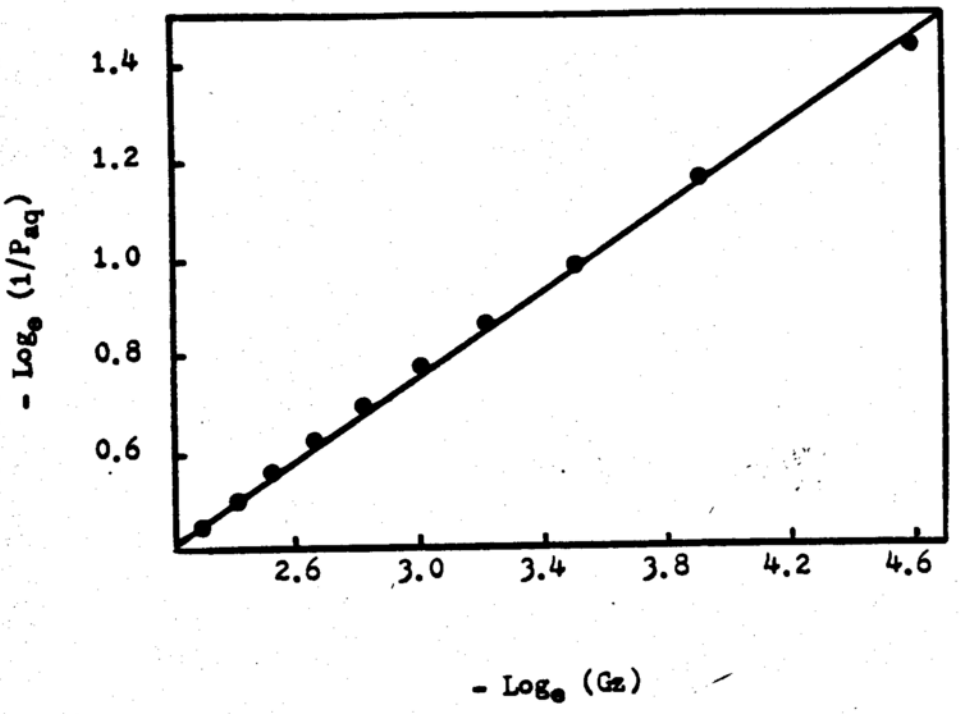

Figure 12
A Log-Log plot of the theoretical aqueous resistance versus the Graetz number. The slope obtained by linear regression is 0.426 which compares to the value of 0.44 found experimentally by Ho, and co-workers for the dependence of progesterone uptake on perfusional flow rate.

membrane resistance (see equation 84). Figure 13 shows the experimentally determined total resistance plotted against the aqueous resistance, which was varied by adjusting the flow rate. The solid line is a line with a slope of one and is the best fit as determined by least squares. Again, the agreement between theory and experimental is very close.

The intercept value obtained in figure 13 is 0.12 ± 0.02. It will be seen subsequently that at a concentration of 0.1 millimolar, leucine uptake is in the first order region of the Michaelis-Menten scheme and that leucine has no passive component to its uptake. Therefore the intercept value corresponds to Km/J*max. Leucine uptake studied at various concentrations ranging over four orders of magnitude will be discussed shortly. At present it is noted that the value obtained for Km/J*max from these experiments, 0.16 ± 0.01, is not significantly different than the value determined from the flow experiments.

It is concluded that the aqueous resistance derived theoretically agrees quite well with that found experimentally for the compounds progesterone and leucine. The aqueous resistance calculated for the progesterone data may be a little high due to a slight difference in the perfusion technique. However, the aqueous resistance in this case still appears to be within 15% of that found experimentally. The point to be made is that the derived expression is an estimate of the aqueous resistance. With that estimate,

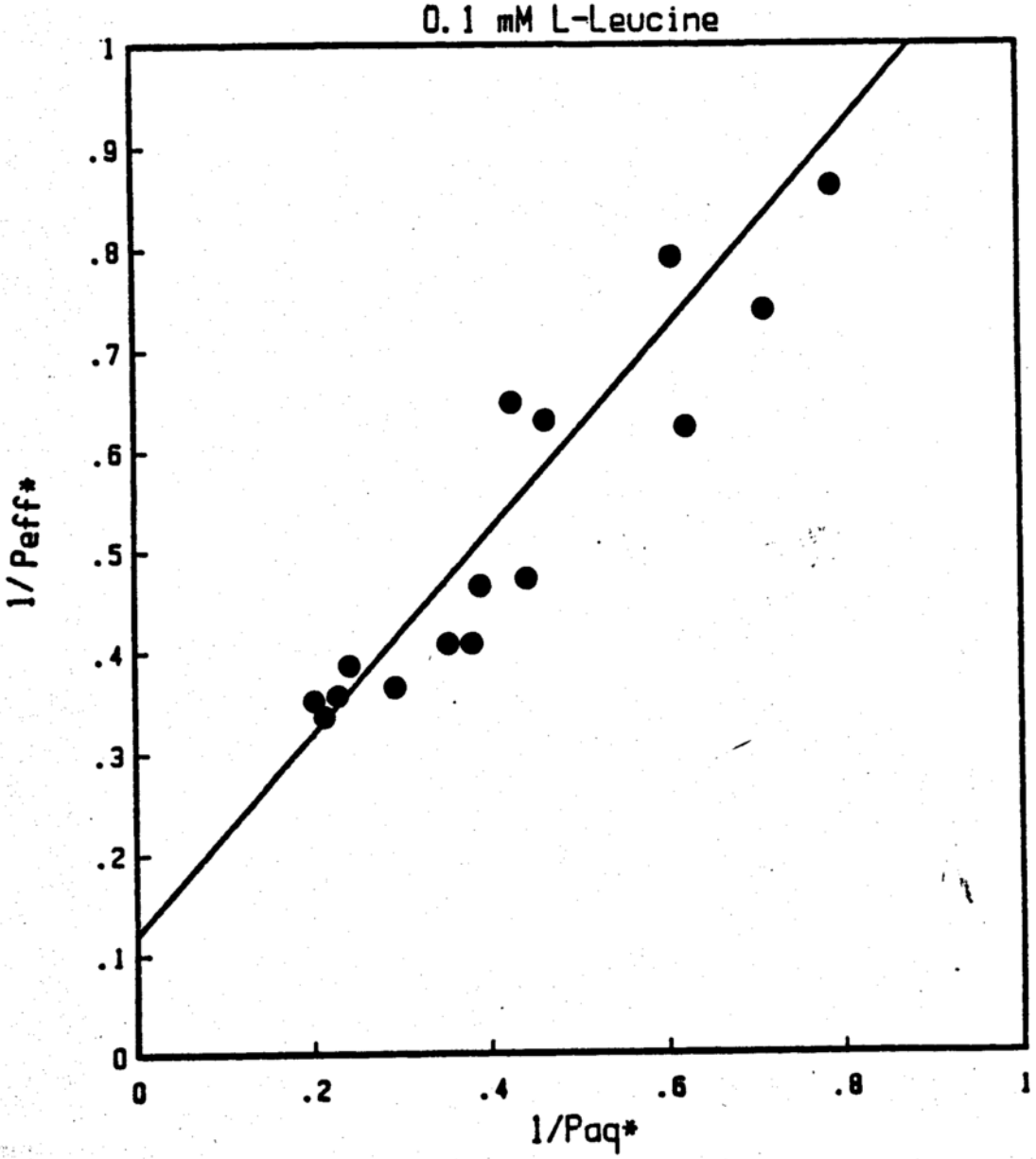

Figure 13
The effective permeability of l-leucine was measure at various flow rates. The theoretical aqueous resistance is calculated from the flow rate. A plot of the total resistance versus the aqueous resistance should result in a line of slope one with the membrane resistance as the intercept. The solid line is the best fit line of slope one.

one can perform experiments such that the aqueous resistance is not allowed to dominate the overall resistance to uptake.

One can get an idea of when the aqueous begins to dominate by looking at the ratio of the inlet to outlet concentration, Cm/Co. The sum of the aqueous and membrane resistance is expressed below.

$$\frac{1}{P^*_{eff}} = \frac{1}{P^*_{aq}} + \frac{1}{P^*_{w}} \qquad (86)$$

The membrane resistance can now be considered some multiple of the aqueous resistance, $1/P^*_w = F/P^*_{aq}$.

$$\frac{1}{P^*_{eff}} = \frac{(F+1)}{P^*_{aq}} \qquad (87)$$

F can be considered the ratio of the membrane resistance over aqueous resistance. Putting in the expression for P^*_{eff}, one can solve for Cm/Co (see equation 81).

$$Cm/Co = 1 - \frac{4\ Gz}{(F+1)} P^*_{aq} \qquad (88)$$

Since P_{aq}^{*} is a function of only Gz, Cm/Co is also a function of only Gz. The values of Gz and Cm/Co are tabulated for various F values in table VI. When F=0, the total resistance is completely dominated by the aqueous resistance. This results in low Cm/Co values for nearly all Gz values. As membrane resistance is added to the aqueous resistance, (F>0), the Cm/Co values increase. For F=1, the membrane and aqueous resistance are equal. When the membrane resistance becomes ten times the aqueous resistance (F=10), the Cm/Co values become so high that it starts becoming difficult to detect the difference between Cm and Co analytically. Therefore, it is seen that some aqueous resistance must be allowed to exist and that the membrane resistance cannot dominate unless the ratio Cm/Co goes to one. It is concluded that the flow rate should be adjusted such that the Cm/Co values are at least 0.85-0.90. This gives a good membrane to aqueous resistance ratio, which guarantees no aqueous resistance domination and at the same time allows enough mass to be loss to prevent analytical problems.

The permeability of leucine as a function of inlet concentration is shown in figure 14. The graph shows 2 plots. One is the effect permeability versus the inlet concentration (dashed line). The other is the intrinsic membrane permeability obtained by

Table VI - Ratio of Outlet to Inlet Concentrations for the Perfusion Experiment as a Funtion of Total Resistance Which is due to Membrane. F is Ratio of Membrane to Aqueous Resistance.

Gz	Cm/Co			
	F=0	F=1	F=2	F=10
.01	.833	.916	.944	.985
.02	.745	.872	.915	.977
.03	.678	.839	.893	.971
.04	.618	.809	.873	.965
.05	.566	.783	.855	.961
.06	.519	.760	.840	.956
.07	.477	.739	.826	.952
.08	.440	.720	.813	.949
.09	.405	.702	.802	.946
.10	.373	.687	.971	.943

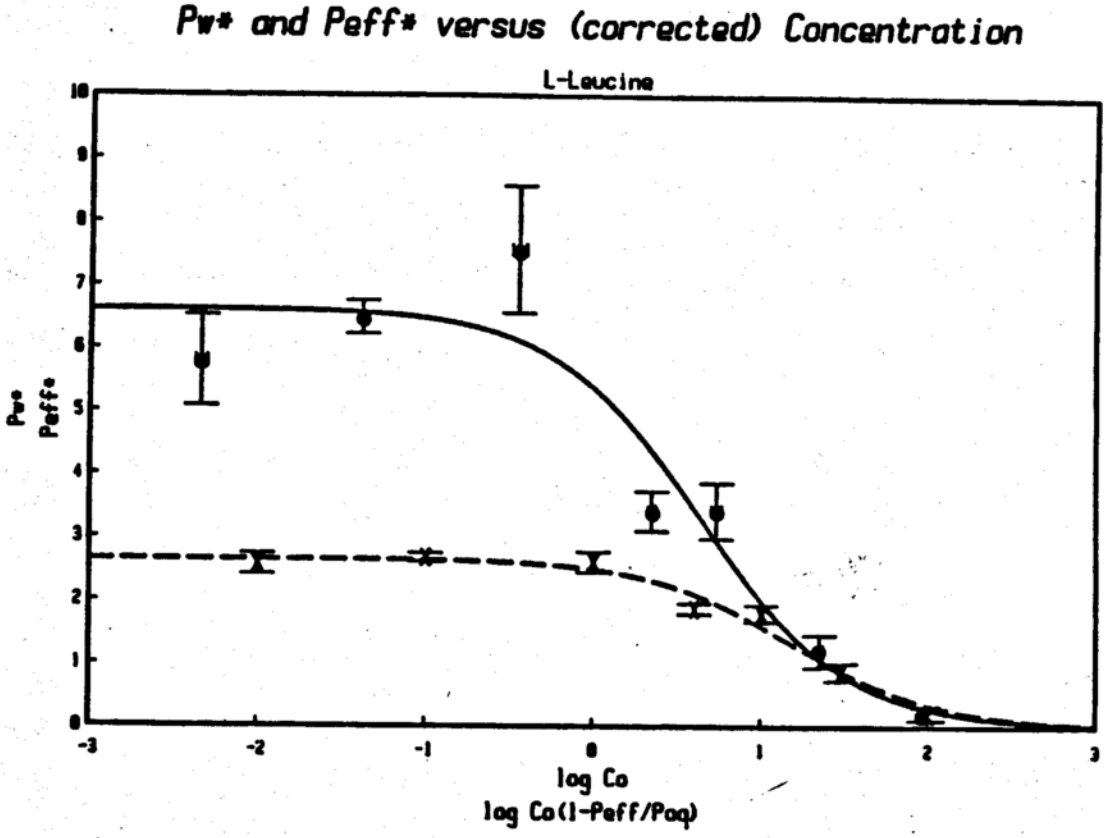

Figure 14
The membrane permeability of l-leucine was measured over four orders of magnitude of concentration. The permeability decreases at high concentrations due to saturation of the carrier mechanism. There appears to be no passive absorption of this compound. The dashed curve shows the effective permeability, P*eff, as a function of concentration. The solid curve is the aqueous corrected permeability, P*w. The Michaelis constant is shifted to a higher value for the dashed curved due to the aqueous resistance.

factoring the aqueous resistance out of the effective permeability. As shown in the analysis (see equation 82), this is plotted against Co(1-Peff/Paq), (solid line).

The membrane permeability drops to zero at high concentrations due to the saturation of the carrier system. Although the flux across the membrane is at its maximum value, the permeability goes to zero at high concentrations since the permeability is the flux divided by concentration. If a passive diffusion mechanism were present, the permeability would be constant at high concentrations (see figure 10).

In these experiments, the flow rate was adjusted at each concentration studied such that as the membrane resistance decreased (at lower concentrations) the aqueous resistance was also decreased to prevent it from dominating. This point is important since one may tend to think of the flow rate as a variable that should be kept constant. One should use the ratio Cm/Co as a guide for adjusting flow rates as discussed previously. Also, it is important to calculate the aqueous, membrane and total resistances. The higher the aqueous to total resistance ratio, the more in error is the membrane resistance calculation, which in fact may even result in a negative value as seen earlier.

From the graph in figure 14 it is obvious that factoring the aqueous resistance out of the total resistance allows easier detection of a saturable mechanism than just using the effective

permeability. The aqueous resistance is independent of inlet concentration. The greater the fraction of the total resistance which is made up of aqueous resistance, the weaker is the functional dependence of the effective permeability on inlet concentrations. Therefore, Peff is less responsive than is Pw to concentration changes in the Km region.

The curves of figure 14 are the best fit curves based on least squares regression analysis. The solid curve is obtained by regression of equation 83. Regression of equation 82 resulted in a passive permeability constant, Pm, not significantly different than zero. The dashed curve is obtained by regression of the following equation:

$$P^{*}_{eff} = \frac{J'_{max}}{K'_{m} + Co}$$

where the prime indicates no correction for the bias due to aqueous resistance.

Regression of equation 83 gave the intrinsic parameters J*max and Km as 24.64 ± 9.41 S.E. (mM) and 4.05 ± 1.51 S.E. (mM) respectively, ($Km/J^{*}max$ = 0.16 +0.01). The aqueous biased parameters obtained by regression are J'max = 39.78 ± 6.82 (mM) and K'm = 15.03 ± 2.84 (mM). The aqueous biased Michaelis constant is

shifted to a much higher value. Even though the Jmax values may not be significantly different, the intrinsic Jmax is lower than the aqueous biased one. These findings are consistant with those of Wilson and Dietschy (1). They studied the uptake into intestinal rings at various shaking rates and found that the experimentally determined maximal flux at high concentrations was consistently lower than the maximal flux found by a double reciprocal plot. They also found higher Km values at low stirring rates. This is a result of the aqueous bias, which tends to always give higher apparent Km and apparent Jmax values.

The intrinsic Km value of 4.05 can be compared to the literature value obtained by everted rings of 1.6 mM (4). Although there is probably no significant difference in the in vivo and in vitro values (no standard error is given in the reference for the in vitro study), it appears that the in vivo Km may be higher. It should be pointed out that the in vivo perfusion study was done over four orders of magnitude of concentration. This was necessary to get into the limiting regions of the membrane permeability. Only a couple of concentrations were close to the Km value. If one wished a better estimate of Km, it would be necessary to study the membrane permeability at more concentrations in the Km region.

In the experiments the flow rate was adjusted to prevent the aqueous resistance from dominating. However, as discussed earlier, a significant aqueous resistance must be allowed to exist because one

wants enough mass loss to distinguish outlet from inlet concentrations. Therefore, the aqueous biased Km is quite high. This is why the apparent Km values tend to be higher with in vivo systems. For example, the apparent Km for the uptake of caratine in rat jejunum is 1.035 mM whereas in everted rings it was found to be only 0.2 mM (29).

If the flow rate is not adjusted or if no knowledge of the aqueous resistance is available, it is possible to bias the Km so much that the Km shift may be out of the concentration range of study or beyond the solubility limit of the compound. This may explain the failure to show saturation of threonine absorption in human perfusion studies while saturation has been demonstrated in everted sac experiments (4).

The aqueous resistance can mask a saturable system even more when a passive mechanism is also present. This is especially true if the passive permeability is fairly significant. Figure 15 shows the data obtained by Ming Hu (75) for the permeability of L-Proline as a function of concentration. The effective permeability does not change very much over the entire concentration range. Different conclusions may be drawn about whether a carrier mediated system is involved depending upon whether the effective permeability or the intrinsic permeability is looked at. As with the leucine experiments, the flow rate was adjusted at each cocentration studied

to prevent aqueous resistance from dominating. Due to the passive component, it would be very easy to mistakenly allow the aqueous resistance to dominate the entire concentration range. This is because the passive component would never allow the membrane permeability to go to zero (membrane resistance go to infinity). Hence, a saturable mechanism may go totally undetected.

It is concluded therefore, that it is important to be able to estimate the aqueous resistance for two reasons. One is to correct the apparent uptake parameters to give the intrinsic values. The other is so that the saturable mechanism is not masked by the aqueous resistance, particularly if a significant passive permeability is also present.

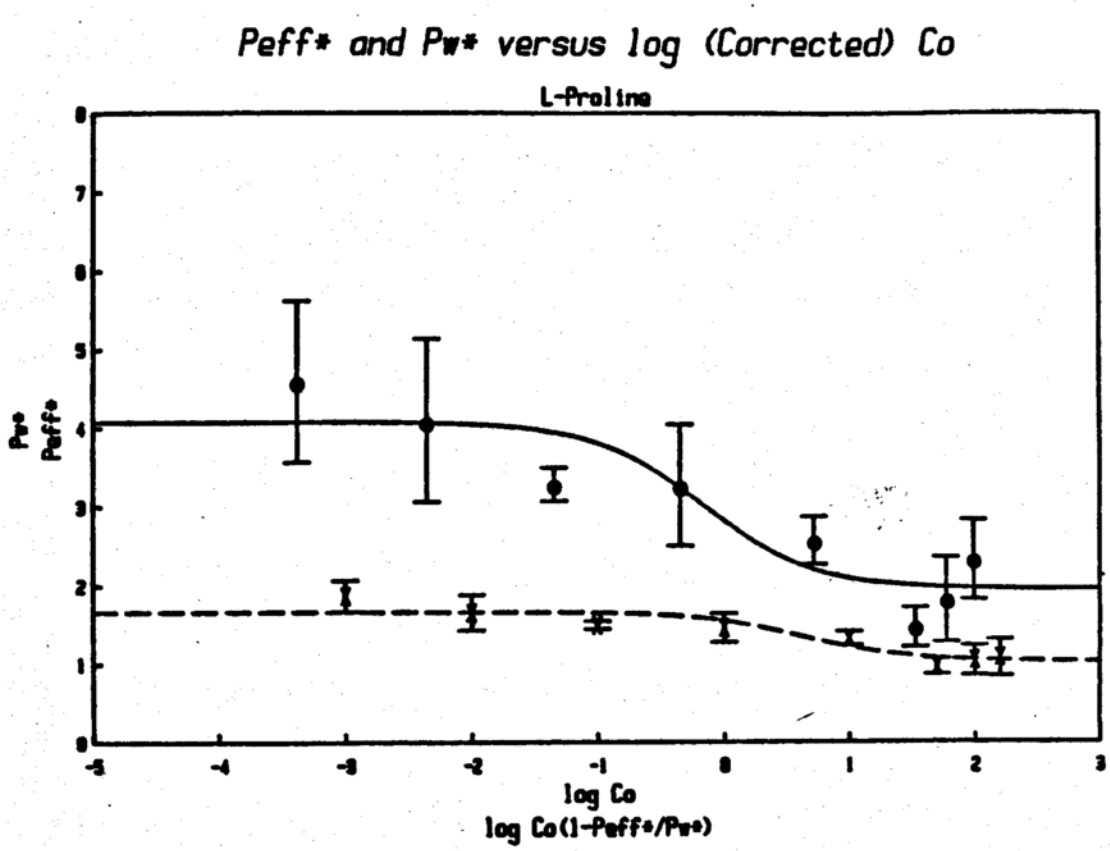

Figure 15
The permeability of l-proline is measured as a function of concentration. The dashed curve is the effective permeability, P*eff, and the solid curve represents the intrinsic permeability corrected for the aqueous resistance, P*w. This compound has a significant passive permeability as seen by the permeabilities at high concentrations. The importance of correcting for the aqueous resistance is shown. Saturation is barely detectable if one only views the effective permeability curve.

SUMMARY AND CONCLUSIONS

Various techniques, both in vivo and in vitro, are employed for studying intestinal absorption. One advantage of the in vivo techniques is that the blood supply to the intestine is left intact. These techniques however, require that a significant aqueous resistance be allowed to exist. In fact, with the ligated loop experiment there is no stirring or shaking of the bulk fluid and, therefore, a large aqueous resistance builds up with time. With in vitro techniques, the problem of the aqueous resistance can be circumvented. One can increase stirring until a plateau absorption rate is achieved, or one can measure uptake at various stirring rates and extrapolate to infinite stirring. Unfortunately, the flow rate of the in vivo perfusion experiment can only be increased to a certain limit to decrease the aqueous resistance. If the flow rate is increased too much, the ratio of the outlet to inlet concentration goes to one. Incidently, this points out another advantage of the perfusion technique. That is that only the perfusate concentration need be assayed and this can easily be done with such standard techniques as HPLC.

The unstirred layer, or aqueous resistance, adjacent to the membrane surface affects absorption rates in both passive and saturable absorption mechanisms. For highly permeable compounds, the aqueous resistance may even be rate limiting to membrane uptake. In

a saturable mechanism, the presence of the aqueous resistance will give a Michaelis constant Km value which is too high. The maximal uptake rate, Jmax, will also be too high if it is determined by a double reciprocal plot. The reason for this is because the uptake rate into the membrane depends on the concentration at the membrane surface, a quantity which cannot be measured directly. Usually the bulk concentration is used, which, in effect, ignores the aqueous resistance.

There has been given much consideration on how to correct the apparent uptake parameters for the aqueous resistance. For the most part, these corrections are based on considering the aqueous resistance layer to be of uniform thickness. The problem, or the gap, lies in the fact that almost no theoretical consideration has been given for describing this thickness. In fact, the present analysis has shown that for the intestinal perfusion the aqueous resistance is not of uniform thickness. Rather, it is zero at the entrance of the perfused segment and increases to its maximum size at the exit.

The present work applied the laws of continuity to study the mass transport in the fluid adjacent to the membrane surface in an intestinal perfusion set-up. The purpose was to derive the membrane surface concentration as a function of the bulk concentration of drug as well as the other parameters of the system, most notably the flow rate. Perhaps the most important contribution of this work has been

in the derivation of the aqueous resistance in the layer adjacent the membrane surface. Also, very little theoretical consideration has been given to simultaneous saturable and passive uptake mechanisms. The present analysis can be applied to any arbitrary uptake scheme and was specifically applied to saturable and passive uptake schemes in parallel.

The boundary layer model was based on a model which assumed laminar flow in a circular duct. Although the intestinal wall is not a smooth surface, it was pointed out in the background section that most absorptive cells, including the specialized cells involved in enzymic or carrier systems, are located primarily at the villi tips. It appears as if the folds of the intestine are not so much to increase surface area as to allow time for the undifferentiated cells of the crypts to undergo morphological changes as they migrate to the villi tips. Also, very poorly absorbed compounds, in particular very hydrophilic ones, may migrate into the unstirred waters of the crypt lumen. Although aqueous in nature, the resistance in this region is not part of the derived aqueous resistance since the conditions of the bulk flow have no influence on the diffusional resistance of this region. Instead, this resistance becomes incorporated into the membrane permeability term and in particular, the passive permeability constant.

The overall objectives of the analysis were set forth and

accomplished as follows:

1) To define the aqueous resistance in an unambiguous manner--The aqueous resistance determined by the analysis is completely independent of the membrane permeability. It is found to be a function of only the Graetz number and therefore can be set a priori in an experimental situation. Knowledge of the aqueous resistance assures that the experiments are not performed in a region where aqueous resistance dominates. As a rule of thumb, if the ratio of the outlet to inlet concentration is at least 0.85-0.90, the aqueous resistance will not dominate.

2) To relate the intrinsic membrane permeability to the intrinsic parameters, Jmax, Km and Pm, of a mechanism consisting of saturable and passive uptake in parallel--Once the aqueous resistance is known, it can be subtracted from the experimentally measured total resistance to give the intrinsic membrane resistance. By finding the relationships between the membrane surface concentration and the bulk drug concentration, it is then shown how the intrinsic membrane permeability can be related to the intrinsic parameters, Jmax, Km and Pm.

3) To develop a simple technique for using the above information in a practical manner--The modified boundary layer analysis, a film model, accomplished this goal. The film thickness, usually unknown in a film model, was derived from the convective-diffusive model. The result is that a simple regression

of the membrane permeability, Pw, on the parameter Co (1-Peff/Paq) will yield the parameters Jmax, Km, and Pm. If there is no saturable absorption and only passive permeability, the membrane permeability is independent of the inlet concentration, Co. In this case Pw = Pm. If there is only a saturable mechanism and no passive permeability, a double reciprocal plot can be used by inverting Pw and Co (1-Peff/Paq). Therefore, although the double reciprocal plot has previously been shown to be inappropriate in membrane uptake due to the aqueous resistance, this analysis shows that it can be used as long as the inlet concentration is corrected by the coefficient (1-Peff/Paq).

The theoretically derived aqueous resistance was compared to the experimental data for progesterone of Ho, Higuchi and co-workers. Progesterone is a highly permeable, highly lipophilic compound and therefore all of the total resistance to uptake is believed to be aqueous in nature. The boundary layer analysis was found to be able to predict the progesterone data quite well. The correctness of the derived aqueous resistance was further confirmed from the flow experiments with the amino acid leucine. It was also shown that leucine is taken up by a saturable carrier mediated mechanism and that there is no passive absorption of leucine.

The membrane permeability is found to be a function of concentration if a saturable uptake mechanism exists. It was shown

that if the aqueous resistance is not factored out of the effective permeability, the Michaelis constant is shifted to a higher value. The shift may be great enough to go beyond the concentration range of study or beyond the solubility limit of the compound. It was also shown that if a compound also has a relatively large passive uptake, a saturable mechanism may be completely masked if the aqueous resistance is not controlled. For these compounds especially, it is important to factor the aqueous resistance out of the effective permeability such that concentration dependent permeability may be observed.

It is concluded that the analysis presented supercedes any analysis thus far involving the intestinal perfusion set-up. The concepts developed here should prove quite useful to anyone performing perfusion experiments and in particular if a compound is suspected of having a concentration dependent uptake.

REFERENCES

1. Wilson, F.A. and Dietschy, J.M., Biochim. Biophys. Acta. 363, 112 (1974).
2. Thomson, A.B. and Dietschy, J.M., Amer. J. Physiol. 239, G372 (1980).
3. Schultz, S.G. and Frizzell, R.A., In "Intestinal Absorption and Malabsorption", Johnson. L., Ed., Raven Press, New York 1975, pp. 77-93.
4. Munck, B.G., Ibid pp 1097-1122.
5. Spencer, R.P. and Samly, A.H., Am. J. Physiol. 200, 501 (1961).
6. Munck, B.G., Membrane Biol. 53, 45 (1980).
7. Daniels, V.G., Newey, H., Smyth, D.H., Biochim. Biophys. Acta. 183, 637 (1969).
8. Larsen, P.R., Ross, J.E., and Tapley, D.F., Biochim. Biophys. Acta. 88,570 (1964).
9. Spencer, R.P., and Brody, K.R., Biochim. Biophys. Acta. 88, 400 (1964).
10. Schultz, S.G., Yu-Tu, L., Alverez, O., and Curran, P.F., J. Gen. Physiol. 56, 621 (1970).
11. Munck, B.G., and Schultz, S.G., J. Gen. Physiol. 153, 157 (1969).
12. Wiseman, G. In "Handbook of Physiology", Heidel, W., ed., vol 3, pp. 1277-1307. (1974), American Physiological Society,

Washington, D.C.

13. Wilson, T.H., "Intestinal Absorption", pp. 1-263 (1962), Saunders Co., London.

14. Mathews, D.M. and Laster, L., Am. J. Physiol. 208, 593 (1965).

15. Wiseman, G., J. Physiol., London 133, 626 (1956).

16. Adibi, S.A., Gastroenterology 56, 903 (1969).

17. Finch, L.R. and Hird, F.J.R., Biochim. Biophys. Acta. 43, 278 (1960).

18. Their, S.O., Segal, S., Fox, M., Blair, A., and Rasenberg, L., J. Clin. Invest. 44, 442 (1965).

19. Mathews, D.M. in "Intestinal Absorption and Malabsorption", Johnson, L. ed., Raven Press, New York, 1975, pp 77-93.

20. Das, M., Radhakrishnam, A.N., Biochem. J. 146, 133 (1975).

21. Burston, D., Wapnir, R.A., Taylor, E., and Mathews, D.M., Clinical Science 62, 617 (1982).

22. Rubino, A., Field, M., and Shwachman, H., J. Biol. Chem. 246, 3542 (1971).

23. Himukai, M. and Hoshi, T., J. Physiol., London 302, 155 (1980).

24. Dietschy, J.M., J. Lipid Res., 9, 297 (1968).

25. Tyror, M.P., Garbuth, J.T., and Lack, L., Amer. J. Med., 51, 614 (1971).

26. Levy, G., Jusko, W., J. Pharm. Sci. 55, 285 (1966).

27. Wood, J.H. and Thakker, K.M., Eur. J. Clin. Pharmacol. 23, 183

(1982).

28. Gladtke, E., von Hattingberg, H., "Pharmacokinetics", Springer, New York, 1979, p. 84.

29. Gudjonsson, H., Li, B.U.K., Shug, A.L., Olsen, W.A., Gastroenterology 88, 1880 (1985).

30. Shaw, R.D., Li, B.U.K., Hamilton, J.W., Shug, A.L., Olsen, W.A., Am. J. Physiol., 245, G376 (1983).

31. Hamilton, J.W., Li, B.U.K., Shug, A.L., Olsen, W.A., Clin. Res. 31, 764A (1983).

32. Barber, H.E., Hawksworth, G.M., and Turner, S.J., Proc. of the B.P.S. p 496, April 1979.

33. Tsuji, A., Nakashima, E., Kagomi, I., and Yamana, T., J. Pharm. Sci. 70, 768 (1981).

34. Quay, J.F. and Foster, L., Physiologist 13, 287 (1970).

35. Quay, J.F., Ibid. 15, 241 (1972).

26. Dixon, C., Mizen, L.W., J. Physiol. 269, 549 (1977).

37. Shindo, H., Fukuda, K., Kawai, K., and Tanaka, K., J. Pharm, Dyn. 1, 310 (1978).

38. Kimura, T., Endo, H., Yoshikawa, M, Muranishi, S., Sezaki, H., Ibid. 1, 262 (1978).

39. Tsuji, A., Nakashima, E., Kagami, I., Honjo, N., Yamana, T., J. Pharm. Pharmacol. 29, 707 (1977).

40. Tsuji, A., Nakashima, E., Kagami, I., Asano, T., Nakashima, R., and Yamana, T., Ibid. 30, 508 (1978).

41. Tsuji, A., Nakashima, E., Asano, T., Nakashima, R., Yamana, T. Ibid. 31, 718 (1979).

42. Umeniwa, K., Ogino, O., Miyazaki, K., and Arita, T., Chem. Pharm. Bull. 27, 2177 (1979).

43. Amidon, G.L., Leesman, G.D., Elliott, R.L., J. Pharm. Sci., 69, 1363 (1980)

44. Higuchi, T., Lee, H.K., Pitman, I.H., Farm. Aikak 80, 55 (1971).

45. Lee, H.K., Lambert, H., Stella, V.J., Wang, D., Higuchi, T., J. Pharm. Sci. 68, 288 (1979)

46. Banerjee, P.K., Ph.D. thesis, University of Wisconsin-Madison (1979).

47. Ganong, W.F., "Review of Medical Physiology", 7th edition, Lange, Los Altos, CA. pp. 356-377.

48. Menge, H., Bloch, R., Schaumloffel, E., and Riecken, E.O., Z. Gesamte Exp. Med. 153, 74 (1970).

49. Altmann, G.G., and Leblond, C.P., Am. J. Anat. 127, 15 (1970).

50. Clarke, R.M., Lab. Anim. 9, 201 (1975).

51. Clarke, R.M., Ecknauer, R., and Feyerabend, G., GUT 17, 895 (1976).

52. Herzberg, G.R., Sheerin, H., and Lerner, J., Comp. Biochim. Physiol. 40A, 229 (1971).

53. Kim, S.Y., Kim, Y.W., Sleisenger, M.H., Biochim. Biophys. Acta. 370, 283 (1974).

54. Smithson, K.W., and Gray, G.M., J. Clin. Invest. 60, 665 (1977).

55. Takesue, Y., Nishi, Y., Memb. Biol. 39, 285 (1978).

56. Takesue, Y., Yoshida, T.O., Akaza, T., and Nishi, Y., J. Biochim. 74, 415 (1973).

57. Guyton, A.C. "Basic Human Physiology: Normal Function and Mechanisms of Disease", W.B. Saunders Co., Philadelphia 1977, pp 655-701.

58. Akedo, H., and Christensen, H.N., J. Biol. Chem. 237, 113 (1962).

59. Trier, J.S., in "Handbook of Physiology", Hiedel, ed., vol. 3, American Physiological Society 1968, pp. 1125-1175.

60. Garvey, T.Q., Hyman, P.E., and Isselbacher, K.J., Gastroenterology, 71, 778 (1976).

61. Webster, H.L., and Harrison, D.D., Exp. Cell Res. 56, 245 (1969).

62. Munck, B.G., J. Physiol, London 223, 699 (1972).

63. Kyoo Hai Ryu and Grim, E., Am. J. Physiol. 242, G364 (1982).

64. Ho, N.F.H. and Higuchi, W.I., J. Pharm. Sci. 63, 686 (1974).

65. Westergaard, H. and Dietschy, J.M., J. Clin. Invest. 54, 718 (1974).

66. Wilson, T.H., Wiseman, G., J. Physiol. 123, 116 (1954).

67. Bates, T.R., Gibaldi, M. in "Current Concepts in Pharmaceutical Sciences: Biopharmaceutics", 1st ed., Swarbrick, J., ed., Lea

and Febiger, Philadelphia 1970, pp 57-99.

68. Dietschy, J.M., and Westergaard, H. in "Intestinal Absorption and Malabsorption", Czaky, T., Ed. Raven Press, New York 1975 pp. 197-207.

69. Agar, W.T., Hird, F.J.R., and Sidhu, G.S., Biochim. Biophys. Acta. 14, 80 (1954).

70. Finch, L.R., and Hird, F.J.R., Ibid 43, 268 (1960).

71. Hagihira, H., Wilson, T.H., and Lin, E.C.C., Am. J. Physiol. 203, 637 (1962).

72. Levine, R.R. and Pelikan, E.W., J. Pharmacol. Expti. Theor. 131, 319 (1961).

73. Elliott, R.L., Ph.D. Thesis, University of Wisconsin-Madison 1979.

74. Komiya, I., Park, J.Y., Kamani, A., Ho, N.F.H., and Higuchi, W.I., Intl. J. Pharmaceutics 4, 249 (1980).

75. Johnson, D.A., de Meere, A., Hu, M., Amidon, G.L., unpublished.

76. Elliott, R.L., Amidon, G.L., and Lightfoot, E.N., J. Theor. Biol. 87, 757 (1980).

77. Dainty, J., Adv. Bot. Res. 1, 279 (1963).

78. Pedley, T.J., Quart. Rev. Biophys. 16, 115 (1983).

79. Dietschy, J.M., Sallee, V.L., and Wilson, F.A., Gastroenterology 61, 932 (1971).

80. Sallee V.L., and Dietschy, J.M., J. Lipid Res. 14, 475 (1973).

81. Thomson, A., Dietschy, J.M., J. Theor. Biol., 64, 277 (1977).

82. Wilson, F.A., Sallee, V.L., and Dietschy, J.M., Science 174, 1031 (1971).

83. Winne, D., Biochim. Biophys. Acta. 298, 27 (1973).

84. Alvarado, F., L'Herminier, M., Proc. Physiol. Soc., Dec. 1978 p.45.

85. Preston, R.L., Schaeffer, J.F., and Curran, P.F., J. Gen. Physiol., 64, 443 (1974).

86. Naftalin, R.J., Biochim. Biophys. Acta. 233, 635 (1971).

87. Dugas M.C., Ramaswamy, K. and Crane, R.K., Ibid. 382, 576 (1975).

88. Dugas, M.C., and Crane, R.K., Fed. Proc., 32, 423 (1973).

89. Wilson, F.A., and Dietschy, J.M., Clin. Res., 20, 783 (1972).

90. Edwards, P.A., Biochim. Biophys. Acta. 345, 373 (1974).

91. Winne, D., Ibid., 464, 118 (1977).

92. Lieb, W.R. and Stein, W.D., Ibid., 373, 178 (1974).

93. Lieb, W.R. and Stein, W.D., J. Theor, Biol. 36, 641 (1972).

94. Koizumi, T., Arita, T., Kakemi, K., Chem. Pharm. Bull. 12, 421 (1964).

95. Winne, D., Arch. Pharmacol., 307 265 (1979).

96. Dawson, A.M., McMichael, H.B., J. Physiol., London, 182, 66 (1966).

97. Lewis, L.D., and Fordtran, J.S., Gastroenterology, 68, 1509 (1975).

98. O'Driscoll, K.M., Corrigan, O.I., J. Pharm. Pharmacol. 35, 815

(1983).

99. Dawson, A.M., McMichael, H.B., Proc, Phys. Soc. 2, 13, (1968).

100. Savina, P.M., Staubus, A.E., Gaginella, T.S., and Smith, D.F., J. Pharm. Sci. 70, 239 (1981).

101. Rey, F., Drillet, F., Schmitz, J., and Rey, J., Gastroenterology, 66 , 79 (1974).

102. Holdsworth, C.D., and Dawson, A.M., Clin. Sci., 27, 371 (1964).

103. Sladen, G.E., and Dawson, A.M., Clin. Sci., 36, 133 (1969).

104. Modigliani, R. and Bernier, J.J., GUT 12, 184 (1971).

105. Smithson, K.W., Jacobs, L.R., Gray, G.M., Science 214, 1241 (1981).

106. Amidon, G.L., Kou, J., Elliott, R.L., and Lightfoot, E.N., J. Pharm. Sci. 69, 1369 (1980).

107. Churchill, R.V., and Brown, J.W., "Fourier Series and Boundary Value Problems", 3rd ed., McGraw-Hill, New York, 1978, pp 23-45.

108. Levich, V.G., "Physicochemical Hydrodynamics", Prentice-Hall, Englewood Cliffs, NJ pp 60-72, 112-115.

109. Bird, R.B., Stwewart, W.E., and Lightfoot, E.N., "Transport Phenomena", Wiley, NY 1960 p. 559, 49.

110. Miyamoto, Y., Hanano, M., Iga, T., and Ishikawa, M. J. Pharm. Dyn. 5, 445 (1982).

111. Karino, A., Hayashi, M., Horie, T., Awazu, S., Minami, H., and Hanano, M., J. Pharm. Dyn. 5, 410 (1982).

112. Kozinski, A., Schmidt, F.P., and Lightfoot, E.N., Ind. Eng. Chem. Fundam. 9, 503 (1970).

113. Abromowitz, M. and Stegan, I., "Handbook of Mathematical Functions" Dover, N.Y., 1972, p. 320.

114. De Simone, J.A., Science, 220, 221 (1982).

115. Yamaoko, K., Tanigawarn, Y., Nagagawa, T., and Uno, T., J. Pharm. Dyn. 4, 879 (1981).

116. Freifelder, D., "Physical Biochemistry: Applications to Biochemistry and Molecular Biology" W.H. Freeman and Co., San Francisco 1976, Chapter 5.

DISSOLUTION OF ENZYME SUBSTRATES

Introduction and Background

The effect of a drug chemically reacting subsequent to its dissolution can greatly affect the dissolution rate (1-11). Studies have included the dissolution and subsequent hydrolysis of the two theophylline prodrugs acetyltheophylline and succinylditheophylline (3,7) as well as the dissolution and enzymatic hydrolysis of chloramphenical palmitate (4). Other studies were concerned with the effect of complexation with caffeine upon dissolution of benzoic acid (10) and salicylamide (6). Dissolution rates of cholesterol have also been found to be dependent on the type and amount of bile acid present in the dissolution media (11).

The effect of reaction on the dissolution rate is of particular significance when the drug is a weak acid or base (1,2,8,9). This is due to the fact that acid/base reaction kinetics are usually rapid compared to diffusion kinetics.

In the development of a prodrug, say an amide or ester derivative, the aqueous hydrolytic rates are not normally as fast as acid/base reactions. In particular, a prodrug suspension formulation whose shelf-life is on the order of weeks is considered pharmaceutically unstable and yet may possess a reaction rate much too slow to affect the dissolution process within the time frame of a single dosage regimen. However, it may be possible to exploit the catalytic power of enzymes such that a pharmaceutically stable but biochemically labile prodrug entity results (12).

In order to determine how fast a reaction must be, one can compare the dissolution rate and subsequent diffusion through a film to the rate of bulk reaction in that film. For dissolution with no chemical reaction the mass per time dissolving is given by the mass flux at the surface, J, times the surface area of the solid, A. Under steady-state conditions this is equal to the diffusional mass flux through a film of thickness h (13, 14).

$$J \cdot A = D/h\ C_s \cdot A \qquad (1)$$

The assumption of sink condition gives the concentration gradient as the solubility of the drug, C_s. The diffusion coefficient is D. The maximum rate of mass reaction per time for an enzymic reaction in the same volume is:

$$r = V_{max} \cdot A \cdot h \qquad (2)$$

Vmax is the maximum velocity of the enzyme given by the product of the catalytic rate constant, Kcat, times the bulk enzyme concentration Eo (15).

The effect of an enzymatic reaction is therefore significant when the quantities in eqs. 1 and 2 are on the same order:

$$R^* = V_{max} \cdot h^2/D \cdot C_s \sim 1 \qquad (3)$$

and becomes increasingly more significant as R* becomes large.

Typical film thicknesses for the rotating disc apparatus described by Wood et al (16) are on the order of 2-3 x 10^{-3} cm for rotational speeds in the 100-300 rpm range (17). The diffusion coefficients for most compounds in dilute aqueous solutions are on the order of 5 x 10^{-6} cm^2/sec. (18,19). Therefore, for this system an enzymatic reaction can be estimated to affect dissolution rates of a substrate when the following relationship holds:

$$K_{cat} \cdot E_o \geq C_s \qquad (4)$$

where Kcat is expressed in reciprocal seconds and Eo and Cs are expressed in equivalent concentration units.

This report develops a closed form solution to the dissolution plus enzymatic reaction problem for the rotating disc hydrodynamics. The spinning disc apparatus was chosen because the hydrodynamic theory for this system had already existed (17) and its application to drug dissolution is well established (20,21). The dissolution rates of two substrates for the proteolytic enzyme alpha-chymotrypsin were studied. These substrates were N-acetylphenylalanine ethyl ester and N-benzoyltyrosine ethyl ester. Both had similar catalytic rate constants, but the latter had an aqueous solubility that was two

orders of magnitude lower than the former. Since the catalytic rate constant is a function of pH (22-26) the reaction rate could be varied by varying both pH and bulk enzyme concentration. It will be shown that the solubility/reaction rate dependency of the dissolution rate may be of particular pharmaceutical significance.

STATEMENT OF THE PROBLEM

Certain pharmaceutical problems may be overcome by altering the solubility of a drug. Doing this may affect the bioavailability of the drug especially if the drug solubility is made very low. The problem is due to the low dissolution rates associated with low solubility drugs. A solution to this problem may be to make a prodrug whose site of bioreconversion is one of the digestive enzymes. The purpose of this research is to examine the effect of enzymatic reactions on substrate dissolution rates and to try to identify the important parameters involved in that process.

Theoretical

Model--The rotating disc apparatus is shown schematically in Fig. 1. When there is no reaction occuring in the solution the mass balance at steady state is given by (17):

$$V_y \, dc/dy = D \, d^2c/dy^2 \qquad (5)$$

The concentration of mass is C and is dependent on y, the direction perpendicular to the solid compact surface (where y=0). Therefore Vy is the fluid velocity in the y direction and the term on the left side of the equation represents convection while the term on the right represents diffusion. This expression is readily derived from the equation of continuity (19). A major contribution by Levich (17) was in deriving the expression for the fluid velocity:

$$V_y = - a \, y^2 \qquad (6)$$

$$a = 0.51 \, \omega^{3/2} \, \nu^{-1/2} \qquad (7)$$

where omega is the rotational speed in radians, nu is kinematic viscosity of water. The solution to eqs. 5-7, subject to the following boundary conditions,

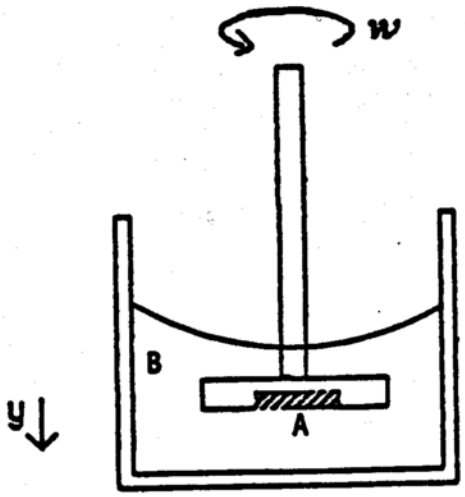

Fig 1

Diagram of the rotating disc apparatus showing the solid compact (A) and the enzymic dissolution media (B). The direction perpendicular to the solid surface is y.

$$C = C_s \quad \text{at} \quad y = 0 \tag{8}$$

$$C = 0 \quad \text{as} \quad y \to \infty \tag{9}$$

gives the Levich solution for dissolution rate:

$$J_L = 0.62\, D^{2/3}\, \nu^{-1/6}\, \omega^{1/2}\, C_s \tag{10}$$

By equating eqs 1 and 10, one calculates the thickness h needed to make the solution to a film model based on Ficks law correct.

$$h = 1.61\, D^{1/3}\, \nu^{1/6}\, \omega^{-1/2} \tag{11}$$

This film thickness applies to the case of diffusion with no reaction.

When in addition to convection and diffusion there exists a homogeneous reaction, mass balance requires inclusion of a reaction term in the continuity equation. In this case the continuity equation is written as (19):

$$V_y\, dc/dy = D\, d^2c/dy^2 + R \tag{12}$$

Where R is the reaction rate expressed in units of mass/volume/time.

Kinetic Considerations--The following reaction scheme is appropriate for alpha-chymotrypsin hydrolysis of substrates and while a commonly encountered scheme it is but one of many possible reaction schemes. A similar analysis (to the one below) would hold for many other enzyme kinetic mechanisms. Consequently the result of this analysis is fairly general.

For alpha-chymotrypsin then, the following kinetic scheme is assumed (15, 27, 28).

$$E + S \underset{k_{-1}}{\overset{k_1}{\rightleftharpoons}} ES \underset{k_{-2}}{\overset{k_2}{\rightleftharpoons}} EP_2 + P_1 \underset{k_{-3}}{\overset{k_3}{\rightleftharpoons}} E + P_2$$

Scheme I

where, for example, S is N-benzoyltyrosine ethyl ester, E is alpha-chymotrypsin, ES is the Michaelis complex, P is ethanol, EP_2 the acyl enzyme, and P_2 is N-benzoyl tyrosine (i.e., the free acid). The reaction term in eq. 12 for the substrate S is thus (where in

notation [S] is equivalent to C):

$$R = k_{-1}\,[ES] - k_1\,[E]\,[S] \tag{13}$$

An analytical solution is not possible for eq. 12 using this reaction term since it contains the additional variables [ES] and [E] which are also unknown functions of y. The complete system of equations that would have to be solved is given below.

$$V_y \frac{d\,[S]}{dy} = D_s \frac{d^2\,[S]}{dy^2} - k_1\,[E][S] + k_{-1}\,[ES] \tag{14}$$

$$V_y \frac{d\,[E]}{dy} = D_E \frac{d^2\,[E]}{dy^2} - k_1\,[E][S] + k_{-1}\,[ES] + k_3\,[EP_2] + k_{-3}\,[E][P_2]$$

$$V_y \frac{d\,[ES]}{dy} = D_{ES} \frac{d^2\,[ES]}{dy^2} + k_1\,[E][S] - [k_{-1} + k_2]\,[ES] + k_{-2}\,[EP_2][P_1]$$

$$V_y \frac{d\,[EP_2]}{dy} = D_{EP_2} \frac{d^2\,[EP_2]}{dy^2} + k_2\,[ES] - [k_{-2} + k_3][EP_2][P_1] + k_{-3}\,[E][P_2]$$

$$V_y \frac{d\,[P_1]}{dy} = D_{P_1} \frac{d^2\,[P_1]}{dy^2} + k_2\,[ES] - [K_{-2} + k_3][EP_2][P_1] + k_{-3}\,[E][P_2]$$

$$V_y \frac{d\,[P_2]}{dy} = D_{P_2} \frac{d^2\,[P_2]}{dy^2} + k_3\,[EP_2][P_1] - k_{-3}\,[E][P_2]$$

Kinetic Scheme I can be simplified (15, 19):

$$E + S \underset{k_m}{\rightleftharpoons} ES' \xrightarrow{K_{cat}} E + P_1 + P_2$$

Scheme II

where

$$k_m = \frac{k_3}{k_2 + k_3} k_s$$

$$K_{cat} = \frac{k_2 k_3}{k_2 + k_3}$$

$$k_s = \frac{k_{-1}}{k_1}$$

The reaction rate term of equation 3 is now given by:

$$R = -K_{cat} [ES']$$

This new expression however still contains an unknown function of y. However a total component balance on all enzymic species (30) shows that the sum total of all species at any point in the system cannot exceed the initial bulk concentration Eo.

$$[E] + [ES] + [EP_2] = [E_o] \tag{19}$$

Therefore, in the simplified Scheme II, the term [ES'] can be estimated to have a value whose upper limit is the bulk enzyme concentration. Using the following for the reaction term in eq. 12 should result in an estimated maximum effect of the enzymatic reaction on dissolution rate and at the same time enormously simplifies the mathematical problem.

$$R = -K_{cat} [E_o] \tag{20}$$

With this expression eq. 12 becomes

$$V_y \, dc/dy = D \, d^2c/dy^2 - K_{cat} \, E_o \tag{21}$$

where Vy is given in eqs 6 and 7.

Boundary Conditions--The boundary conditions for the problem are:

$$1.\quad \text{at } y = 0\ ,\ C = C_s \tag{22}$$

$$2.\quad \text{at } y = y_o,\ C = 0 \tag{23}$$

The second boundary condition is a statement of sink conditions. However, unlike the case with no chemical reaction, letting y go to infinity leads to a divergent solution. Also yo, the reaction zone thickness, should decrease in size as the reaction rate increases. That is, the sink is brought closer to the solid surface due to the fact that a shorter reaction time allows for a shorter diffusion time. Fortunately the reaction zone thickness cannot be arbitrarily assigned and even more important can be derived uniquely. A mass balance reveals that all the material which dissolves reacts in the reaction zone:

$$J = \int_0^{y_o} K_{cat}\, E_o\, dy = K_{cat}\, E_o\, y_o \tag{24}$$

$$y_o = J/(K_{cat} \cdot E_o) \tag{25}$$

One should not confuse yo with h derived from a stagnant film model. In fact, it will be shown that as the reaction rate goes to zero, the reaction zone thickness goes to infinity as is the case with no reaction solved by Levich.

Dimensional Analysis/Solution--It is convenient to make the problem dimensionless. This is done by letting

$$C^* = C/C_s \tag{26}$$

$$Z = y/L \tag{27}$$

$$dZ = dy/L \tag{28}$$

$$dZ^2 = dy^2/L^2 \tag{29}$$

where L is a chosen characteristic length which is as yet unspecified. Making these substitutions (along with the appropriate expression of Vy) into eq. 21 the following equation results:

$$\frac{d^2 C^*}{dZ^2} + \frac{a L^3}{D} Z^2 \frac{d C^*}{dZ} = \frac{K_{cat} E_o L^2}{C_s D} \tag{30}$$

Putting eq 30 into self-adjoint form:

$$\frac{d}{dZ}\left[\exp\left[\frac{a L^3}{D}\frac{Z^3}{3}\right]\frac{d C^*}{dZ}\right] = \frac{K_{cat} E_o L^2}{C_s D}\exp\left[\frac{a L^3}{D}\frac{Z^3}{3}\right] \tag{31}$$

It is seen that the most convenient choice for the characteristic length L is

$$L = \left[\frac{3D}{a}\right]^{1/3} \tag{32}$$

Substituting a into eq. 32 it is found that the chosen characteristic length is 1.119 times the film thickness h derived in the film model for this system with no reaction.

The dimensionless problem becomes

$$\frac{d}{dZ}\left[\exp(Z^3)\ \frac{d\,C^*}{dZ}\right] = 1.252\ R^*\exp[Z^3] \tag{32}$$

where

$$R^* = \frac{K_{cat}\cdot E_o\cdot h^2}{C_s\cdot D} \tag{34}$$

and has the physical interpretation as explained in the introduction. R* can be rewritten as

$$R^* = \frac{K_{cat}\ E_o\ C_s\cdot D}{(J_L)^2} \tag{35}$$

where J_L is the Levich dissolution rate with no reaction.

The solution to eq. 33, subject to the following boundary conditions

$$Z = 0 \quad , C^* = 1 \tag{36}$$

$$Z = Z_o \quad , C^* = 0 \tag{37}$$

is given as:

$$C^* = 1.252 \; R^* \int_0^Z \int_0^V \exp [s^3 - V^3] \, ds \, dv + C_1 \int_0^Z \exp [-V^3] \, dv + C_2 \tag{38}$$

$$C_2 = 1 \tag{39}$$

$$C_1 = \frac{-(1 + 1.252 \; R^* \int_0^{Z_o} \int_0^V \exp [s^3 - V^3] \, ds \, dv)}{\int_0^{Z_o} \exp (-V^3) \, dv} \tag{40}$$

The dissolution rate written in units of flux is given as:

$$J = - D \left. \frac{dC}{dy} \right|_{y = 0} \tag{41}$$

In dimensionless units this is equivalent to:

$$J^* = - 0.894 \left. \frac{d C^*}{dZ} \right|_{Z = 0} = - 0.894 \; C_1 \tag{42}$$

$$J^* = J/J_L \tag{43}$$

where J* is dissolution rate with reaction normalized to the dissolution rate under the same conditions with no reaction. Finally, to get the relationship between R* and Zo, eq. 24 is put in dimensionless form and equated to eq. 43.

$$\frac{1}{R^*} = 1.252 \left[Z_o \int_0^{Z_o} \exp\left[-V^3\right] dv - \int_0^{Z_o} \int_0^{V} \exp\left[s^3 - V^3\right] ds\, dv \right] \tag{44}$$

The dimensionless form of eq 24 is

$$J^* = 1.119\, R^*\, Z_o \tag{45}$$

In practice R* would be given, Zo computed (eq. 44) and the flux calculated from eq. 45.

Table I gives the relationship between R*, Zo and the normalized dissolution rate J*. The values in Table I were determined by numerical integration of eq. 44 using Simpsons rule (31).

Limiting Case/Approximate Solution--If the rate of reaction is large, the drug molecule cannot diffuse very far from the solid surface before it will have reacted. The reaction zone thickness, Zo, will therefore become very small with large R*. Order of magnitude analysis approximates the diffusive and convective terms,

Table I. Theoretical Values for R* Z_o, and J*.

R*	Z_o	J*
0.0	∞	1.0
0.03559	26.0	1.0277
0.04437	21.0	1.0366
0.07366	13.0	1.0724
0.27933	4.0	1.2511
0.40064	3.0	1.3405
0.68875	2.0	1.5371
1.8755	1.0	2.1000
6.5443	0.5	3.6640
17.797	0.3	5.9875
39.984	0.2	8.9455
159.62	0.1	17.8820

respectively, below.

$$\frac{\Delta C^*}{(\Delta Z)^2} = \frac{1}{Z_o^2} \tag{46}$$

$$3 Z_o \frac{\Delta C^*}{\Delta Z} = 3 Z_o \tag{47}$$

The ratio of the convective term to the diffusive term is therefore equal to $3 Z_o^3$, which is very small for large R* values. Therefore the convective term is negligible with high reaction rates. This is because the fluid velocity is proportional to the distance from the solid surface squared (see eq. 6) and that distance is never large within the small reaction zone associated with a rapid reaction.

The continuity equation in this limiting case is

$$\frac{d^2 C^*}{dZ} = 1.252 R^* \tag{48}$$

Solving this equation along with the boundary conditions of eqs. 36 and 37 and using the relationship of R* and Zo given by eq. 45 gives:

$$J^* = (2 R^*)^{1/2} \tag{49}$$

It can be shown that this function is the limit of the previous solution for high R* values. At a value of R* equal to 1.6 this

solution is within 8% of the full solution and is already within 1% at an R* value of 6.4.

Because the solution given by eqs. 44 and 45 are somewhat difficult to use in practice, an approximation to that solution was sought. It was found that the solution given below approximates the solution within 4% for all R* values.

$$J^* = \frac{1}{1 + 2.16\ (R^*)^{0.58}} + (2\ R^*)^{1/2} \qquad (50)$$

A graph of the normalized dissolution rate vs R*, the dimensionless reaction rate, is given in Fig. 2.

By setting the solution for dissolution rate with reaction equal to an expression similar to eq. 1 the film thickness for a model using film theory can be obtained. Doing this, it is found that the ratio of the film thickness with reaction to that with no reaction given by Levich is:

$$\frac{h_R}{h_L} = \frac{1 + 2.16\ (R^*)^{0.58}}{1 + (2\ R^*)^{1/2}\ (1 + 2.16\ (R^*)^{0.58})} \qquad (51)$$

which is always less than or equal to one.

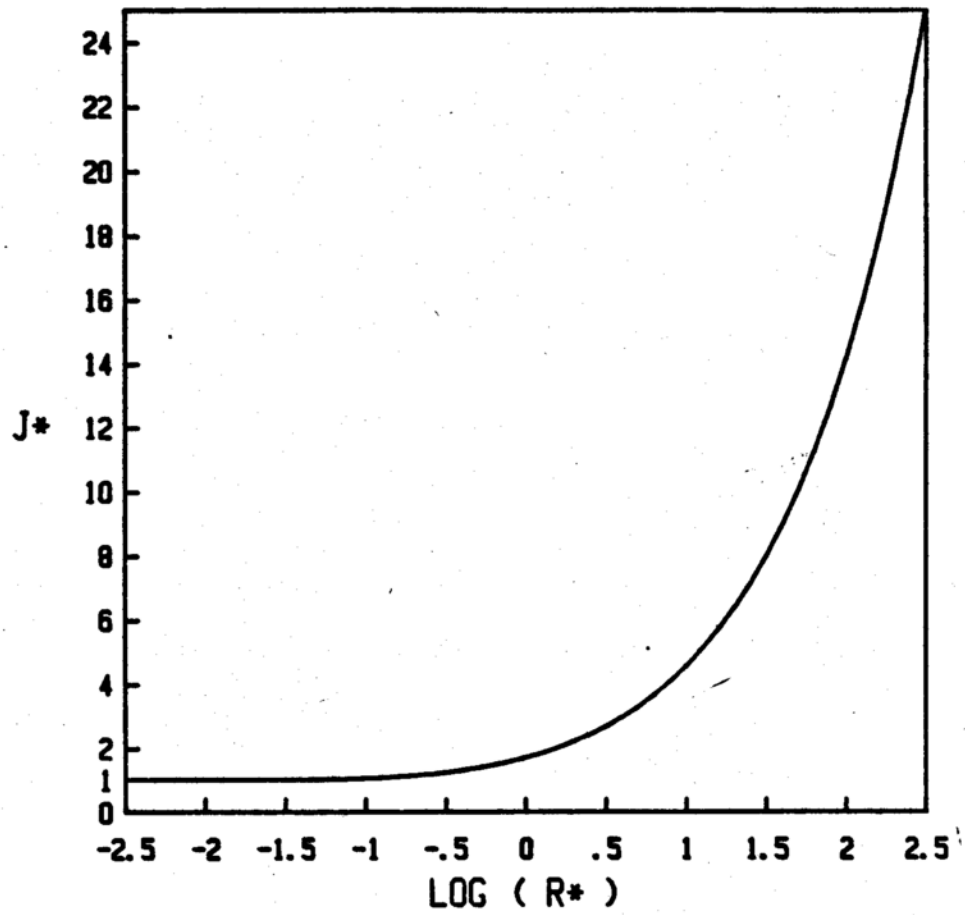

Fig 2

Theoretical plot of J*, the dissolution rate with reaction divided by the dissolution rate predicted by Levich for no reaction versus the logarithm of R*, the reaction rate parameter.

Experimental

Materials--N-benzoyltyrosine (U.S. Biochemical Corp., Cleveland, OH), N-Benzoyl-tyrosine ethyl ester, N-acetylphenylalanine, and N-acetylphenylalanine ethyl ester (Sigma Chemical Co., St. Louis, MO) were obtained in pure crystalline form and used as received. The enzyme alpha-chymotrypsin (Sigma Chemical Co., St. Louis, MO) was three times crystallized. Enzymic solutions were made with Tris (Sigma Chemical Co., St. Louis, MO) buffer using deionized water (Milli-Q^{R}, Continental Water Systems, El Paso, TX) which was degassed using a slight vacuum for approximate 30 min or more. The enzyme solutions contained 0.05M Tris buffer as well as 0.05M calcium chloride. In the kinetic experiments, the substrate solution contained 0.05M Tris, 0.05M calcium chloride and 2% V/V HPLC grade acetonitrile. The activity of the enzyme was checked periodically using a spectrophotometric titration with N-trans-cinnamoylimidazole (Sigma Chemical Co., St. Louis, MO)(32). See appendix A for details of the spectrophotometric titration.

Dissolution Experiments--The rotating disc used was similar to the one described by Wood et al. (16). The diameter was 1.1cm. The compounds studied were compressed directly in this disc at a pressure of 7,000 psi which was maintained for 3-4 min. The disc was rotated at various speeds using a motor equipped with a constant speed

control unit (Cole-Parmer Instrument Co., Chicago, IL). The rotational speed was calibrated and monitored repeatedly throughout each dissolution experiment using a tachometer (Cole-Parmer Instrument Co., Chicago, IL, Model 8312-20). The dissolution cell consisted of a jacketed beaker maintained at 25 ± 0.1°C. The dissolution media was the enzyme solution described earlier and had enzyme concentrations that ranged from 0 to 2.4×10^{-5}M. The dissolution volume was 250 ml. Each dissolution run was over a 30 min period. Steady-state occurred in less than 10 min. A 200 ul sample was taken periodically and assayed using reverse phase HPLC (Kratos, Ramsey, NJ, Models 773 and 400). The mobile phase was 35:65, MEOH:H_2O, adjusted to pH 2.1 using phosphoric acid. The wavelengths were 237 and 254 for BTEE and APEE respectively. It was found that when no enzyme was present, aqueous hydrolysis of the ester was negligible within the time frame of the experiment. Also, even the smallest concentration of enzyme (10^{-8}M) would cause complete hydrolysis of the ester within the time frame of sampling although the reaction rate was too small to affect dissolution rate.

The dissolution rate is calculated as follows: A standard curve is made using an external standard technique. For every three sample injections, a known concentration is injected. A linear relationship between concentration and peak height is observed. The slope of the standard curve is determined, SL_1. The peak height of the samples were also linear with time and that slope is determined,

SL_2. The dissolution flux was determined by the following equation:

$$J = (SL_2/SL_1) \cdot \frac{V}{A}$$

where V is the dissolution volume and A is the surface area of the solid compact.

In addition to varying enzyme concentration, the rotational speed was varied and in the case of N-benzoyltryosine ethyl ester the pH was also varied from 7.0 to 7.8 in increments of 0.2 ± 0.05 pH units (Radiometer, Copenhagen, Denmark Model PHM 64).

Diffusion Coefficients--The diffusion coefficients were obtained by measuring the dissolution rates as a function of rotational speed with no enzyme present. A least squares regression was applied to the Levich solution of eq. 10. The values for the diffusion coefficients obtained in this manner were $4.94 \pm 0.04 \times 10^{-6}$ cm^2/sec and $6.98 \pm 0.08 \times 10^{-6}$ cm^2/sec for N-benzoyl- tyrosine ethyl ester and N-acetylphenylalanine ethyl ester, respectively. See appendix B for details.

Solubility--The aqueous solubility was measured by placing excess solid in vials containing deionized water. The vials were placed in a water bath at 25 ± 0.1°C. The vials were vortexed three times daily. Samples were assayed daily for one week. The samples were removed, filtered and diluted 1/10. The ester concentration was

determined by HPLC assay. Solubilities measured after 48 hours were not found to be significantly different than those measured after one week. N-benzoyltyrosine ethyl ester had a measured solubility of $4.66 \pm 0.06 \times 10^{-4}$M while N-acetylphenylalanine ethyl ester had a value nearly two orders of magnitude higher, $1.38 \pm 0.05 \times 10^{-2}$M.

Kinetic Experiments--For N-acetylphenylalanine ethyl ester the value for K_{cat} at pH 7.8 reported by Hammond et al (33) was used. This value is 160 sec^{-1}. For N-benzoyltyrosine ethyl ester, Bender et al (34) reported a value for K_{cat} of 200 sec^{-1} at pH 7.8. However, the dissolution of this compound was studied at various pH values and therefore the catalytic rate constant had to be determined at each of these pH values.

The method used to measure the reaction rates was the modified spectrophotometric method described by Hummel (35). The spectrophotometer used was a Perkin-Elmer Lambda 3B equipped with a model 3600 data station. The spectrophotometer was fitted with jacketed cell holders to maintain a constant temperature of $25 \pm 0.1^{\circ}C$. The enzyme concentrations were 10^{-8}M. The initial substrate concentrations were in the range of 30 to 600 uM, the lowest concentration being at least 2 times the Km value. This gave greater reproducibility for determining Vmax and hence Kcat. In order to avoid solubility problems, 2% (v/v) acetonitrile was added

to the substrate solution. A weighted least squares linear regression analysis was done on the single reciprocal plot of the data (36, 37):

$$\frac{S_o}{V_o} = \frac{K_m}{V_{max}} + \frac{S_o}{V_{max}} \qquad (52)$$

where So is the initial substrate concentration and Vo is the initial rate. Details of the kinetic data analysis are given in Appendix C.

Results and Discussion

The experimental results are given in Tables II-V. The experiments utilizing N-benzoyltyrosine ethyl ester were repeated at least three times and therefore the mean and standard deviation are reported. N-acetylphenylalanine ethyl ester on the otherhand included no repeats.

Solubility Dependence--The difference between the two compounds is fairly evident. While the catalytic rate constants for these compounds are nearly the same, the solubilities differ greatly. N-acetylphenylalanine ethyl ester has a much higher solubility and therefore enzymatic reaction has little impact on this compound's dissolution. This is because with high solubility, the dissolution rate is very high even without reaction, as predicted by the Levich solution. It would therefore take a very large reaction rate to consume the entire mass undergoing dissolution within a small reaction zone. As seen in eq. 34, it would take extraordinarily high Kcat and/or bulk enzyme concentrations to give large R* values for highly soluble drugs.

The dissolution rate with no reaction depends on the solubility to the first power. However, examining the limiting case solution with high reaction (see eq. 49) it is seen that the dissolution rate is proportional to the solubility to the one-half power.

Table II--Dissolution Rate Data for N-Benzoyltyrosine Ethyl Ester and N-Acetylphenlalanine Ethyl Ester with Zero Bulk Enzyme Concentration ($E_o = 0$) and Varying rpm at pH = 7.8.

	$J \times 10^9$ (moles/cm^2/sec) $\pm$ s.d.	
rpm	N-BTEE	N-APEE[a]
100	0.599 $\pm$ 0.064	--
125	--	23.68
150	0.713 $\pm$ 0.029	--
200	0.836 $\pm$ 0.031	30.82
250	0.916 $\pm$ 0.064	34.40
300	1.005 $\pm$ 0.061	37.62

[a]Average of two points

Table III--Dissolution Rate Data for N-Benzoyltyrosine Ethyl Ester and N-Acetylphenylalanine Ethyl Ester with Constant rpm and Varying Bulk Enzyme COncentration at pH = 7.8.

N-BTEE (rpm = 200)		N-APEE (rpm = 125)	
$E_o \times 10^{-5}$ M	$J^{*a} \pm$ s.d.	$E_o \times 10^{-5}$ M	$J^{*a,b}$
0.347	2.89 ± 0.01	0.398	1.011
0.695	3.78 ± 0.19	0.796	1.021
1.045	4.22 ± 0.17	1.194	1.040
1.389	4.40 ± 0.35	1.554	1.046
1.736	4.573 ± 0.19	1.592	1.051
2.39	5.550 ± 0.39	2.030	1.067
--	--	2.33	1.074
--	--	3.18	1.113

[a]Experimentally determined dissolution rate normalized to the dissolution rate with no reaction as predicted by eq. 10.

[b]Single point determination.

Table IV--Dissolution Rate Data for N-Benzoyltyrosine Ethyl Ester and N-Acetylphenylalanine Ethyl Ester with Constant Bulk Enzyme Concentration and varying rpm at pH = 7.8.

	$J^{*a} \pm$ s.d.	
rpm	N-BTEE (E_o = 2.39 x 10^{-5}M)	N-APEE[b] (E_o = 2.03 x 10^{-5}M
100	7.44 ± 0.25	--
125	--	1.067
150	6.36 ± 0.26	--
200	5.55 ± 0.39	1.046
250	5.62 ± 0.17	0.997
300	5.18 ± 0.15	1.001

[a]Experimentally determined dissolution rate normalized to the dissolution rate with no reaction as predicted by eq. 10.

[b]Single point determination.

Table V--Dissolution Rate Data for N-Benzoyltyrosine Ethyl Ester with Constant Bulk Enzyme Concentration (E_o=2.39x10^{-5}M) and Constant Rotational Speed (rpm = 200) and with varying pH.

pH	J x 10^9 (moles/cm^2/sec) ± s.d.
7.8	4.59 ± 0.32
7.6	3.76 ± 0.40
7.4	3.32 ± 0.42
7.2	2.93 ± 0.11
7.0	2.63 ± 0.12

$$J = [2 K_{cat} E_0 D C_s]^{1/2} \quad (53)$$

The importance of the solubility dependence is understood when one considers the effect of making a prodrug whose solubility is orders of magnitude less than its parent drug. Ordinarily this means a decrease in dissolution rate proportional to the solubility decrease (see eq. 1). While in some cases this effect may be desired for prolonged release (3), in other cases the decrease in dissolution rate may be detrimental to bioavailability. The chemical reaction may, however, compensate for this decrease due to lower solubility. As seen in the graph of Fig. 2, it is possible that this compensation may reasonably be one to perhaps two orders of magnitude. In fact it is possible that while the prodrug derivative may have a lower solubility than its parent, it may actually have a higher dissolution rate if R* is large enough.

Applications of the above principle are particularly interesting in considering suspension formulations. Suspensions degrade via zero-order kinetics and the rate constant is proportional to the drug solubility. Making a prodrug with a solubility orders of magnitude lower will increase shelf-life stability tremendously. If the prodrug is made as a substrate for one of the digestive enzymes, rapid dissolution and bioreconversion may result upon oral administration.

Bulk Enzyme Concentration Dependence--At pH = 7.8 the rotational speed was kept at a constant value of 200 rpm while the bulk enzyme concentration was varied. The results for N-benzoyltyrosine ethyl ester are shown graphically in Fig. 3. The theoretical curve was calculated using the literature value for Kcat (200 sec^{-1}) (34). Good agreement between theory and experiment exists. Calculation of R* values show most of the data to be in the limiting case region. From eq. 54 it is seen that in the limiting case, the dissolution rate is proportional to the bulk enzyme concentration to the one-half power.

rpm Dependence--At a constant enzyme concentration of 2.4 x 10^{-5}M, the rpm was varied. Figure 4 shows that the increase in dissolution rate due to reaction is greater for slower rotational speeds. This is due to the fact that at slower speeds the boundary layer thickness is increased. The drug has a longer time to diffuse and hence a greater probability of reacting within the reaction zone.

The pharmaceutical implications are two-fold. First, if the reaction is very large the dissolution rate is independent of the hydrodynamics. An interphase transport problem with no reaction is a convective-diffusive problem. With a large reaction term, the

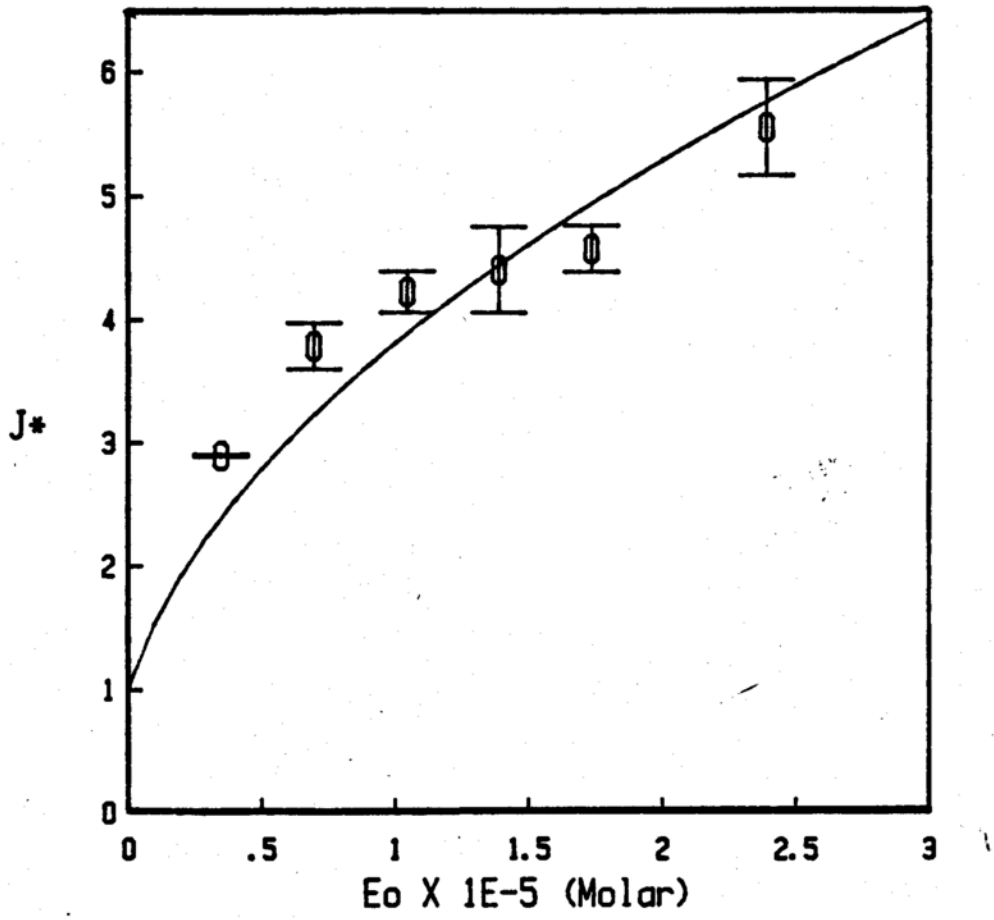

Fig 3

The normalized dissolution rate, J* of N-benzoyltyrosine ethyl ester versus the bulk enzyme concentration E_o. The solid line is the theoretical curve predicted by eq. 50. The error bars represent the standard deviation of the experimental data.

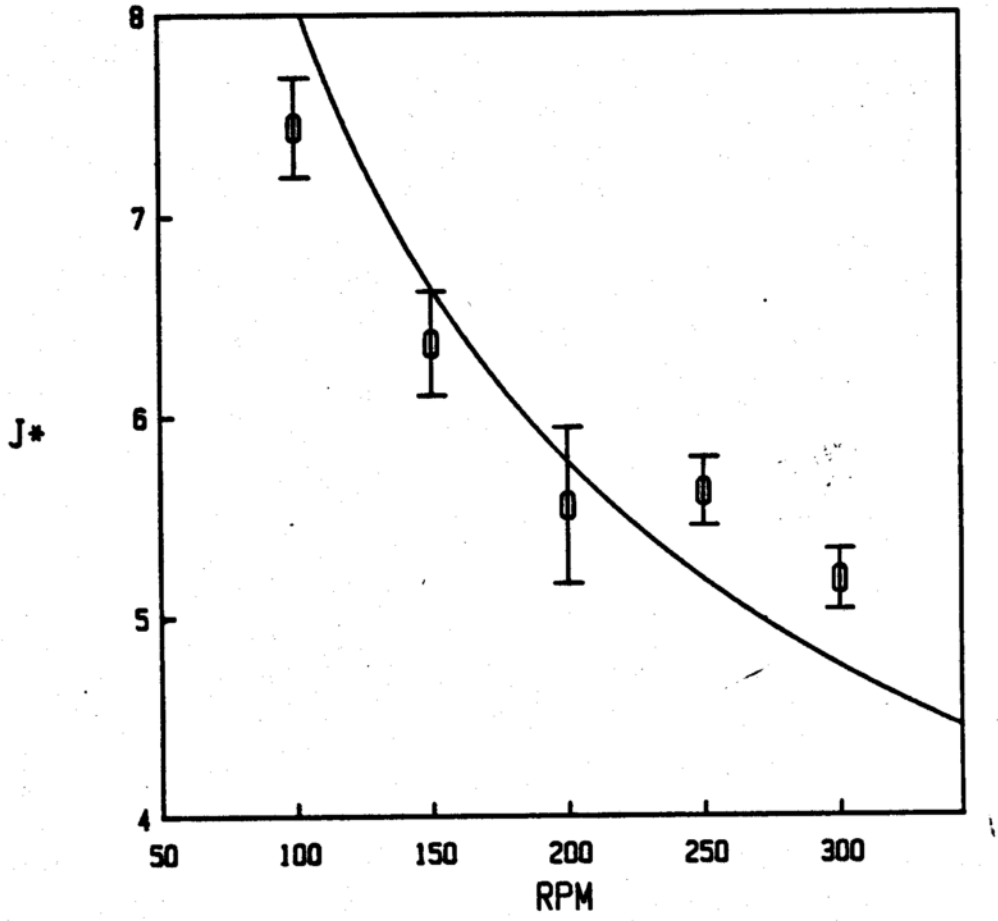

Fig 4

The normalized dissolution rate J* of N-benzoyltyrosine ethyl ester versus the rotational speed. The solid line is predicted by theory and error bars represent the standard deviation. The curve shows that the increase in dissolution rate due to reaction decreases as convection increases.

problem becomes one of reaction-diffusion. Interphase transport rates become more dependent on the reaction rate and less dependent on the sometimes unknown hydrodynamics of the system. Examination of the limiting case solution reveals the lack of the rotational speed variable.

Secondly, a reaction does not have to be as large in a system with no convection in order to influence interphase transport rates. This suggests the possibility of incorporating a chemical reaction in a hydrogel or other polymeric phase for the purpose of chemically controlled drug delivery. The effect of a homogeneous chemical reaction in the biophase of the skin has already been shown to greatly effect the transdermal absorption of drugs (38).

pH Dependence--The catalytic rate constant for the hydrolysis of esters varies with pH (22-26). There are two ionizable groups of alpha-chymotrypsin whose states of ionization are important in terms of the activity of alpha-chymotrypsin. One is the imidazole group of histidine located at the active site and the other is the amino group of the terminal isoleucine. The result of these two ionizable groups is that the catalytic rate constant has an optimum value around pH = 9.0 (15, 23). The isoleucine residue has a pK value around 9.23 and therefore in the range of pH for the dissolution studies, consideration will be given only to the ionization of the histidine residue. The dependence of Kcat on pH is given below for the rate

limiting case ($K_2 >> K_3$) where deacylation of the acyl enzyme intermediate is the rate limiting step (25):

$$(K_{cat})_{pH} = \frac{k_3}{1 + \frac{[H+]}{K_a}} \qquad (54)$$

where Ka is the ionization constant for the histidine residue.

The values of Kcat for N-benzoyltyrosine ethyl ester were determined from pH 7.0 to 7.8. They are presented in Table VI. The Michaelis constant, Km was found to be 0.016 mM with a standard deviation of 0.005 and was independent of pH value (23, 25). A least squares regression of the data in Table VI according to eq. 54 gave K_3 = 191 sec^{-1} ± 11.5 s.d. and pKa = 7.27 ± 0.025 s.d. The pKa determined was slightly higher than the value found by others: pKa = 6.7; (23, 28) 6.9 (24), 7.14 (39).

The dissolution rate for N-benzoyltyrosine ethyl ester versus pH is shown in Fig. 5. The theoretical curve was calculated by using the function in eq. 54 and the K_3 and Ka values determined from the kinetic experiments. It is seen that the theoretical is in agreement with experimental.

In the previous figures, the Kcat at pH 7.8 used to calculate the theoretical curves was 200 sec^{-1} the value reported by Bender et al (34), and not 150 sec^{-1} as determined in the present kinetic studies. Least squares regression analysis on all the data determined at pH = 7.8 resulted in a catalytic rate constant

Table VI--Kinetic Rate Constant K_{cat}, for N-Benzoyltyrosine Ethyl Ester with varying pH.

pH	K_{cat} (sec^{-1}) ± s.d.
7.8	150 ± 10.0
7.6	125 ± 9.6
7.4	102 ± 7.5
7.2	91 ± 6.6
7.0	68 ± 4.3

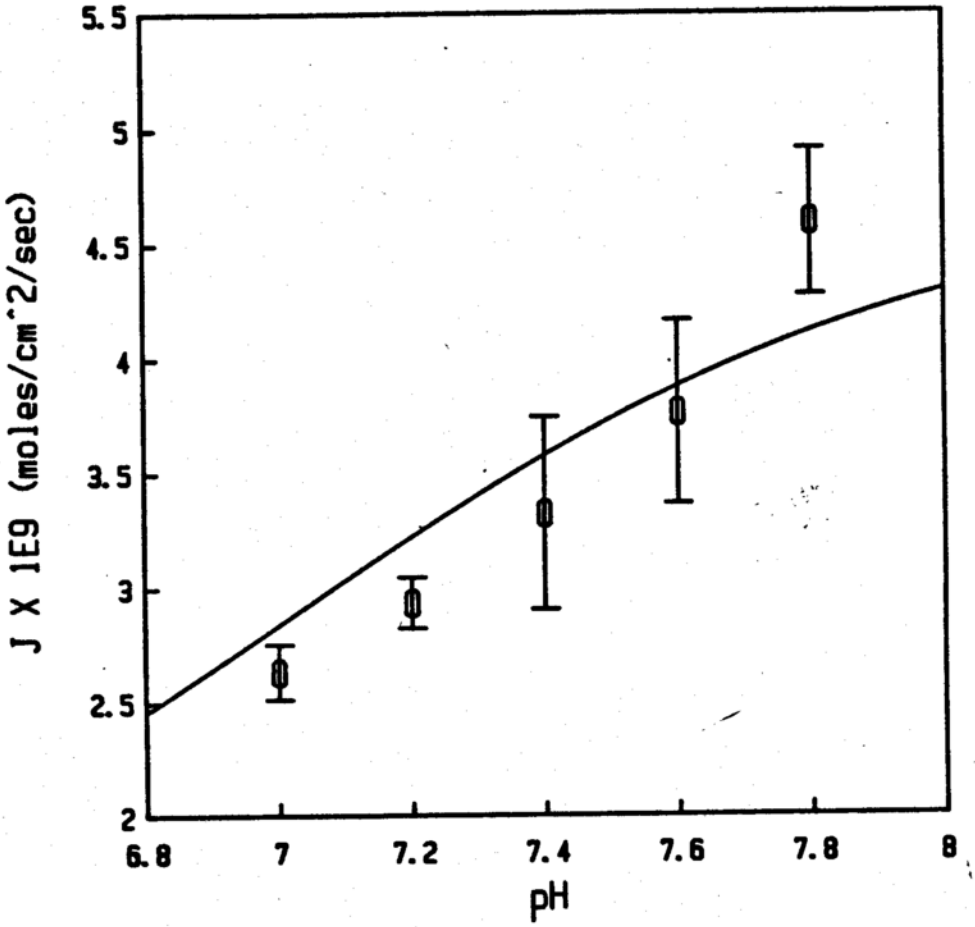

Fig 5

The dissolution rate of N-benzoyltyrosine ethyl ester versus pH. The theoretical solid line is calculated using eq. 54 for the dependence of the catalytic rate constant on pH. The error bars represent the standard deviation of the experimental data points.

of Kcat = 206 sec^{-1}. Although there is some discrepancy between using the values 200 and 150, most theoretical values calculated using Kcat = 150 sec^{-1} are 87% of those using Kcat =200 sec^{-1}. This is due to the fact that at high reaction rates the dissolution rate is proportional to Kcat to the one-half power. Table VII shows all the data at pH 7.8 where the dissolution rate predicted depends on the choice of the value for Kcat. Even for the less favorable choice of Kcat = 150 sec^{-1}, the agreement seems very good considering the complexity of the problem and the simplicity of the solution.

Comparison of Theory and Experimental--Because of the simplifying assumptions made and because of the powerful use of dimensional analysis, the solution consists of only two variables, R* and J*. This makes it possible to represent all the data for all compounds on one curve (as was seen in Fig. 2). All the data for N-acetylphenylalanine ethyl ester and N-benzoyltyrosine ethyl ester of Tables II-V are shown graphically in Fig. 6. Again what is most readily apparent is that the dissolution rate of the higher solubility compound, N-acetylphenylalanine ethyl ester, was only slightly affected by the presence of enzymatic reaction. Although a perfect fit is not seen for all the data, the overall trend is truly apparent.

Deviation of experimental from theory has many explanations.

Table VII--Comparison of Predicted and Experimental Dissolution Rates at Two Different Catalytic Rate Constant Values for all N-Benzoyltyrosine Ethyl Ester Data at pH = 7.8.

$(R^*/K_{cat}) \times 10^2$	J_{exp}/J_{pred} (K_{cat} = 150)	J_{exp}/J_{pred} (K_{cat} = 200)
1.17	1.36	1.21
2.34	1.33	1.17
3.52	1.24	1.08
4.68	1.13	0.99
5.37	1.25	1.09
5.85	1.06	0.93
6.44	1.25	1.09
8.06	1.11	0.96
10.74	1.10	0.96
16.11	1.06	0.92

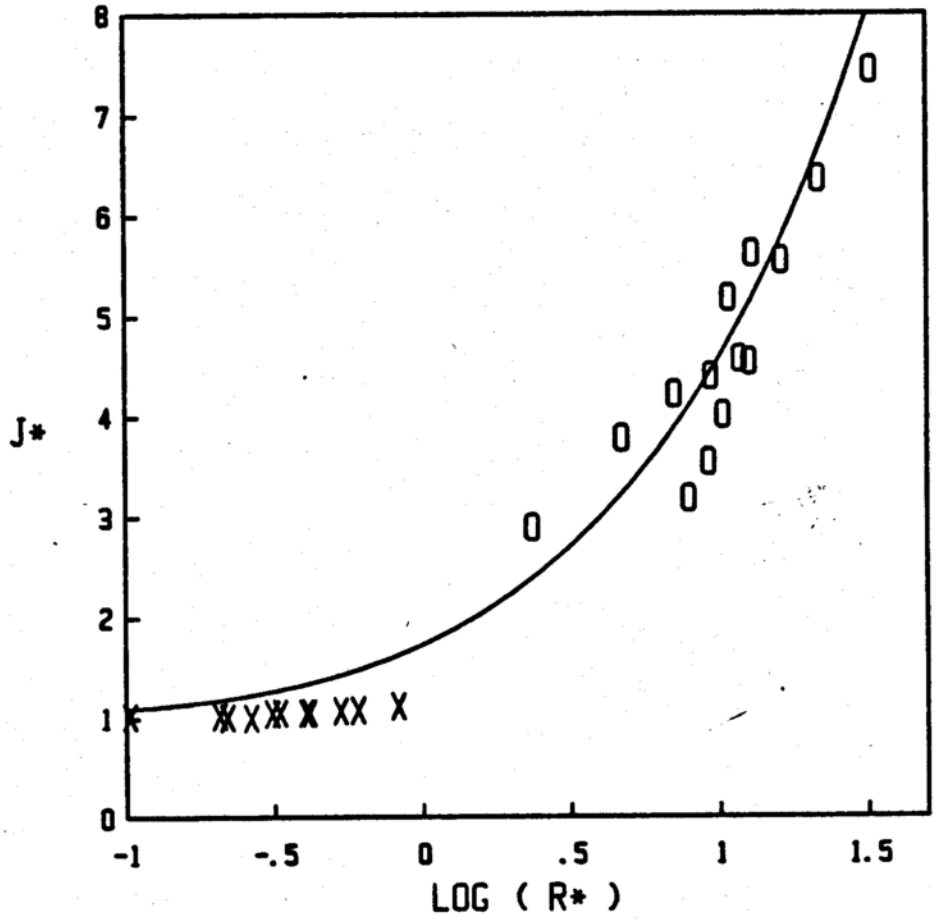

Fig 6

The normalized dissolution rate versus the logarithm of the reaction parameter R*, for N-acetylphenylalanine ethyl ester (X), and N-benzoyltyrosine ethyl ester (O). The difference due to the relative solubilities of the two compounds is clearly shown. Data is for all rotational speeds, bulk enzyme concentrations and pH values.

One is that the total component balance given earlier (Equation 19) does not apply within the reaction zone. There may be a build-up of enzyme within this zone due to diffusion of enzyme in from the bulk. Therefore the maximum effect of the reaction may be higher than estimated. Another consideration is that the liberation of hydronium ions due to reaction results in a pH gradient wihin the reaction zone (8).

Further insight into these deviations could be obtained from a numerical solution to the complete set of continuity equations (eq. 14). However, given the numeric difficulties inherent in a boundary value problem of this system size and the number of parameters involved, it appears a numerical solution may not provide more insight than the simple solution obtained here.

Summary and Conclusions

Enzymatic reactions were determined to be fast enough to affect the dissolution rate of a solid substrate. Dimensional analysis led to the definition of the single most important parameter, R*, which determines the relative importance of the reaction rate in regard to the diffusional process. This parameter may be simply regarded as the ratio of the diffusion time to the reaction time when these times are defined as follows:

$$t_R = C_s/V_{max} \tag{55}$$

$$t_D = h^2/D \tag{56}$$

The dimensionless parameter R* is obtained from a model using simplifying assumptions in regard to the kinetic scheme. An analytical solution to the true system (eq. 14) is not possible. A numeric solution to that system would not give as good a qualitative description as the R* parameter model. The latter model was found to correctly predict the trends found experimentally.

Perhaps the most pharmaceutically significant parameters in R* are the solubility and Kcat. The catalytic rate constants for ester hydrolysis by alpha-chymotrypsin are on the order of 100-200 sec^{-1} while amide hydrolysis is on the order of 1 sec^{-1}. The model therefore suggests that in certain prodrug strategies an

ester derivative may have advantages over an amide.

Experimentally it was found that N-acetylphenylalanine ethyl ester had much lower increases in dissolution rates than the less soluble N-benzoyltyrosine ethyl ester. This is due to the fact that higher solubility drugs already have a high rate of dissolution. It was concluded that the decrease in dissolution rate due to making a prodrug derivative whose solubility is lower than the parent drug may be compensated for by the presence of the enzymatic reaction. It is further concluded that although highly soluble compounds may not have their dissolution rates increased by chemical reaction, there may be a significant effect on the interphase transport rates from a medium in which the compound's concentration is kept low.

A final conclusion is that the model predicts the possibility of reaction controlled interphase transport. It is seen that the solution goes from convectively controlled diffusion to one of reaction controlled. Experimentally it was shown that as the rotational speed was decreased (convection decreased), the impact of enzymatic reaction increased.

APPENDIX A

Spectrophotometric Determination of the Operational normality of alpha-Chymotrypsin

The titration method used to determine the operational normality of chymotrpsin is similar to the one described by Schonbaum, Zerner, and Bender (32). The present studies used a Perkin- Elmer lambda 3B spectrophotometer equipped with a model 3600 data station. The titrant used in this method is N-trans-cinnamoylimidazol (NTC) which forms a stable acyl intermediate with chymotrypsin at pH 5.

Modification of the method used is as follows. Rather than making a concentrated enzyme stock solution and adding 100 microliters of the stock solution to 3 milliliters of buffer in the sample cell, three milliliters of a more dilute enzyme stock solution was added directly. This was done since the enzyme solutions were always made fresh and never stored for prolonged periods.

The NTC stock solution is approximately .08 grams of NTC in 100 milliliters of HPLC grade acetonitrile. The buffer solution is .1 molar acetate adjusted to pH 5. The enzyme stock solution is approximately 0.19 grams per 100 milliliters of buffer. The exact weights of enzyme and NTC are recorded.

The procedure is as follows:

1) Buffer vs Buffer to zero spectrophotometer

2) Buffer solution is placed in reference cell and 3 milliliters

of enzyme solution is placed in sample cell - absorbance is recorded (A4).

3) To the sample cell described in 2 is added 100 microliters of stock NTC - absorbance is recorded (A3).

4) Contents of sample cell are discarded. Fresh buffer is added and spectrophotometer is zeroed. To the buffer in the sample cell is added 100 microliters of NTC - absorbance is recorded (A1).

The operational normality is calculated from the following equation which differs from reference 32 due to the dilution factors.

$$N = \frac{A_2 - A_3}{8.613 \times 10^3}$$

$$A_2 = A_4 + 0.9677\ A_1$$

The value 0.9677 corrects for the dilution (i.e. 3.0/3.1) The value 8.613×10^3 is equal to the molar extinction coefficient of NTC minus the delta molar extinction coefficient of NTC-chymotrypsin versus chymotrypsin times the dilution factor.

$$8.613 \times 10^3 = (9.32 - 0.42) \times 10^3 \times (0.9677)$$

APPENDIX B

Determination of Aqueous Diffusion Coefficients

The diffusion coefficients were determined by measuring the dissolution rate as a function of rotational speed in the absence of enzymatic reaction. The data for N-benzoyltyrosine ethyl ester and N-acetylphenylalanine ethyl ester is shown below.

DISSOLUTION RATE OF BTEE

AS A FUNCTION OF ROTATIONAL SPEED

RPM	$J_L \times 10^9$ (moles/cm^2/sec) ± S.D.
100	0.599 (.064)
150	0.713 (.029)
200	0.836 (.031)
250	0.916 (.064)
300	1.005 (.060)

DISSOLUTION RATE OF APEE

AS A FUNCTION OF ROTATIONAL SPEED

RPM	$J_L \times 10^9$ (moles/cm^2/sec)
125	23.68
200	30.70
250	34.51
300	37.84

The experiments were not repeated for N-acetylphenylalanine ethyl ester. The data reported for N-benzoyltyrosine ethyl ester is the mean and standard deviation of at least 3 trials.

The Levich solution can be written as:

$$J_L = 0.432\, D^{2/3}\, C_s\, RPM^{1/2}$$

To find the diffusion coefficient, a linear regression of the dissolution rate versus RPM to the one-half power is performed on a line forced through the origin. The slope is calculated by minimizing the sum of squares.

$$S.S. = \sum (SL \cdot x_i - y_i)^2$$

$$SL = \frac{\sum y_i x_i}{\sum x_i^2}$$

The variance of the slope is given by the following equation (36, 40):

$$VarSL = \frac{\sum y_i^2 - SL\sum x_i^2 y_i^2}{(n-1)\sum x_i^2}$$

The number of data points is n.

The diffusion coefficient is calculated from the slope.

$$D = \left[\frac{SL}{0.432\ C_s}\right]^{3/2}$$

The variance of the diffusion coefficient, D, is a function of the slope variance and the variance of the solubility, VarCs:

$$VarD = (D_{SL})^2\ VarSL + (D_{C_s})^2\ VarC_s$$

where Dsl and Dcs are the partial derivatives of the diffusion coefficient with respect to the slope and the solubility respectively.

APPENDIX C

KINETIC DATA ANALYSIS

The modified spectrphotometric method of Hummel (35) involves having the substrate initially in both the reference and sample cells of the spectrophotometer. The wavelength used was 254 nanometers. The delta molar extinction coefficient of N-benzoyltyrosine ethyl ester versus N-benzoyltyrosine was needed. A Beers Plot for each compound was made for each pH studied. Although the variances for the molar extinction coefficients of each compound are small, they are additive when the molar extinction coefficients are substracted. The delta molar extinction coefficients as a function of pH are given in the table below along with the associated variance, VarE.

DELTA ABSORBANCE AT VARIOUS pH VALUES

pH	delta absorbance (A.U. / mM)	VarE x 10^4
7.0	.9985	10.0
7.2	.9583	9.22
7.4	.8896	7.6
7.6	.8491	8.6
7.8	.792	10.1

The procedure for the kinetic studies is as follows. To both the reference and sample cells is added 1.5 milliliters of substrate solution. To the reference cell, an additional 1.5 milliliters of plain buffer solution is added and mixed. To the sample cell is added and mixed 1.5 milliliters of enzyme solution. At time zero, the absorbance reading is zero and starts to increase. The data station of the spectrophotometer reads and electronically records the absorbance once every second for 2 minutes. A Perkin-Elmer kinetic software program, KINS, regresses the data and gives the initial slope in absorbance units per second along with the variance of the slope, VarSL. The initial rate is calculated by dividing the initial slope by the delta molar extinction coefficient, delta e.

$$Vo = \frac{Slope}{delta\ e}$$

The variance of the initial rate, VarVo is calculated from the following equation.

$$VarVo = \left[\frac{Slope}{(delta\ e)^2}\right]^2 VarE + \frac{1}{(delta\ e)^2} VarSL$$

In the single reciprocal plot, the initial substrate concentration divided by the initial rate, So/Vo, is regressed against the initial substrate concentration, So.

$$\frac{S_o}{V_o} = \frac{K_m}{V_{max}} + \frac{S_o}{V_{max}}$$

The x variable So, is assumed to have a negligible variance. The y variable, So/Vo, has the following variance (36).

$$VarY = \left(\frac{So}{Vo^2}\right)^2 VarVo$$

Weighting is done with one over VarY

$$w = \frac{1}{VarY}$$

Therefore, the sum of squares is given as:

$$s.s. = \sum w_i (y_i - ax_i - b)^2$$

The linear regression gives the slope, 1/Vmax, the intercept, Km/Vmax, and the associated variances of the slope and intercept (SLP, INT, VarSLP, VarINT).

$$INT = \frac{(\sum w_i x_i^2 \sum w_i x_i/y_i - \sum w_i x_i \sum w_i x_i^2/y_i)}{DM}$$

$$SLP = \frac{(\sum w_i \sum w_i x_i^2/y_i - \sum w_i x_i \sum w_i x_i/y_i)}{DM}$$

$$VarSLP = \frac{\sum w_i}{DM} VC \qquad VarINT = \frac{\sum w_i x_i^2}{DM} VC$$

$$DM = \sum w_i \sum w_i x_i^2 - \left(\sum w_i x_i \right)^2$$

$$VC = \frac{\sum w_i \left(x_i/y_i - (SLP)(x_i) - INT \right)^2}{(n - 2)}$$

where n is the number of data points. Since the catalytic rate constant is Vmax divided by the bulk enzyme concentration, Eo, it is calculated as follows:

$$K_{cat} = \frac{1}{SLP \cdot Eo}$$

The variance of Kcat is given below

$$Var K_{cat} = \left[\frac{1}{Eo \cdot SLP^2} \right]^2 VarSLP + \left[\frac{1}{SLP \cdot E_o^2} \right]^2 Var E_o$$

where VarEo is the variance of the bulk enzyme concentration. The Michaelis constant is calculated by dividing the intercept by the slope.

$$Km = \frac{INT}{SLP}$$

The variance of Km can be calculated from the following equation.

$$VarKm = \left[\frac{1}{SLP} \right]^2 VarINT + \left[\frac{INT}{SLP^2} \right]^2 \cdot VarSLP$$

REFERENCES

1. Higuchi, W.I., Nelson, E., Wagner, J.G. J. Pharm. Sci. 1964, 53, 333-335.
2. Hamlin, W.E., Higuchi, W.I. Ibid, 1966, 55, 205-207.
3. Higuchi, T., Lee, H.K., Pitman, I.H. Farm Alkak 1971, 80, 55-90.
4. Andersgaard, H., Finholt, P., Gjermunsen, R., Hoyland, T. Acta Pharm. Suecica 1974, 11, 239-248.
5. Higuchi, T., Stella, V.J. "Prodrugs as Novel Drug Delivery Systems"; ACS Symposium Series 14; American Chemical Society: Washington, DC, 1975; pp 51-66.
6. Donbrow, M., Touitou, E. J. Pharm. Pharmacol. 977, 29, 524-528.
7. Lee, H.K., Lambert, H., Stella, V.J., Wang, D., Higuchi, T. J. Pharm. Sci. 1979, 68, 288-295.
8. Mooney, K.G., Mintun, M.A., Himmelstein, K.J., Stella, V.J. Ibid, 1981, 70, 13-22.
9. Mooney, K.G., Mintun, M.A., Himmelstein, K.J., Stella, V.J. Ibid, 1981, 70, 22-32.
10. Touitou, E., Donbrow, M. Intl. J. Pharmaceutics 1981, 9, 97-106.
11. Hirotsune, I., Carey, M.C. J. Lipid Res. 1981, 22, 254-270.

12. Amidon, G.L., Pearlman, R.S., Leesman, G.D., "Design of Biopharmaceutical Properties Through Prodrugs and Analogs"; American Pharmaceutical Association: Washington, DC, 1977, pp 281-315.

13. Noyes, A.A., Witney, W.R. J. Amer. Chem. Soc. 1897, 19, 930-934.

14. Nernst, W. Z. Physikal Chem. 1904, 47, 52-55.

15. Gray, C.J. "Enzyme-Catalysed Reactions"; Van Nostrand Reinhold Co.: London, 1971, pp 72-74, 148-166.

16. Wood, J.H., Syrato, J.E., Letterman, H. J. Pharm. Sci. 1965, 54, 1068.

17. Levich, V.G. "Physicochemical Hydrodynamics": Prentice-Hall Inc., Englewood Cliffs, NJ, 1962, pp 60-72.

18. Longsworth in "American Institute of Physics Handbook" 3rd Ed., McGraw Hill: New York, NY, 1972, pp 221-229.

19. Bird, R.B., Stewart, W.E., Lightfoot, E.N., "Transport Phenomena" Wiley: New York, 1960; pp 502-516, 559.

20. Prakongpan, S., Molokhia, A.H., Kwan, K.H., Higuchi, W.I. J. Pharm. Sci. 1976, 65, 685-689.

21. Tsuji, A., Nakashima, E., Hamano, S., Yamana, T. Ibid 1978, 67, 1059-1066.

22. Cunningham, L.W., Brown, C.S. J. Biol. Chem. 1956, 221, 287-299.

23. Bender, M.L., Clement, G.E., Kezdy, F.J., Heck, H. J.

Amer. Chem. Soc. 1964, 86, 3680-3689.

24. Kaplan, H., Laidler, K.J. Canad. J. Chem. 1967, 45, 547-557.

25. Martinek, K., Yatsimirskii, A.K., Berezin, I.V. Molekul. Biol. 1971, 5, 96-109.

26. Casado, J., Seoane, F., Cachaza, J.M. Rev. Roumaine de Chimie 1979, 24, 1451-1456.

27. Gutfreund, H., Sturtevant, J.M. Biochem. J. 1956, 63, 656, 661.

28. Gutfreund, H., Sturtevant, J.M. Proc. Natl. Acad. Sci. (US) 1956, 42, 719-728.

29. Segel, I.H. "Enzyme Kinetics"; Wiley-Interscience: New York, 1975; pp 29-34.

30. Olander, D.R. A.I.Ch.E. Journal 1959, 6, 233-239.

31. MACC, "Numerical Integration Routines"; University of Wisconsin; Madison, WI, 1976.

32. Schonbaum, G.R., Zerner, B., Bender, M.L. J. Biol. Chem, 1961, 236, 2930-2935.

33. Hammond, B.R., Gutfreund, H. Biochem. J. 1955, 61, 187-189.

34. Bender, M.L., Schonbaum, G.R., Hamilton, G.A. J. Polym. Sci. 1961, 49, 75-103.

35. Hummel, B.C.W. Can. J. Biochem. Physiol. 1959, 37, 1393-1399.

36. Connors, K.A. Interest 1984, 23, 1-61.

37. Kenneth A. Connors, personal communication.

38. Yu, C.D., Fox, J.L, Ho, N.F.H., Higuchi, W.I. J. Pharm. Sci. 1979, 68, 1341-1346.

39. Kezdy, F.J., Bender, M.L. Biochemistry 1962, 1, 1097-1106.

40. Draper, N., Smith, H. "Applied Regression Analysis"; John Wiley and Sons Inc.: New York 1966, p 44-81.

OVERALL SUMMARY

There may be several reasons accounting for the poor oral bioavailability of pharmaceutical compounds. They include first pass metabolism, poor drug permeability through the intestinal membrane and poor drug dissolution and/or low drug solubility. In order to ascertain the cause of a drug's poor bioavailability it sometimes becomes necessary to experimentally isolate and evaluate each step of the drug absorption process.

A major problem inherent in most experimental systems is that the sample is usually drawn from a well stirred bulk media. However, in an interphase transport problem, it is usually the viscid region near the interface of the two phases that is of interest. For instance, it is the concentration near the membrane surface which determines the rate of mass uptake by the membrane. It becomes necessary to know, at least qualitatively, how the bulk sample represents a physical process or some physical quantity in a region removed from the bulk media (e.g. how does bulk concentration relate to membrane surface concentration?). This knowledge can be gained emperically from experimental trials as well as theoretically through hydrodynamic considerations. Ideally, experiments should be designed to test theoretical concepts.

If several experimental set-ups can be chosen from, it makes the most sense to chose the one which has the best known hydrodynamics. However, other factors can also complicate the interpretation of

physical data, including chemical reactions. One possibility is when the sample comes from the phase where mass is leaving as a result of a chemical reaction in another phase. A second possibility is when the sample comes from the phase in which the chemical reaction is occuring. The non-linearity of Michaelis-Menten type reactions may complicate matters even more.

In this thesis, two experimental problems of pharmaceutical interest were identified and analysed. Both involved interphase transport with Michaelis-Menten kinetics. Both experimental systems had well characterized hydrodynamics such that the effect of reaction could be isolated in each case. The first problem was that of the intestinal perfusion experiment. In this experiment, the mass loss from the moving bulk fluid is measured. The uptake by the membrane phase was considered as a chemical reaction involving first order kinetics in parallel with a Michaelis-Menten type reaction. The effective permeability which is measured by the mass loss in the bulk fluid had to be related to the intrinsic membrane permeability. A key finding was that the aqueous resistance to membrane uptake was independent of the membrane permeability. Therefore, it is concluded that a surface reaction, or a reaction in the phase opposite the sample phase, has no effect on the aqueous resistance of the sample phase. The reaction changes the concentration at the phase interface, Cw, and therefore affects only the concentration potential in the sample phase.

In the second problem, mass was transferred from a solid phase into a reactive bulk phase. Here, the reaction occurs in the sample phase. In this particular problem, the concentration potential is fixed. The effect of the chemical reaction in this case is to decrease the overall aqueous resistance in the fluid adjacent the solid phase surface. This effect is significant when the reaction time is on the order of the diffusion time through the aqueous boundary layer. In general, if the phase opposite the sample phase were not a solid, say a polymeric phase with a concentration gradient within it, the chemical reaction of the sample phase would also affect the concentration at the interface and therefore the concentration potential of the sample phase. The effect of chemical reaction in this case would be on both the aqueous resistance and concentration potential.

The results of this work should prove useful in providing many guidelines for the development and evaluation of pharmaceutical compounds and oral dosage forms. Particular applications can be found with pharmaceutical compounds which are either prodrugs or substrates for the carrier mediated transport systems of the brush border region of the intestinal membrane.